[redacted]

UNCLASSIFIED

WT-68-SAN

OPERATION GREENHOUSE

SCIENTIFIC DIRECTOR'S REPORT

ANNEX 1.5 NEUTRON MEASUREMENTS

PART II—SPECTRUM AND AIR ATTENUATION STATIC MEASUREMENTS

SECTION 2

NUCLEAR EXPLOSIONS

1951, SANITIZED VERSION

[redacted]

[redacted]

RESTRICTED DATA

This document contains restricted data as defined in the Atomic Energy Act of 1946. Its transmittal of its contents in any manner to an unauthorized person is prohibited.

[redacted]

UNCLASSIFIED

[redacted]

This document consists of 176 plus 4 pages
(counting preliminary pages)

[redacted]

Scientific Director's Report of Atomic Weapon Tests at Eniwetok, 1951

Annex 1.5

Neutron Measurements

Part II—Spectrum and Air Attenuation Static Measurements

Section 2

[redacted]

This document contains restricted data as defined in the Atomic Energy Act of 1946. Its transmittal or disclosure of its contents in any manner to an unauthorized person is prohibited.

[redacted]

[redacted]

Distribution

	Copy
DEPARTMENT OF DEFENSE	
Armed Forces Special Weapons Project (Sandia)	1–3
Armed Forces Special Weapons Project (Washington)	4–15
ARMY	
Army Field Forces	16
Assistant Chief of Staff, G-3	17
Assistant Chief of Staff, G-4	18–19
Chief Chemical Officer	20–23
Chief Signal Officer	24–27
Chief of Engineers	28–29
Chief of Ordnance	30–34
Operations Research Office (Johns Hopkins University)	35–36
NAVY	
Bureau of Medicine and Surgery	37
Chief of Naval Operations	38
Chief of Naval Research	39
Naval Medical Research Institute	40
Naval Radiological Defense Laboratory	41–43
AIR FORCE	
Air Force Cambridge Research Center	44
Air Research and Development Command	45–48
Air Targets Division, Directorate of Intelligence (Phys. Vul. Branch)	49–50
Assistant for Atomic Energy	51–52
Assistant for Development Planning	53
Assistant for Materiel Program Control	54
Deputy Chief of Staff for Development (AFDRD)	55
Director of Operations (Operations Analysis Division)	56
Director of Plans (AFOPD-P1)	57
Director of Requirements	58–59
Director of Research and Development	60–61
Eglin Air Force Base, Air Proving Ground	62–63
Ent Air Force Base, Air Defense Command	64–65
Kirtland Air Force Base, Special Weapons Center	66–68
Langley Air Force Base, Tactical Air Command	69–70
Maxwell Air Force Base, Air University	71–72
Offutt Air Force Base, Strategic Air Command	73–75
1009th Special Weapons Squadron	76
Rand Corporation	77–78
Scott Air Force Base, Air Training Command	79–80
Wright Air Development Center	81–83
Wright Air Materiel Command	84–85
ATOMIC ENERGY COMMISSION	
Atomic Energy Commission, Washington	86–88
Division of Military Application (for supplemental distribution)	89–92
Los Alamos Scientific Laboratory, Report Library	93–107
Sandia Corporation	108–109
Technical Information Service, Oak Ridge (surplus)	110–148
University of California Radiation Laboratory (York)	149
Weapon Test Reports Group, TIS	150

[redacted]

[redacted]

NEUTRON MEASUREMENTS

Part II—Spectrum and Air Attenuation Static Measurements

Section 2

Neutron-spectra Measurements

by

JOHN C. ALLRED

DONALD D. PHILLIPS

and

LOUIS ROSEN

Approved by: FREDERICK REINES
Director, Program 1

Approved by: ALVIN C. GRAVES
Scientific Director

Los Alamos Scientific Laboratory
Los Alamos, New Mexico

January 1952

[redacted]

[redacted]

Acknowledgments

The authors are greatly indebted to Lee Stewart and John Green for performing a great many of the calculations relevant to this report. To Lee Stewart the authors are further indebted for assuming most of the burden of assembling and arranging the data, tables, and figures that went into this report and for deciphering the writing in the first written draft. We are also indebted to Alice H. Armstrong for supervising much of the plate analysis and to the following for the exacting and tedious work of analyzing the plates: Pat Agee, May Bergstresser, Rexine Booth, Julia Carlson, Juanita Frazer, Juanita Gammel, Caroline Hart, Catherine Lacey, Opal Milligan, Enid Nordeen, Pearl Norwood, Muriel Osborn, Lee Stewart, and Dorothy Squires.

Values of mean free paths and error assignment to them were calculated by least-squares analyses. All these calculations were performed by Lee Stewart with the aid of Don Dodder, to whom we are also indebted for many helpful discussions.

The authors take pleasure in acknowledging the help and support received from William Ogle during the course of these experiments. The pleasure derived from collaborating with William Ogle and all the members of Group J-3 of the Los Alamos Scientific Laboratory to a large extent offsets the somewhat less than ideal conditions under which these experiments were of necessity performed.

Finally we wish to thank Julia Carlson, Martha Downs, and Kathryn Uken for typing the manuscript.

[redacted]

[redacted]

CONTENTS

[redacted]

[redacted]

CONTENTS (Continued)

[redacted]

[redacted]

CONTENTS (Continued)

ILLUSTRATIONS

[redacted]

ILLUSTRATIONS (Continued)

[redacted]

ILLUSTRATIONS (Continued)

[redacted]

ILLUSTRATIONS (Continued)

TABLES

[redacted]

TABLES (Continued)

CHAPTER 8 RESULTS

[redacted]

Chapter 1

General Introduction

1.1 BACKGROUND OF REPORT

A preliminary report on the photographic neutron experiment was written Feb. 1, 1951. Since neither the philosophy of the experiment nor the method of carrying it out underwent significant changes after January 1951, the preliminary report is reproduced here as the first three chapters of this report. Chapter 4 outlines the changes which were introduced as well as the expanded objectives which dictated the nature of the most important of these changes.

The Greenhouse series of experiments involved four nuclear detonations. These may be briefly described as follows (listed in the order of firing):

1. Dog shot—DELETED
Yield: 82.9 ± 1.3 kt.

2. Easy shot—DELETED
Yield: 46.7 ± 0.6 kt.

3. George shot—DELETED
Yield: 214.5 ± 6.6 kt.

4. Item shot—DELETED
Yield: 45.7 ± 0.5 kt.

1.2 OBJECTIVES OF EXPERIMENT

The photographic neutron experiment (Phonex) is designed to yield the prompt-neutron spectra generated in various types of nuclear detonations with particular emphasis on the scheduled thermonuclear tests. All measurements are to be made in collimated geometry and at a number of distances from the various explosions, thus making possible observations of essentially the prompt neutrons only, as well as a determination of the mean free path of these neutrons in air as a function of their energy. Mean-free-path determinations are essential if it is to be possible to deduce the absolute number of neutrons, as a function of energy, emanating from a bomb. It is fortunate for calculatory purposes that considerable data are already available on the mean free path of neutrons in air over a reasonable region of the energy spectrum under consideration. The objectives of this experiment may then be summarized as follows:

1. Determination of whether a thermonuclear reaction takes place, in those cases where deuterium and tritium are present, as evidenced by production of 14-Mev neutrons.
2. Determination of the amount of tritium burned from a measurement of the number of 14-Mev neutrons produced in a given thermonuclear reaction.
3. Measurement of neutron spectra from various types of fission weapons.

In order to permit a realistic design of the various components entering into this experiment, certain data have to be assumed on the basis of previous experiments and/or calculations. The data necessary for present computations fall into two general categories—data which are independent of bomb characteristics and data which are functions of bomb characteristics. Table 1.1 lists the data falling within the first category; Table 1.2 lists the

data falling within the second category.

Figure 1.1 is a graph of the attenuation data taken by L. D. P. King of the Los Alamos Scientific Laboratory for M-1 concrete (limonite, cement, and scrap iron) using fission spectrum gammas. Although these data seem to be very good, the 8.5-cm mean free path was used in the following calculations so that errors made in the calculated shielding requirements would lead to a conservative design of the shields.

1.3 EXPERIMENTAL METHOD

Figure 1.2 shows schematically the experimental arrangement to be utilized in this experiment. The hydrogenous (polyethylene) neutron converter is irradiated by a cone of neutrons of maximum half angle of 0.8°. The axis of this cone passes through the bomb core. This degree of collimation essentially ensures that the converter sees only the prompt unscattered neutrons from the bomb. A fraction

TABLE 1.1 DESIGN DATA INDEPENDENT OF BOMB CHARACTERISTICS

Mean free path in air for 14-Mev neutrons ($\lambda_{n\text{-}14}$)	150 yd	From Ogle's* measurements at Sandstone and Coon's* measurements at Los Alamos
Mean free path in air for fission spectrum neutrons (λ_{nf})	180 yd	From Ogle's measurements at Sandstone
Mean free path in air for fission gammas ($\lambda_{\gamma f}$)	340 yd	From Ogle's measurements at Sandstone
Mean free path in limonite concrete and scrap iron (M-1 mix) for fission gammas ($\lambda_{\gamma L}$)	8.5 cm	Based on data from Oak Ridge. Data of L. D. P. King* give somewhat lower value (6.85 cm).
Mean free path in M-1 mix for slow neutrons (λ_{NSL})	<0.7 in.	Based on data from L. D. P. King
Mean free path in M-1 mix for fast neutrons (λ_{NFL})	6.0 cm	Based on data from L. D. P. King
Maximum slow-neutron background to which nuclear plates may safely be exposed	$10^{10}/cm^2$	This produces approximately 75 proton tracks per 10^{-6} cm^3 of dry emulsion. Protons arise from $N^{14}(n,p)C^{14}$ reaction.
Maximum fission spectrum neutron background to which nuclear plates may be safely exposed	$5 \times 10^9/cm^2$	This flux produces approximately 40 proton-recoil tracks per 10^{-6} cm^3 of dry emulsion.
Maximum fission spectrum gammas to which nuclear plates may be safely exposed	2 r	

*Of the Los Alamos Scientific Laboratory.

PAGE 3 IS DELETED.

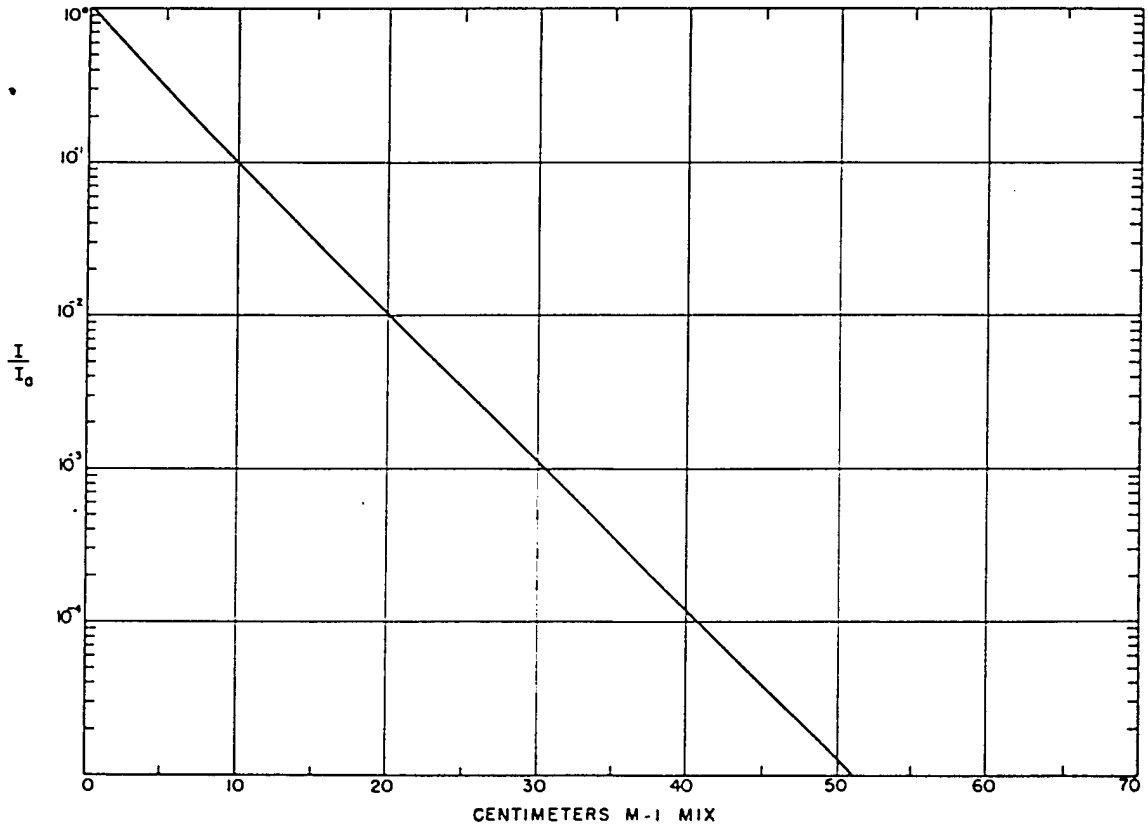

Fig. 1.1 Attenuation vs Thickness of Limonite Concrete for Fission Spectrum Gammas

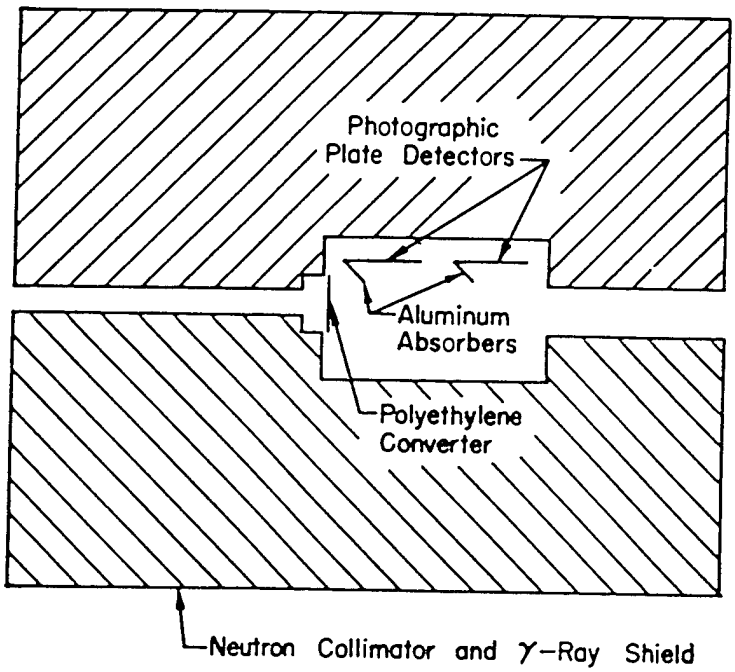

Fig. 1.2 Schematic Diagram of Collimator and Camera

of the proton recoils projected by the neutrons from the polyethylene radiator pass through the absorbers and then impinge upon photographic plate detectors. The absorbers and emulsion thicknesses are so chosen that protons projected by the highest energy neutrons with the incident neutron direction. The angle θ is given by the position on the plate at which the proton penetrated the emulsion surface. The absolute neutron intensity in any given energy interval at the converter can be determined from the number of protons of corre-

TABLE 1.3 PLANNED CONDITIONS AND GEOMETRY FOR EXPOSURE OF EACH PLATE

Collimation Camera Unit	Converter Thickness (mg/cm^2)	Plate Designation	Aluminum-absorber Thickness (mils)	Angle θ	D (cm)	Emulsion Type	Emulsion Thickness (μ)	ΔE (Mev)
C-1								
C-2	DELETED							
C-3								

*This plate is to be used as a control. Emulsion side faces camera wall rather than converter.

being investigated will be stopped within the sensitive volume of the detectors. The neutron energy corresponding to a given proton recoil is determined from the range of the proton in the emulsion, the thickness of the aluminum absorber, the radiator thickness, and the angle (θ) which the proton recoil makes sponding energy observed on the plates per unit solid angle subtended at the radiator, the diameter of the collimator hole, the number of H atoms per square centimeter of converter, and the differential neutron-proton scattering cross section averaged over the energy interval under consideration.

Data will be obtained at five or six distances from each bomb. The stations are to be spaced at 200-yd intervals from the base of the bomb tower. Each station will consist of a single shielding block containing three cylindrical channels or tubes. Behind each tube will be housed one camera, and in each camera there will be one converter, eight nuclear plates, and appropriate absorbers. The cameras are vacuumtight and will be evacuated prior to installation to a pressure of less than 1 mm Hg. This is sufficient to prevent neutron and gamma-ray scattering in the gas, as well as scattering and energy degradation of recoil protons from the radiator. The reason for utilizing three camera units at each station is to make possible a determination of neutron-energy spectra over the energy region from 2 to 16 Mev. For the low-energy portion of the spectra, very thin radiators and no absorbers will be used. For the high-energy portion where intensity is a problem, thick radiators can be used without compromising energy resolution, and relatively thick absorbers must be used to ensure that the plates will not be blackened by the large number of proton recoils projected by low-energy neutrons. Without this device it would be impossible, in the case of a fission bomb, to observe the high-energy protons in the presence of low-energy protons.

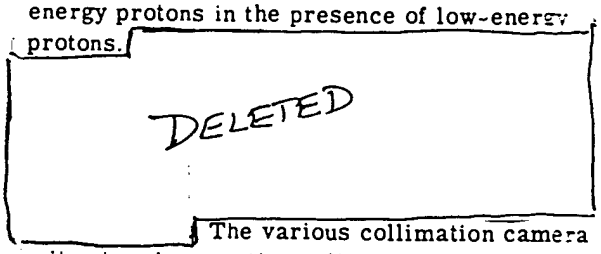

The various collimation camera units at a given station will be called C-1, C-2, and C-3 and the various plates in each camera P-1, P-2, P-3, etc. Table 1.3 then gives the values for converter thickness; aluminum-absorber thickness; angle, θ, between collimator axis and line from center of converter to center of detector; distance, D, from center of converter to center of detector; type of emulsion; thickness of emulsion; and neutron energy interval, ΔE, being investigated.

All plates will be developed as follows:

(1) 30 min in one part D-19 to six parts water. No agitation.

(2) 2 min in running water.

(3) 4 hr in acid hypo with good agitation. Hypo to be changed after 2 hr. After 15 min in hypo, surface silver to be rubbed off with light finger pressure.

(4) 2-hr wash in running water. All water to be distilled and filtered. Temperatures of solutions, darkroom, and wash water to be 68 ± 1°F.

The plates will be analyzed using binocular microscopes with oil-immersion 45 × to 90 × objectives and 6 × to 12 × compensating eyepieces.

1.4 COLLIMATION AND SHIELDING

1.4.1 Angular Apertures of Collimator; Effect of Neutron Scattering in Air

It is quite certain that this experiment will be successful if the converter is permitted to see only prompt neutrons which proceed from the bomb directly to the converter and if the nuclear plates can be simuitaneously shielded adequately from neutrons, thermal radiation, and gamma radiation. It remains, therefore, to inquire into the air-scattering of neutrons and the degree of shielding necessary to prevent the detectors from becoming unduly heated or overexposed by neutron and gamma radiation. As to the latter, consideration must be given not only to the direct transmission of the shielding material contained in the collimator block but also to the effect of the collimator tubes and converters since they serve as scatterers of neutrons and gamma rays and as converters of neutrons to gamma rays.

Calculations by Ogle show that the number of 14-Mev neutrons elastically scattered by air that will enter a given collimation tube and proceed without scattering to the converter is given by Eq. 1.1 (see Appendix IA for derivation of this equation).

$$\frac{N_{scattered}}{N_{direct}} = e^{R/2\lambda} - 1 \frac{\alpha}{\pi \sin^2 \theta \sqrt{R/2\lambda}}, \quad (1.1)$$

where $N_{scattered}$ = number of scattered 14-Mev neutrons.

N_{direct} = number of direct 14-Mev neutrons.

θ = mean scattering angle of neutrons for one collision.

R = distance between bomb and collimator.

λ = mean free path of 14-Mev neutrons in air considering both elastic and inelastic processes = 140 m.

α = solid angle subtended by collimation-tube aperture at a point on the converter = 1.4×10^{-4} steradian.

At 600 yd from the zero point,

$$\frac{N_{scattered}}{N_{direct}} = 2.90 \times 10^{-3}.$$

Since the mean free path for, say, 3-Mev neutrons is not radically different from the mean free path for 14-Mev neutrons, elastically scattered neutrons should not produce a significant contribution to the measured spectrum in the energy region of interest.

1.4.2 Heating of Collimator Block

The energy generated by a so-called 200-kt bomb is approximately 8.4×10^{21} ergs. Assume that all the energy intercepted by the collimator block is absorbed, and further assume an energy attenuation of $(1/R^2)$. It is then found that at the closest station the maximum energy that the collimator block can possibly absorb is 4.2×10^{15} ergs. Since the collimator weighs 30 tons and its specific heat is essentially that of iron, the maximum temperature rise of the collimator if heated uniformly throughout will be 3.7°C.

1.4.3 Shielding Requirements Assuming a Solid Block Made of M-1 Mix; No Collimator Tubes

As a first approximation to the shielding requirements, the thickness of M-1 mix necessary when the detectors are surrounded by a hole-free shield will be calculated. Table 1.4 shows the neutron and gamma-ray fluxes expected at various distances from a 200-kt bomb and the shielding thicknesses required to reduce these fluxes to permissible values. Section 1.2 gives all the constants upon which this table is based. Since the mean free path for gammas given in Sec. 1.2 was measured in the presence of pile neutrons, it is not necessary to consider the effect of gamma-ray production by neutron absorption in the shield. Of course, this argument does not hold in the case of a thermonuclear reaction, but experiments with 14-Mev neutrons, to be described in one of the following sections, have essentially eliminated this uncertainty.

The calculated particle or gamma-ray flux at any distance D is given by

$$\frac{Q}{4\pi D^2} e^{-D/\lambda}, \qquad (1.2)$$

where Q is the effective source strength, D is the distance of station from bomb, and λ is the mean free path.

The thickness of the M-1 mix required is calculated from

$$I/I_0 = e^{-t/\lambda}, \qquad (1.3)$$

where $(I/I_0)^{-1}$ is the attenuation required, t is the thickness of mix, and λ is the mean free path of particles or radiations being considered.

It will be seen from Table 1.4 that the γ radiation poses the most serious shielding problem. Therefore this problem will be considered primarily, since it appears that if the plates can be adequately shielded against γ radiation they will automatically be shielded against other radiations, with the possible exception of slow neutrons which proceed down the collimation tube. These slow neutrons will be eliminated by boron containing 3 g/cm^2 of B^{10} placed in the entrance and exit collimator tubes. This thickness of B^{10} is equivalent to 36 mean free paths for neutrons for which the $B^{10}(n,\alpha)Li^7$ cross section is 100 barns (the thermal-neutron cross section for this reaction is 2000 barns). The B^{10} will therefore reduce the slow-neutron flux by something like a factor of e^{36} which is more than adequate.

However, the gamma-ray problem is more serious. The three most important mechanisms for irradiating the photographic plate detectors are (1) radiation transmitted through shield, (2) radiation scattered by collimation tube and then rescattered by the back wall of the cavity containing the camera, and (3) radiation scattered by the converter and then proceeding either directly or after additional scatterings to the detectors.

Mechanism 1 has already been considered. As far as mechanisms 2 and 3 are concerned,

TABLE 1.4 REQUIRED SHIELDING

Distance from Base of Tower (yd)	Slow-neutron Flux (Ogle at Sandstone) (neutrons/cm²)	Minimum Attenuation Factor Required	Minimum Thickness of M-1 Mix Required (cm)	Fast-neutron Flux (Calculated) (neutrons/cm²)	Minimum Attenuation Factor Required	Minimum Thickness of M-1 Mix Required (cm)	Total Gammas (Scoville's Data) (r)	Minimum Attenuation Factor Required	Minimum Thickness of M-1 Mix Required (cm)	Gammas (Prompt Calculated) (r)
200										
400										
600										
800										
1000										
1200										
200										
400										
600										
800										
1000										
1200										

DELETED

[redacted]

6

only the γ radiation needs to be considered since the effect of scattered neutrons must be quite small compared to the effect of scattered gammas. This reasoning becomes clear when it is remembered that the tolerance for the neutron irradiation of the detectors is extremely large. Also, the relative contribution of neutrons to gamma blackening must be a second-order effect; i.e., although there are approximately as many scattered neutrons as gammas, the neutrons must be converted to gammas and these gammas must get back to the detector before any appreciable gamma blackening due to neutrons can occur.

1.4.4 Collimation-tube Scattering

Estimates based on rather detailed calculations by B. R. Suydam[1] show that, for our geometry, the intensity of gamma radiation reaching the detectors which is due to scattering in the collimation tube is a factor of 10^5 below that of the radiation intensity outside the collimator. It is therefore seen that this effect is roughly equivalent to the intensity transmitted through the collimator.

1.4.5 Gamma-ray Scattering by Converter

The thickest converter which will be used is 22 mg/cm^2 of polyethylene. Since the mean free path of 2.0-Mev gammas is approximately 36 g/cm^2, it is apparent that our converter is equivalent to 6×10^{-4} mean free path. The transmission then is given by $I/I_0 = e^{-6 \times 10^{-4}}$ mean free path. The fraction scattered is therefore $(1 - I/I_0) = 6 \times 10^{-4}$, and of this fraction not more than 5 per cent will ever reach the detectors. It is therefore seen that this effect is probably negligible compared to collimation-tube scattering.

1.4.6 Summary of Shielding Requirements and Predicted Exposures of Detectors to Penetrating Radiation

As a consequence of calculations similar to the preceding but based on somewhat more favorable values for the mean free path of gammas and neutrons in limonite concrete, all collimators were built with 42-in.-thick front faces and 23-in.-thick top and sides. The top and sides were made thinner because the gammas, and to a somewhat lesser extent the neutrons, are more or less unidirectional. As far as the neutrons are concerned, 23 in. would be sufficient even for the surface facing the bomb. This is not so for the gammas. However, most of the gammas which are incident on the top and sides come in at a grazing angle, thus making the effective shielding much thicker. Those gammas which are scattered enough so that the shielding path is essentially 23 in. are degraded in energy as well as intensity. Table 1.5 shows the energy distribution with angle of 2- and 4-Mev scattered gammas. If it is assumed that the effective gamma intensity perpendicular to the top and sides is 5 per cent of the intensity on the front and if 0.7 Mev is taken as the mean energy of these scattered gammas, the radiation in roentgens transmitted through the 1 cm^2 of side or top surface is

TABLE 1.5 ENERGY DISTRIBUTION WITH ANGLE OF 2- AND 4-MEV SCATTERED GAMMAS

θ (deg)	$E_S(E_0 = 2$ Mev) (Mev)	$E_S(E_0 = 4$ Mev) (Mev)
10	1.9	3.6
30	1.3	2.7
60	0.67	0.8
90	0.4	0.44
180	0.22	0.23

approximately a factor of 10 less than that transmitted through 1 cm^2 of the front face.

All collimators for all stations were built alike for reasons of economy of design and construction. Additional lead, limonite, and dirt shielding will be used at the 400- and 600-yd stations on the first test. In front 8 in. of lead will be used, with 4 in. of lead on top. The side shielding will be bolstered by 18 in. of limonite concrete and 18 in. of sand. All this is for the purpose of ensuring that usable data will be obtained on the first shot. Radiation measurements will be made inside all collimators on the first shot in order to determine the effectiveness of the shielding. In case of trouble, these measurements should serve as a reliable guide for the following shots.

DELETED

This estimate is on the

TABLE 1.6 [DELETED]

Distance from Bombs (yd)	Gamma-ray Intensity (r)	Intensity on Detectors (r)
200	[DELETED]	
400		
600		
800		
1000		
1200		

basis of supplementary shielding at the 200- and 400-yd stations only. Also, the 200-yd station will have 2 in. of lead in front of two of the collimator holes. It is of interest that the attenuation factor of the collimator for gammas is essentially determined by scattering in the collimation tube.

1.5 TREATMENT OF DATA AND INTERPRETATION OF RESULTS

The analysis of the photographic plates consists in making a range analysis of all proton tracks, over a measured area of plate, which start on the surface of the emulsion and proceed away from the converter within the angular region defined by the converter-detector geometry, adequate allowance being made for absorber scattering. The acceptability criteria just presented should effectively eliminate the necessity for making a background correction. For ease of analysis, the horizontal projections of the tracks produced by the proton recoils are measured, and these are then converted into absolute ranges on the basis of the radiator-detector geometry, i.e.,

$$R_T = \frac{R_M}{\cos \theta}$$

where R_T is the proton range in dry emulsion, R_M is the measured length of track (horizontal projection), and θ is the angle between proton recoil and incident neutron. The incident-neutron direction is taken to coincide with the collimation axis. To the range in the emulsion thus obtained must be added the emulsion equivalent of the absorber used in front of the plates and the emulsion equivalent of one-half the converter thickness. This summation is now equivalent to the range in dry emulsion which a recoil proton would have had if it had been projected from an infinitesimally thin converter directly to the emulsion without traversing any absorber. It has been shown experimentally that 1 mg/cm^2 of polyethylene is equivalent to 1.1 cm of air or 4.58 μ of dry C-2 emulsion for 5.2-Mev alpha particles. This is also borne out quite well from calculations based on atomic stopping powers. It is assumed that this relation will hold for protons and will be more or less independent of energy. Since the half thickness of the converter is always less than 10 per cent of the range of the lowest energy protons being measured, the energy resolution is not seriously impaired, and furthermore a considerable error in the above assumptions will produce negligible error in the end result.

Table 1.7 gives the range of protons in dry C-2 emulsion and in aluminum as a function of energy[2,3] and also the C-2 emulsion equivalent of aluminum as a function of energy. From the sixth column in the table it can be seen that the emulsion equivalent of aluminum for protons is practically independent of energy from 3.0 to 14.5 Mev.

Therefore 1 mg/cm^2 of aluminum will be taken to be equivalent to 3.27 μ of C-2 emulsion. The maximum error that will be made due to assuming a constant value of (range in emulsion)/(range in aluminum) is less than 0.1 Mev at 14 Mev.

Figure 1.3 is a graph of the range-energy relation for protons in Ilford C-2 emulsion. Figure 1.4 is a graph of the range of protons vs energy in aluminum.

It is now possible to obtain for a given proton track a value for the range the proton would have had in C-2 emulsion if none of its energy had been dissipated in the converter and absorber. This permits the determination of the energy of this proton by referring to the range-energy curve plotted in Figure 1.3.

The data can now be reduced to the number of protons projected per unit solid angle at a given angle (determined by the radiator-detector geometry) as a function of proton energy.

The next step involves conversion of the proton energies to corresponding incident-

TABLE 1.7 RANGE OF PROTONS IN C-2 EMULSION AND IN ALUMINUM AS A FUNCTION OF ENERGY

E (Mev)	Range of Protons in Dry C-2 Emulsion* (μ)	ΔR_E/Mev (μ)	Range of Protons in Aluminum (mg/cm^2)	ΔR_{Al}/Mev (mg/cm^2)	$\Delta R_E/\Delta R_{Al}$/Mev (μ/mg/cm^2)
2.0	39.8		10.8		
2.5	56.0	35.0	15.6	10.2	3.43
3.0	74.8		21.0		
3.5	96.0	44.2	27.3	13.5	3.27
4.0	119.0		34.5		
4.5	144.5	52.0	42.1	15.8	3.29
5.0	171.0		50.3		
5.5	201.5	61.5	59.0	18.8	3.27
6.0	232.5		69.1		
6.5	265.0	67.0	79.2	20.9	3.21
7.0	299.5		90.0		
7.5	336.0	74.5	101.3	23.2	3.21
8.0	374.0		113.2		
8.5	414.5	83.5	125.6	25.6	2.26
9.0	457.5		138.8		
9.5	502.0	89.0	152.4	27.9	3.19
10.0	546.5		166.7		
10.5	596.0	99.5	181.4	29.9	3.33
11.0	646.0		196.6		
11.5	698.0	105.0	212.5	32.4	3.24
12.0	751.0		229.0		
12.5	806.0	111.0	246.1	34.7	3.20
13.0	862.0		263.7		
13.5	921.0	120.0	281.8	36.9	3.25
14.0	982.0		300.6		
14.5	1046.0	130.0	319.0	38.7	3.36
15.0	1112.0		339.3		
15.5	1171.0	140.0	359.0	40.2	3.48
16.0	1252.0		379.5		

*Range in NTA emulsion, ±2 per cent; range in E-1 emulsion, ±1 per cent.

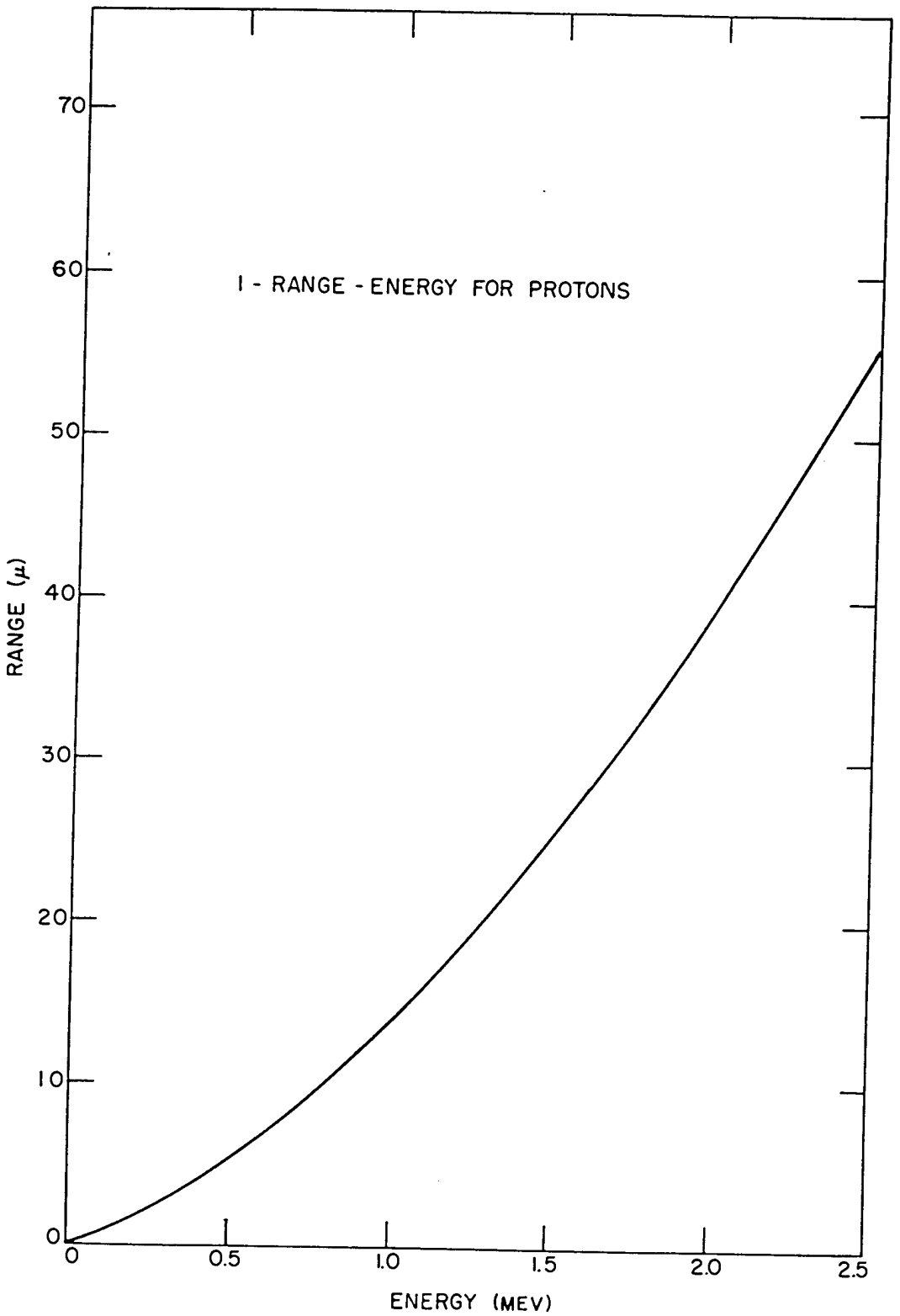

Fig. 1.3 Range-Energy Relations for Protons in Ilford C-2 Emulsion

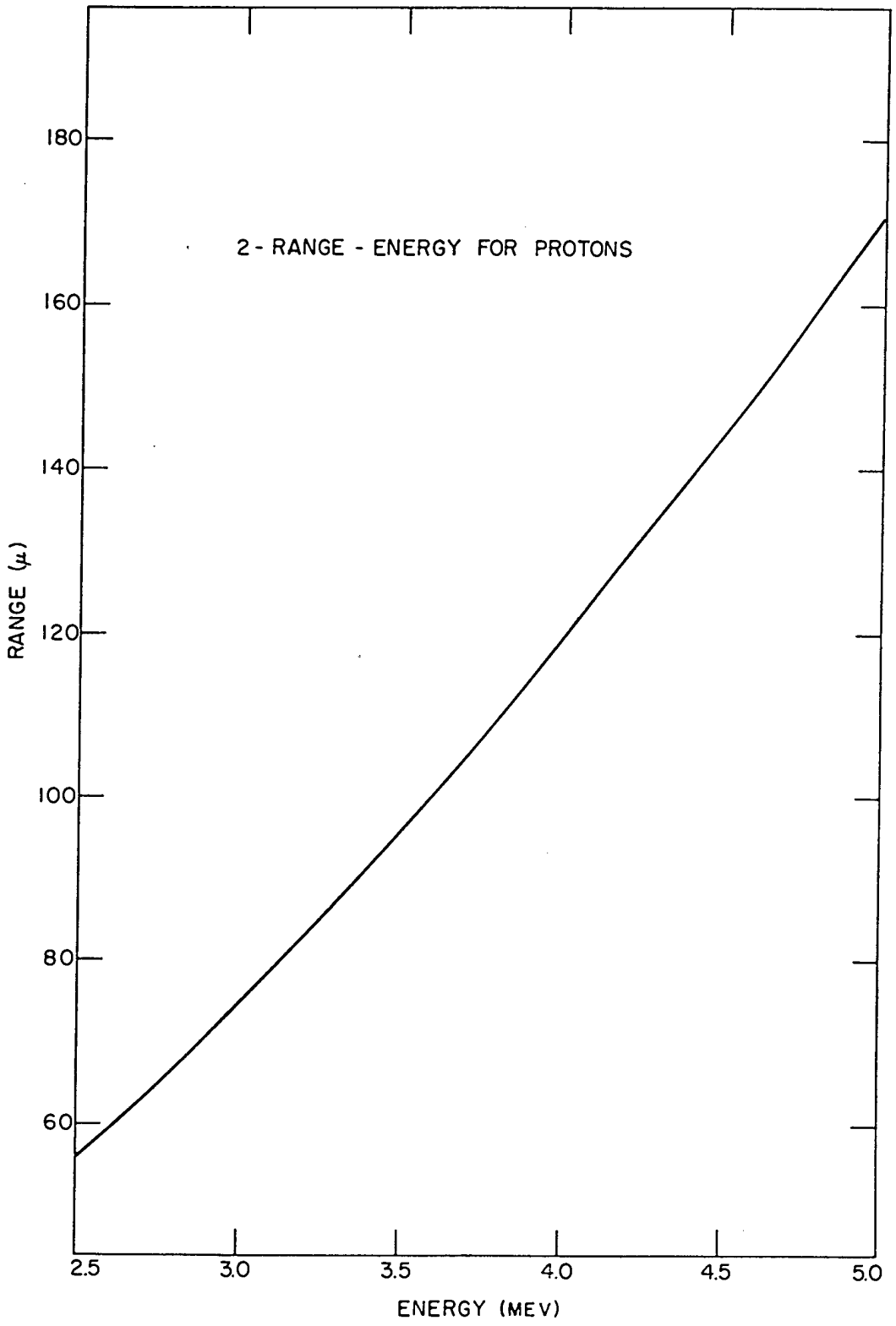

Fig. 1.3 Range-Energy Relations for Protons in Ilford C-2 Emulsion

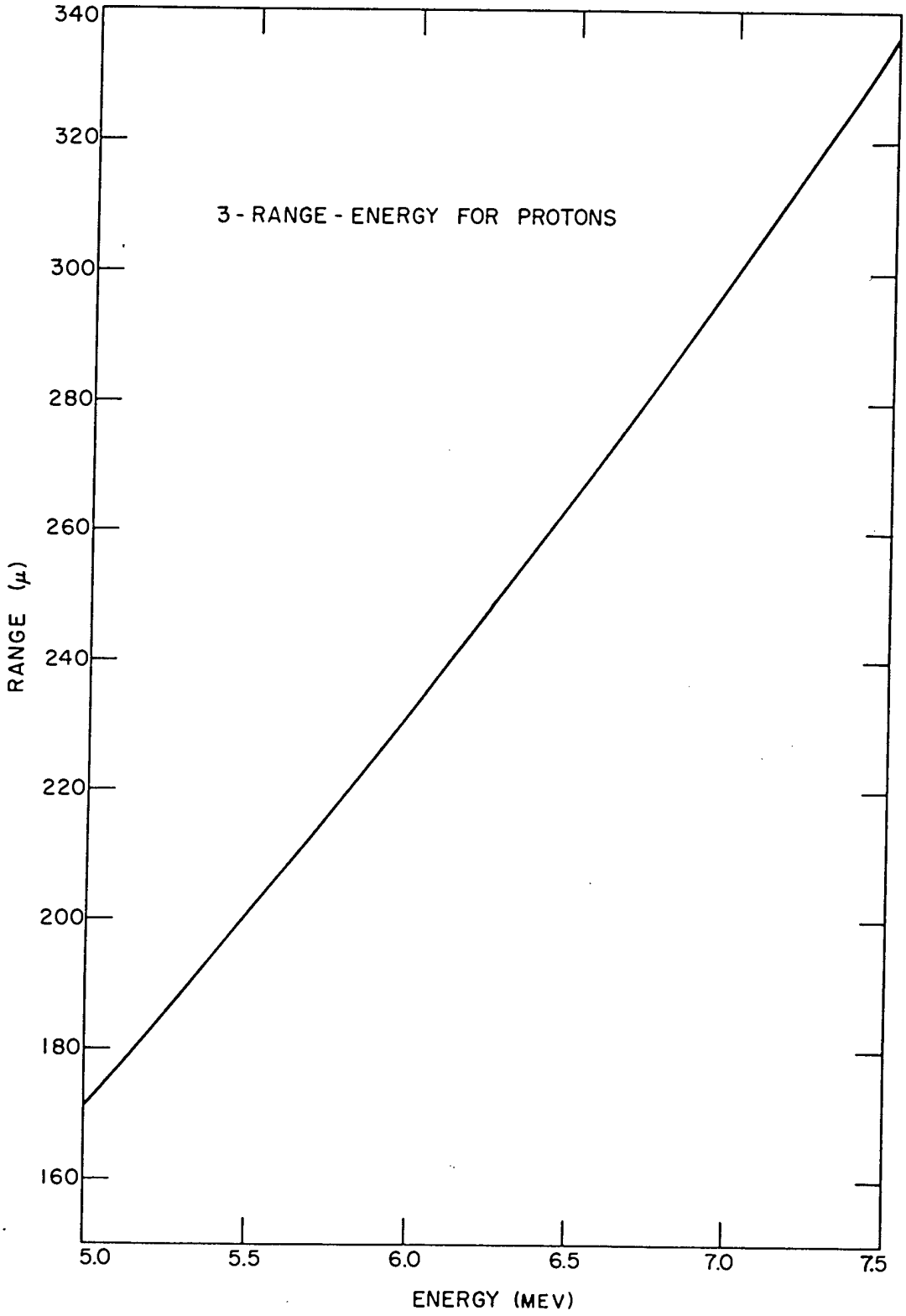

Fig. 1.3 Range-Energy Relations for Protons in Ilford C-2 Emulsion

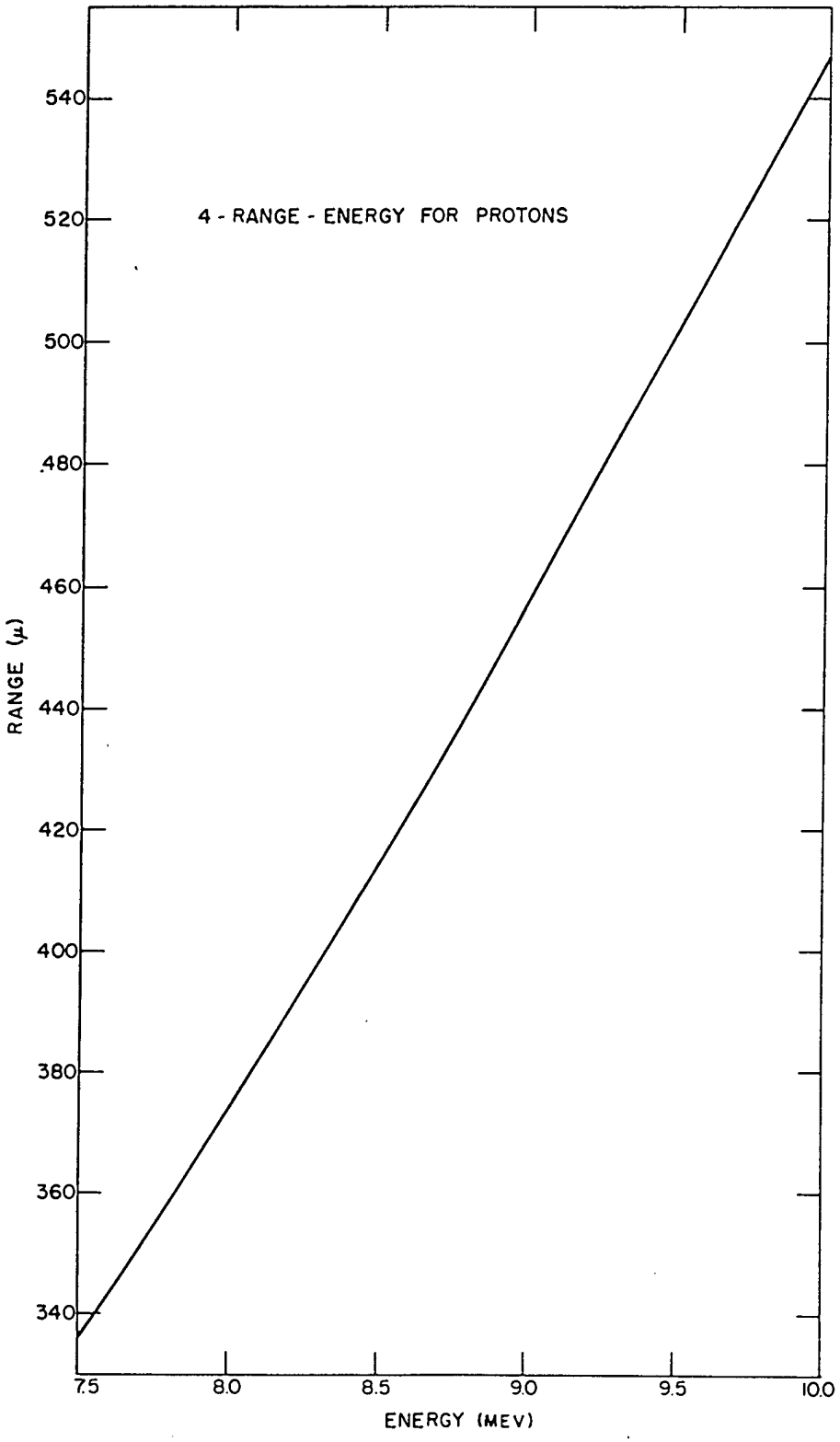

Fig. 1.3 Range-Energy Relations for Protons in Ilford C-2 Emulsion

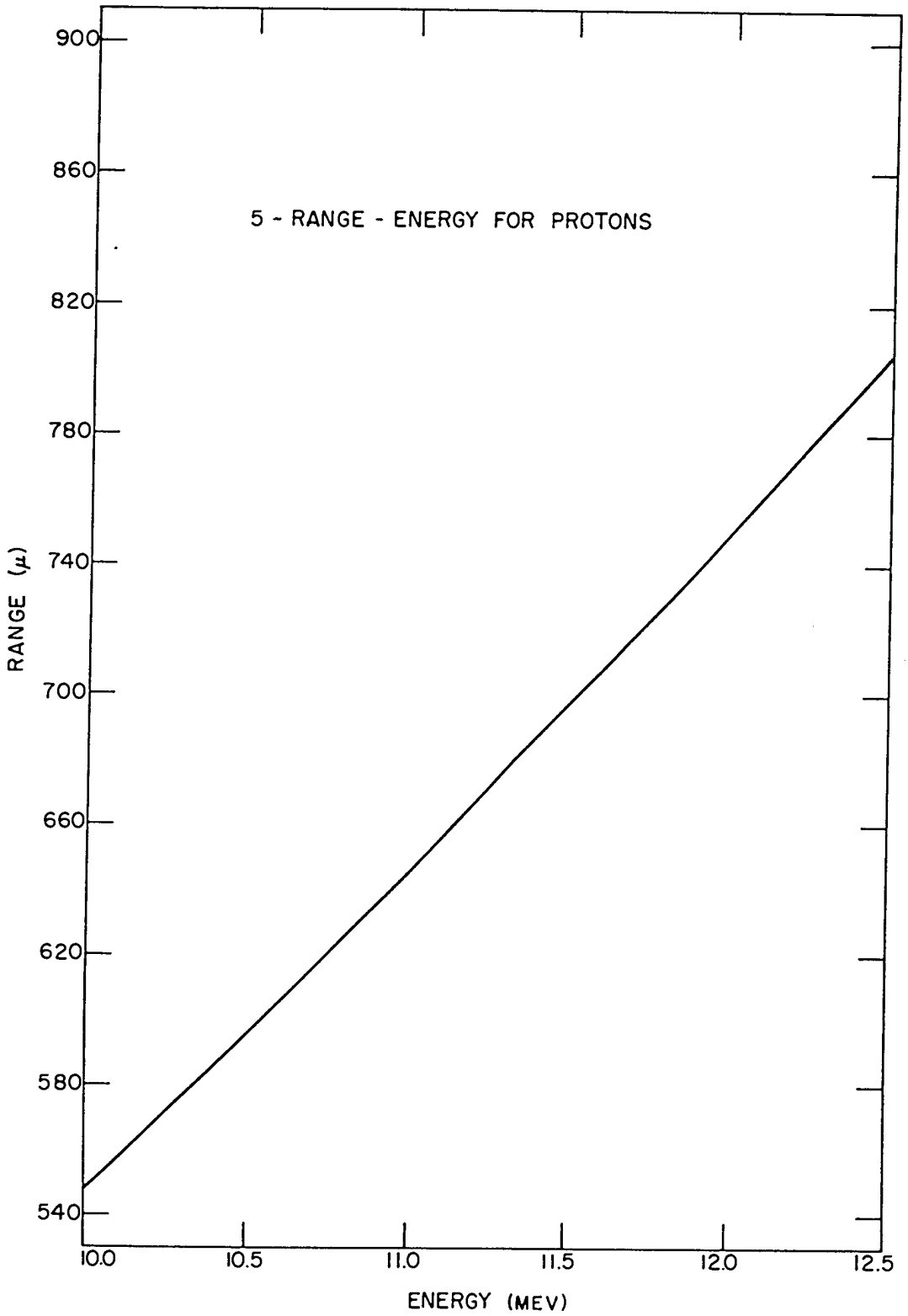

Fig. 1.3 Range-Energy Relations for Protons in Ilford C-2 Emulsion

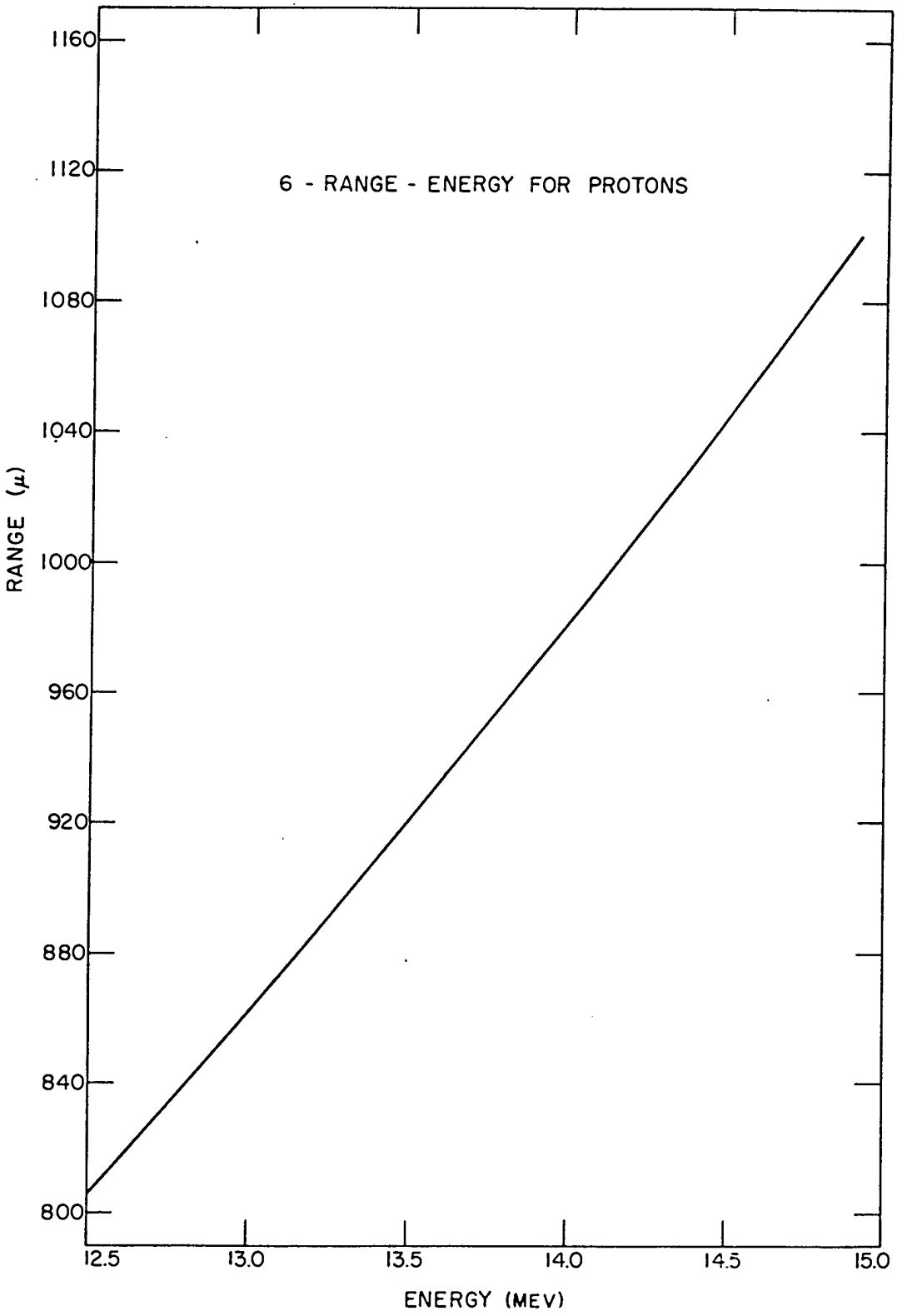

Fig. 1.3 Range-Energy Relations for Protons in Ilford C-2 Emulsion

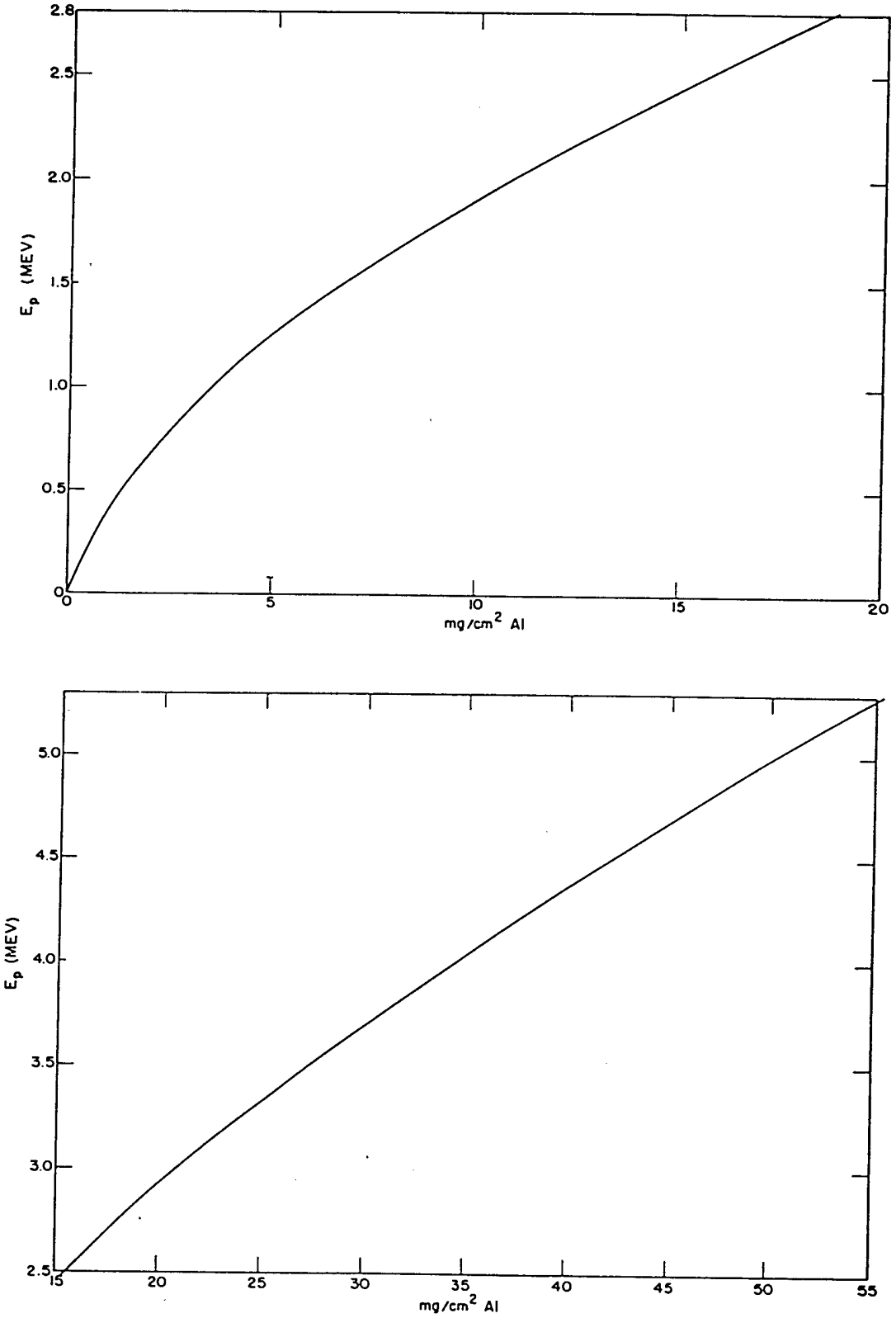

Fig. 1.4 Range-Energy Relations for Protons in Aluminum

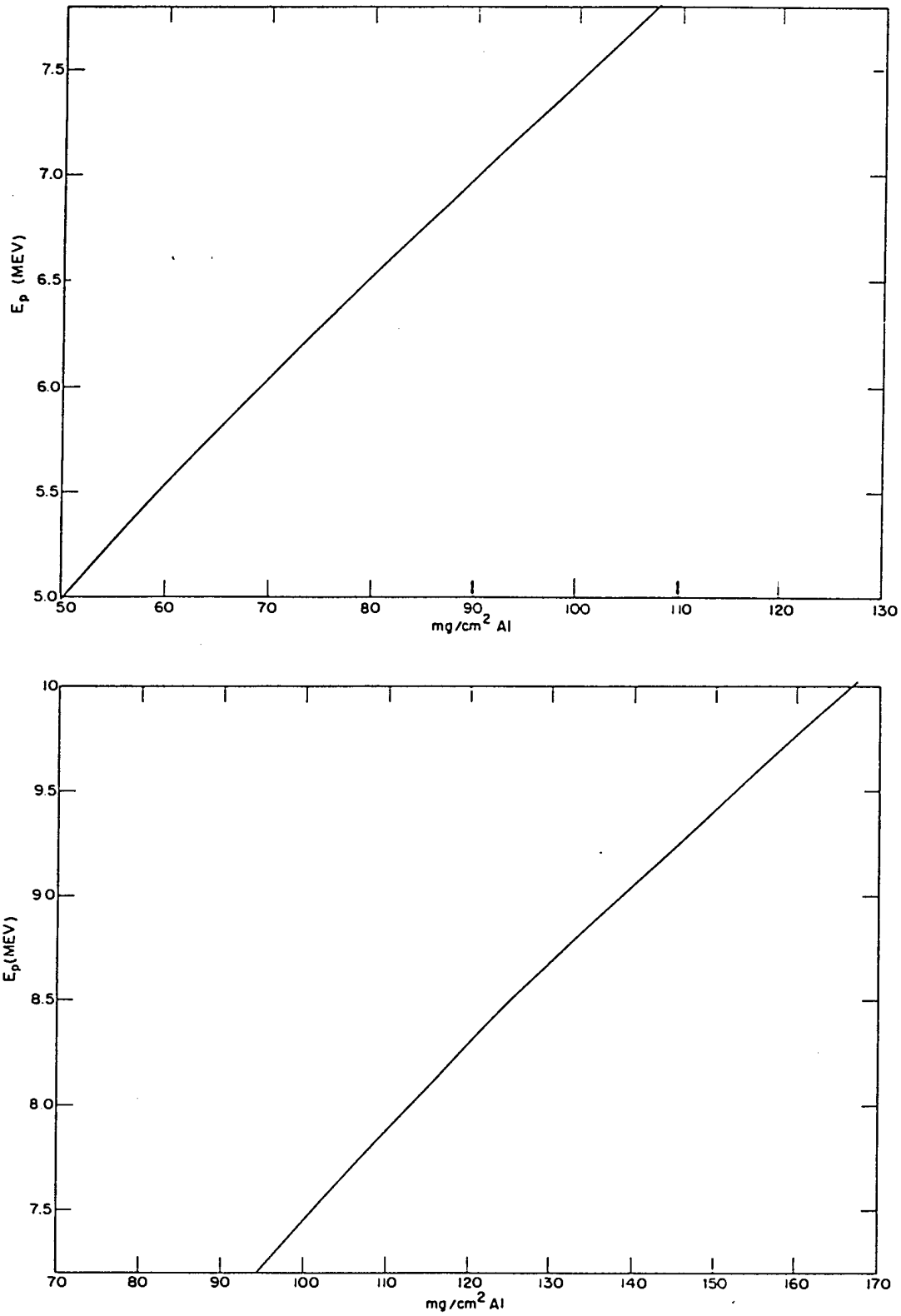

Fig. 1.4 Range-Energy Relations for Protons in Aluminum

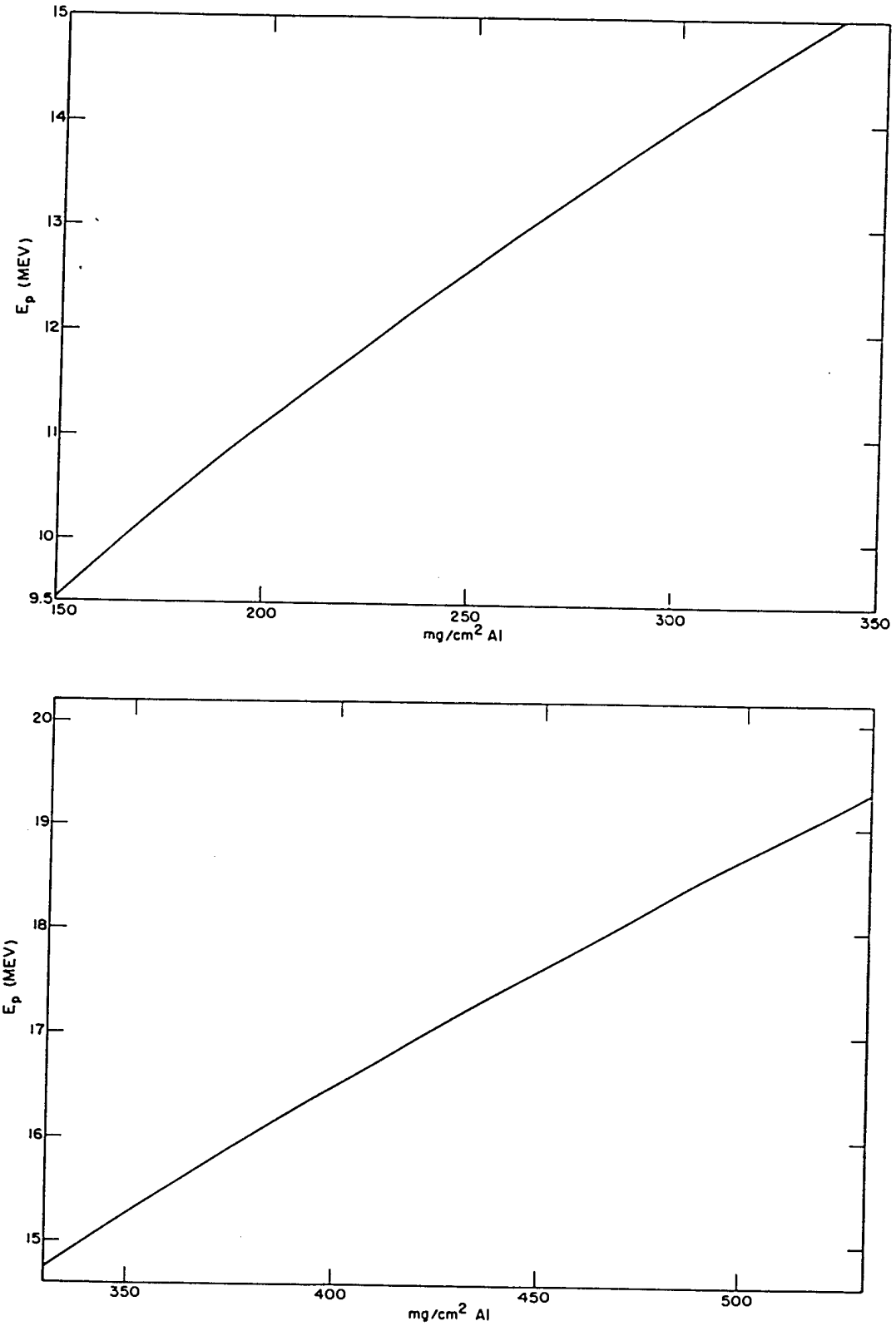

Fig. 1.4 Range-Energy Relations for Protons in Aluminum

neutron energies. Energy and momentum considerations show that

$$E_n = \frac{E_p}{\cos^2 \theta},$$

where E_n is the incident-neutron energy, E_p is the energy transmitted to the proton, and θ is the angle between the incident-neutron direction and the projected-proton direction. Since this operation has been performed, it is possible to plot the data as the number of protons recorded per unit solid angle subtended at the converter vs the incident-neutron energy. It now remains only to infer the neutron intensity at the converter from the observed proton intensity at the detector. For this purpose it is convenient to define the following notations:

F_n = number of neutrons per square centimeter per unit energy interval at energy E_n incident on the converter.

N_p = number of protons per unit energy interval at energy E_p projected per unit solid angle in the center-of-mass system from the converter by neutrons of energy E_n.

A = area of detector analyzed.

N = N_p times the solid angle in the center-of-mass system subtended by A at converter.

n_o = number of hydrogen nuclei per square centimeter of converter $(CH_2)_x = (8.58 \times 10^{19})t$.

t = converter thickness in milligrams per square centimeter.

A_c = area of collimation tube = area of converter exposed to collimated neutron beam = 1.27 cm^2.

$D = \sqrt{x^2 + y^2}$ = distance from center of converter to center of A.

θ = arctan (y/x) = angle which projected proton makes with incident neutron in the laboratory coordinate system.

Ω = solid angle subtended by A at the converter in the center-of-mass coordinate system.

Θ = solid angle subtended by A at the converter in the laboratory coordinate system.

$\sigma_{n\text{-}p}(E)$ = total neutron-proton scattering cross section for neutrons of energy E.

Figure 1.5 is a graph of the total n-p scattering cross section vs energy. The curve drawn is a weighted average of the following:

1. Experimental data of Bailey, Bennett, Bergstralh, and Richman, Phys. Rev., 70: 583 (1946).

2. Experimental data of Barschall, Coon, and Taschek [all of the Los Alamos Scientific Laboratory (LASL)] at 14 Mev.

3. Experimental data of R. Sherr, Phys. Rev., 68: 240 (1945).

4. Experimental data of W. Sleator, Jr., Phys. Rev., 72: 207 (1947).

5. Theoretical data of Louis Goldstein, Los Alamos Scientific Laboratory Report, LA-702.

6. Theoretical data of Bohm and Richman, Phys. Rev., 71: 570 (1947).

The least accurately known region appears to be in the neighborhood of 7 Mev, but even here it is felt that the accuracy is better than 10 per cent.

Essentially all the differential scattering cross-section measurements on n-p scattering indicate isotropic scattering in the center-of-mass system up to 14 Mev. Although the data at 14 Mev are not so conclusive in this respect as the lower-energy data, it is felt that, even at this energy, the error incurred owing to an assumption of isotropy is less than 5 per cent. In fact, 5 per cent is probably a good estimate for the maximum error to be assigned to any deduced differential cross section in the energy region of importance here (3 to 16 Mev).

In order now to determine the neutron spectrum incident on the converter, it should be noted that, corresponding to a given neutron energy interval dE_n, the total number of protons projected from the converter is given by the product of the number of neutrons in this energy interval which are incident upon the converter and the probability that a neutron of energy E_n will suffer a collision with a hydrogen nucleus in the converter. The number of neutrons in the energy interval dE_n which are incident upon the converter is simply $F_n\, dE\, A_c$. The probability that a neutron will project a proton from the radiator is given by the product of the n-p scattering cross section at the appropriate energy and

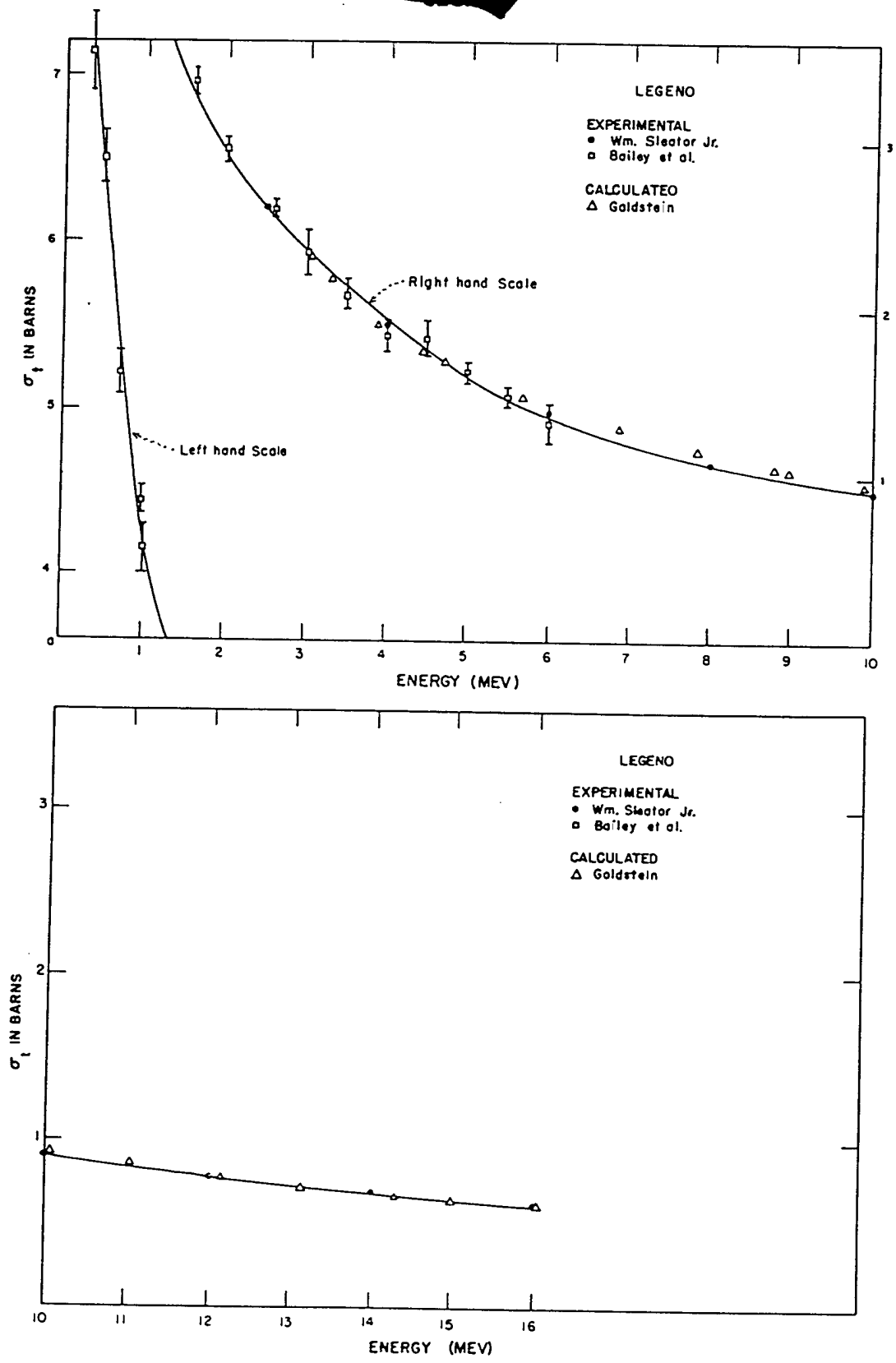

Fig. 1.5 Total n-p Scattering Cross Section vs Energy

the number of H^1 atoms per square centimeter of radiator.

Since the n-p scattering has been shown to be isotropic in the center-of-mass coordinate system over the energy region of interest here, it is now possible to write an expression for the number of protons projected at the angle θ per unit solid angle in the center-of-mass system by neutrons of energy E_n. This expression takes the form, using previously defined notation,

$$N_p\, dE_p = F_n A_c n_o \frac{\sigma_{n\text{-}p}(E)}{4\pi}\, dE_r;$$

since $E_p = E_n \cos^2\theta$,

$$dE_p = \cos^2\theta\, dE_n$$

and

$$N_p = \frac{F_n A_c n_o \sigma_{n\text{-}p}(E)}{4\pi \cos^2\theta}. \qquad (1.4)$$

The number of protons corresponding to neutrons in the energy interval dE_n at the energy E_n recorded by the detector will be the number of protons corresponding to this neutron energy interval projected from the converter per unit center-of-mass solid angle (Eq. 1.4) multiplied by the solid angle in the center-of-mass system projected at the converter by the plate area analyzed.

By the usual transformation from the laboratory system to the center-of-mass system, it is found that the solid angles are related by

$$\Omega_{CM} = (4\cos\theta)\Theta_{lab}. \qquad (1.5)$$

Therefore the center-of-mass angle is subtended by A_p at the converter,

$$\Omega_{CM} = \frac{4A_p \sin\theta\cos\theta}{D^2}. \qquad (1.6)$$

Finally, the number of protons projected by neutrons of energy $E \pm \Delta E/2$ and recorded on the detector area A is given by

$$N = N_p\Omega. \qquad (1.7)$$

[redacted] DELETED

[redacted] DELETED It is now apparent that

$$F_n = \frac{\pi D^2 N}{\sigma_{n\text{-}p}\, n_o\, A_c A_p \sin\theta\cos\theta} = \frac{\pi(x^2+y^2)^2}{n_o\sigma_{n\text{-}p}A_c A_p xy}. \qquad (1.8)$$

Figure 1.6 and Table 1.9 give values of $(x^2+y^2)^2/xy$ vs x for various y values. A curve of number of neutrons per square centimeter incident on the converter as a function of energy can now be plotted. To convert this neutron flux as a function of energy to an absolute number of neutrons emanating from the bomb as a function of energy, the following relation is used:

$$F_n = \frac{Q(E)}{4\pi R^2}\, e^{-R/\lambda}, \qquad (1.9)$$

where F_n = neutron flux in the energy interval E as determined at the converter.
$Q(E)$ = number of neutrons emanating from bomb in the same energy interval.
R = distance from bomb to converter.
λ = mean free path in air for neutrons of energy E.

To convert the Q(E) outside the bomb to a $Q_o(E)$ inside the bomb, the calculated attenuation of the bomb material for neutrons of various energies must be utilized. An accurate calculation of this factor is now being made by T Division of the Los Alamos Scientific Laboratory.

[redacted] Deleted

Since the number of fission neutrons produced in any given energy interval will be directly calculable from the measured efficiency of the bomb and the known fission neutron spectrum, it should be possible to determine the absolute number of 14-Mev neutrons generated by the D-T reaction rather accurately and without recourse to attenuation factors either in the bomb material or in air, with the possible exception of a slight correction for the difference in attenuation of neutrons in the

[redacted]

Pages 25 and 26 are DELETED.

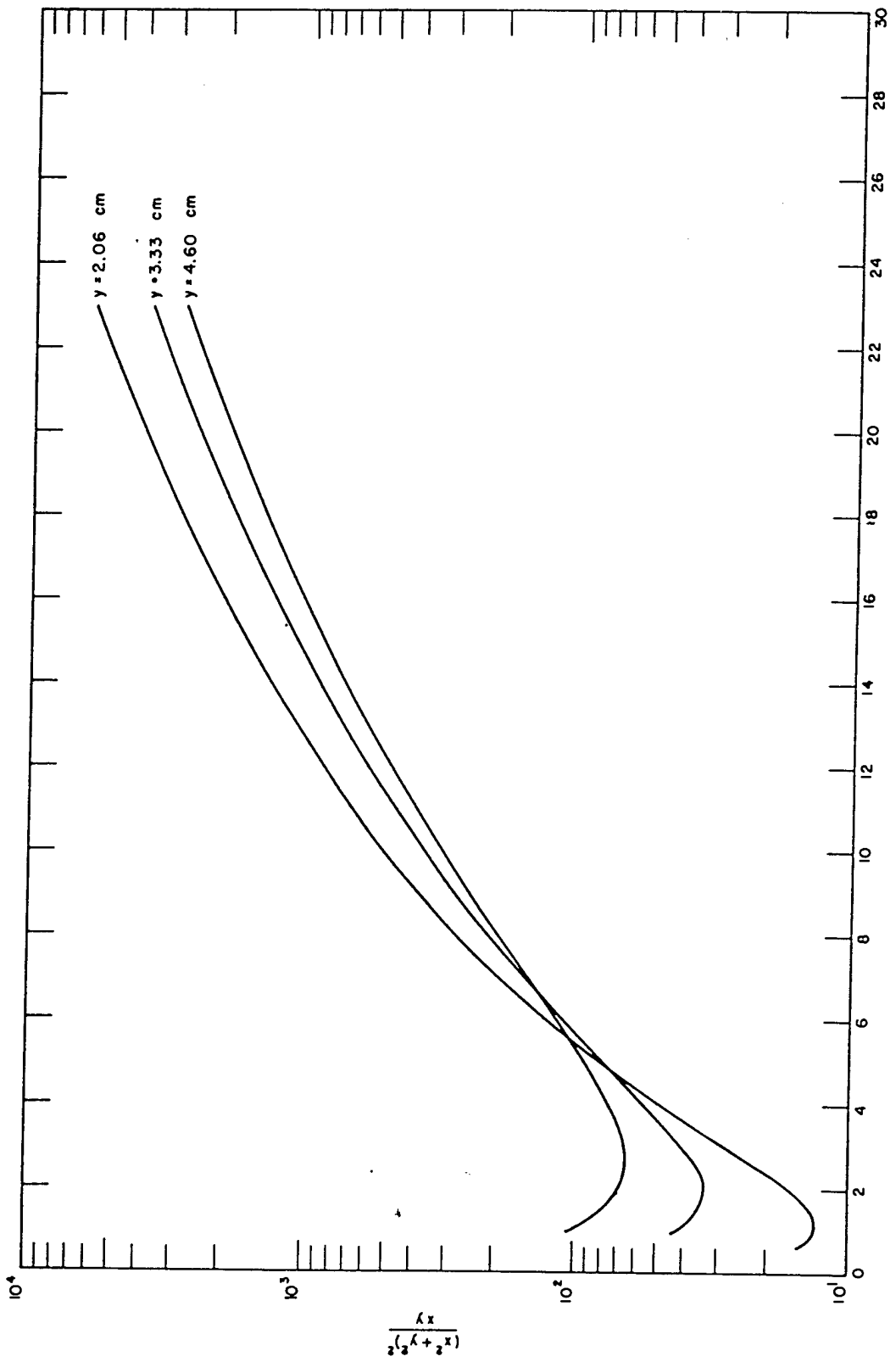

Fig. 1.8 Values of the Function $(x^2 + y^2)^2/xy$ vs x for Various Values of y, Where x and y Are the Longitudinal and Radial Coordinates of the Track Position with Respect to the Converter

comparison region, since these will have an energy of less than 14 Mev.

It should be pointed out that existing experimental evidence strongly indicates that inelastically scattered neutrons in the bomb material or in the air will in general be reduced in energy to below the region of interest in these experiments. This should therefore cause no confusion in the evaluation of the data.

TABLE 1.9 CALCULATED VALUES OF $(x^2 + y^2)^2/xy$ VS x FOR VARIOUS VALUES OF y

x (cm)	$(x^2 + y^2)^2/xy$ y = 2.06 cm	y = 3.33 cm	y = 4.60 cm
0.5	19.57	---	---
1.0	13.32	43.90	106.7
2.0	16.47	34.19	68.77
3.0	28.45	40.44	65.92
4.0	49.73	55.10	75.08
5.0	82.99	78.25	92.68
6.0	130.0	110.9	118.4
7.0	196.5	154.8	152.9
8.0	282.6	211.4	197.1
9.0	391.8	283.3	252.1
10.0	527.4	370.4	319.1
11.0	692.0	477.1	399.4
12.0	888.9	602.4	494.1
13.0	1121	749.6	604.6
14.0	1391	920.0	732.1
15.0	1698	1114	878.0
16.0	2055	1339	1044
17.0	2455	1591	1230
18.0	2905	1873	1439
19.0	3408	2188	1671
20.0	3967	2538	1928
21.0	4583	2923	2211
22.0	5260	3347	2521
23.0	6006	3807	2861

In cases where lead absorbers are used in front of the collimation channels, appropriate corrections will have to be applied to the neutron spectra according to the attenuation thus produced. The foregoing comments on inelastically scattered neutrons also apply here.

The above evaluations will permit us to arrive at a value for the amount of tritium burned in the D-T reaction. It should be remembered that an additional tiny amount (approximately 1 per cent of that burned by D-T) will have been burned by means of the T-T reaction.

Evaluation of Errors. The various factors which produce errors in the final evaluation of the neutron spectrum inside a bomb as well as the estimated errors relevant to these factors are as follows:

Factor	Error (%)
Attenuation of bomb materials	15
Attenuation of air	10
Small-angle scattering in air and in collimation tube	4
Number of H atoms in converter exposed to direct neutron beam	6
n-p scattering cross section (this includes error in assumption of spherical symmetry in C.M.)	5
Solid-angle calculations (mainly due to uncertainty of angle which surface of emulsion makes with line of center of converter to center of area of plate analyzed)	6
End effects in collimator	10
Statistical errors	5
Background errors	2

It is estimated that the total probable error should be less than 30 per cent.

REFERENCES

1. Los Alamos Scientific Laboratory Report, LAB-J-1001.
2. J. Rotblat, private communication.
3. J. H. Smith, Phys. Rev., 71: 32 (1947).

Chapter 2

Design of Collimators and Cameras

2.1 GENERAL DESIGN FEATURES OF COLLIMATORS

The general features of the collimators are shown in Figs. 2.1 to 2.4. Each collimator was constructed of six sections since it was not certain that loads greater than 5 or 6 tons could be handled in the field. There are front and rear top sections, front and rear middle sections, and front and rear bottom sections. The front middle section contains three collimator tubes, each $\frac{1}{2}$ in. in internal diameter and 3 ft in length. The rear middle section contains three tubes of 6 in. in internal diameter and 45 in. in length. Each of the 6-in. tubes is coaxial with one of the small collimator tubes. A camera (Fig. 2.5) is placed inside each of the 6-in. tubes immediately behind the small collimator tube. A heavy plug 2 ft long fits into each large tube behind each camera. Each plug contains an axial hole which serves as an exit port for the neutrons and gammas which have come down the collimator tube and passed through the camera.

Each of the six sections of the collimator block is constructed of 1-in. boiler plate and is filled with a heavy limonite and scrap-iron concrete mix; this mix was designated as M-1 in Sec. 1.2. The six sections are bolted together vertically and longitudinally with a total of 30 bolts, each 2 in. in diameter, as shown in Fig. 2.1.

The prototype collimator was built in C Shop at LASL and was tested as described in Chap. 3. After the tests, certain changes in design were made, and an order for 12 collimators was placed with Consolidated Western Steel Corporation of Los Angeles. One change was the lengthening of the collimator block from 72 to 82 in. in order to make room for the front and rear extensions on the camera (see Sec. 2.2). The external dimensions of the collimator block exclusive of bolts are 82 in. long by 60 in. wide by 55 in. high. The tube openings at both front and back of the collimator are covered by removable steel blast plates $\frac{3}{4}$ in. thick. The front plate has three holes, 1 in. in diameter, extending halfway through it and immediately in front of the three collimator tubes. The front of each collimator tube, for a depth of $\frac{3}{4}$ in., was enlarged from an internal diameter of $\frac{1}{2}$ to $\frac{17}{32}$ in. This was done to allow the insertion of a cylindrical steel cup having a $\frac{1}{64}$-in. wall and containing about 2.7 g of powdered boron metal which was 98 per cent B^{10}. A similar but larger cup containing normal boron carbide was placed in the exit port of each of the rear plugs.

The empty collimators were shipped to Eniwetok and filled with type A limonite concrete mix, having an average measured unit weight of 265 lb per cubic foot, the formula for which follows:

Ingredient	Pounds per Cubic Yard of Concrete
Cement	940
Limonite	1880
Steel scrap	4100
Water*	337

*The water content of this mix was to be adjusted to provide the proper slump.

It was found that plenty of heavy equipment was available so that the filled collimators could be handled in thirds rather than sixths.

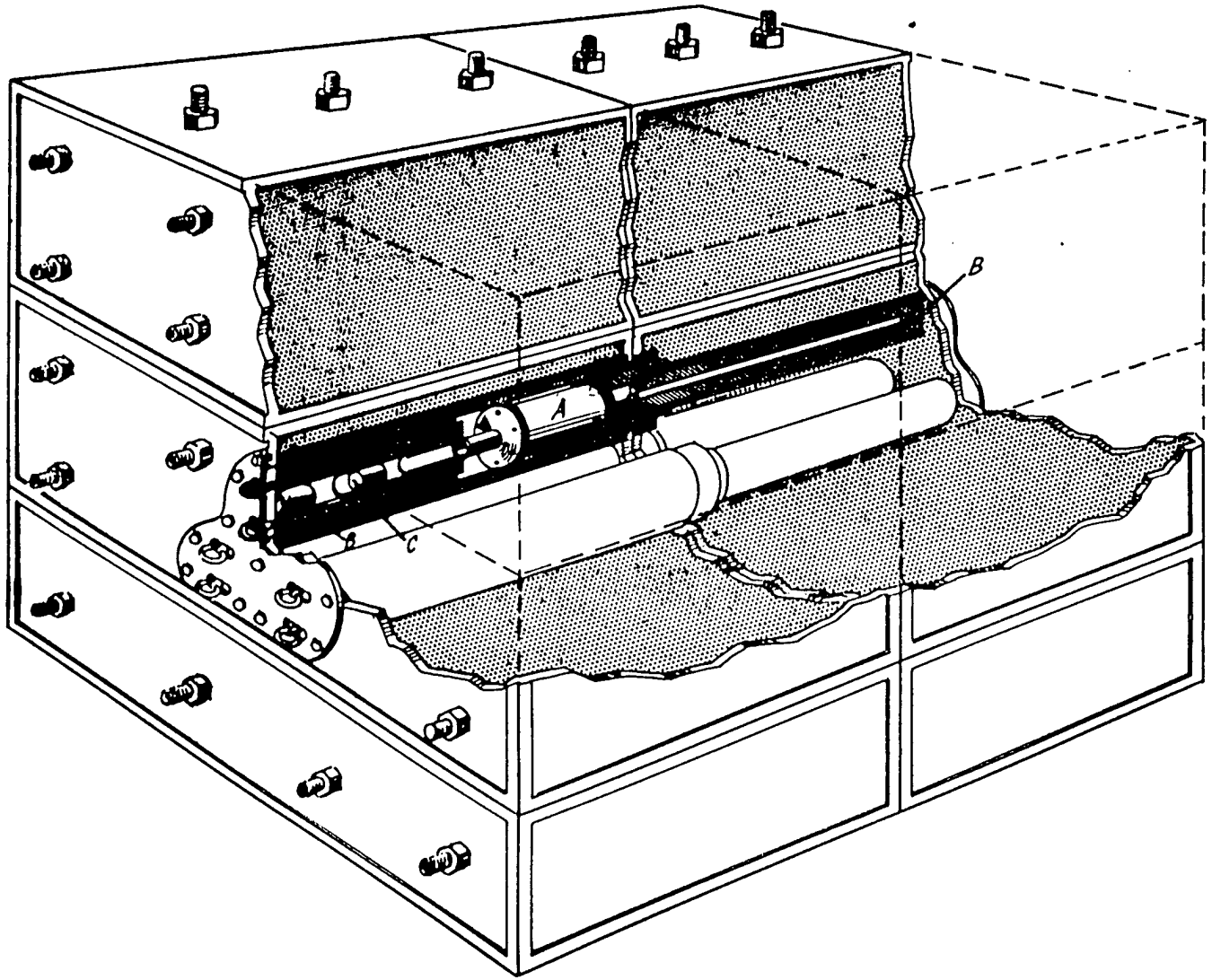

Fig. 2.1 Collimator Block. (A) Camera in place behind collimator tube; (B) small boron absorber at front of collimator tube and larger boron absorber in exit part; (C) cylinder containing threshold detectors used in Annex 1.5 experiment.

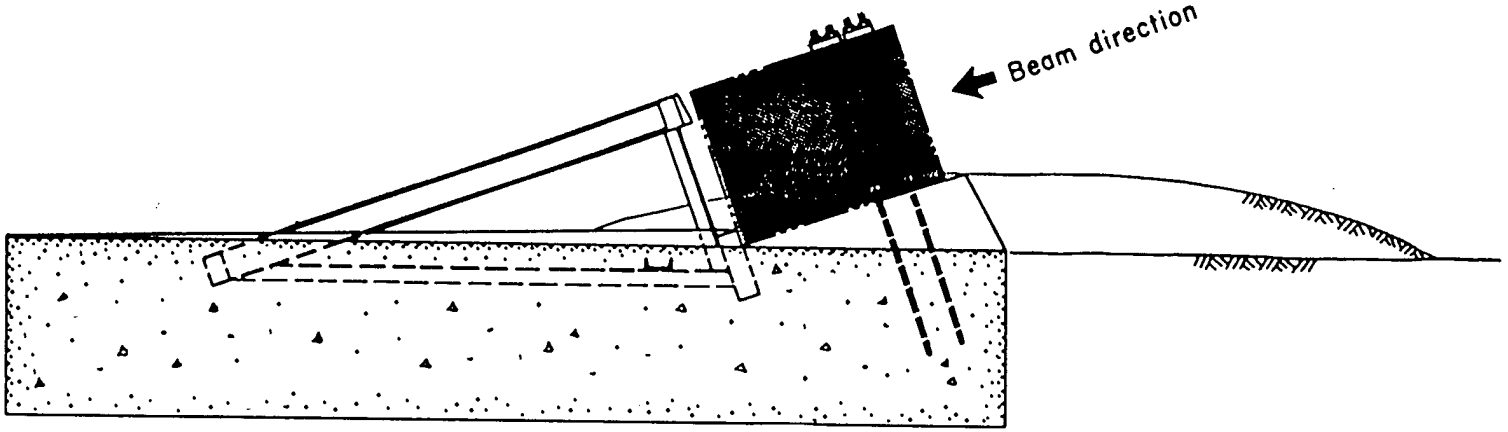

Fig. 2.2 Type of Mounting Used for Collimator Blocks (Shown Shaded) at Near Stations

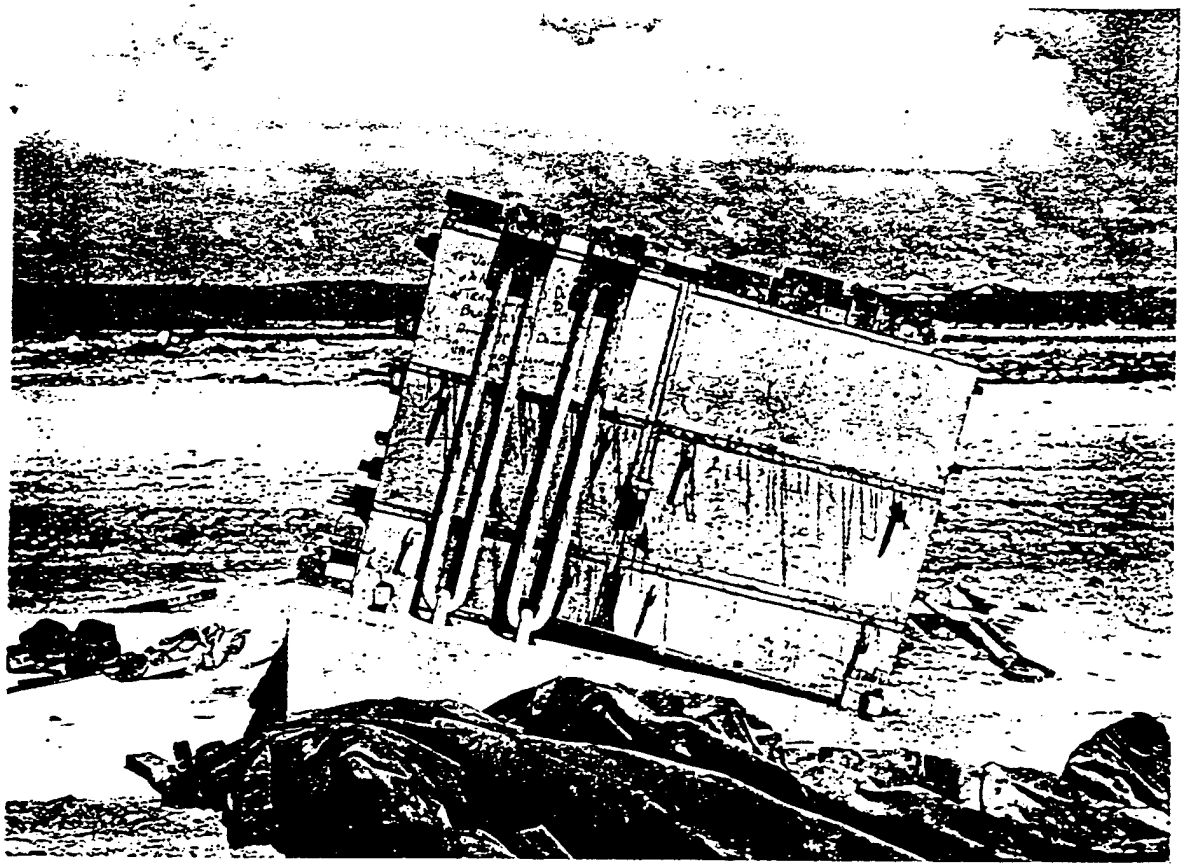

Fig. 2.3 Side View of Collimator Block Mounted at Station E-10

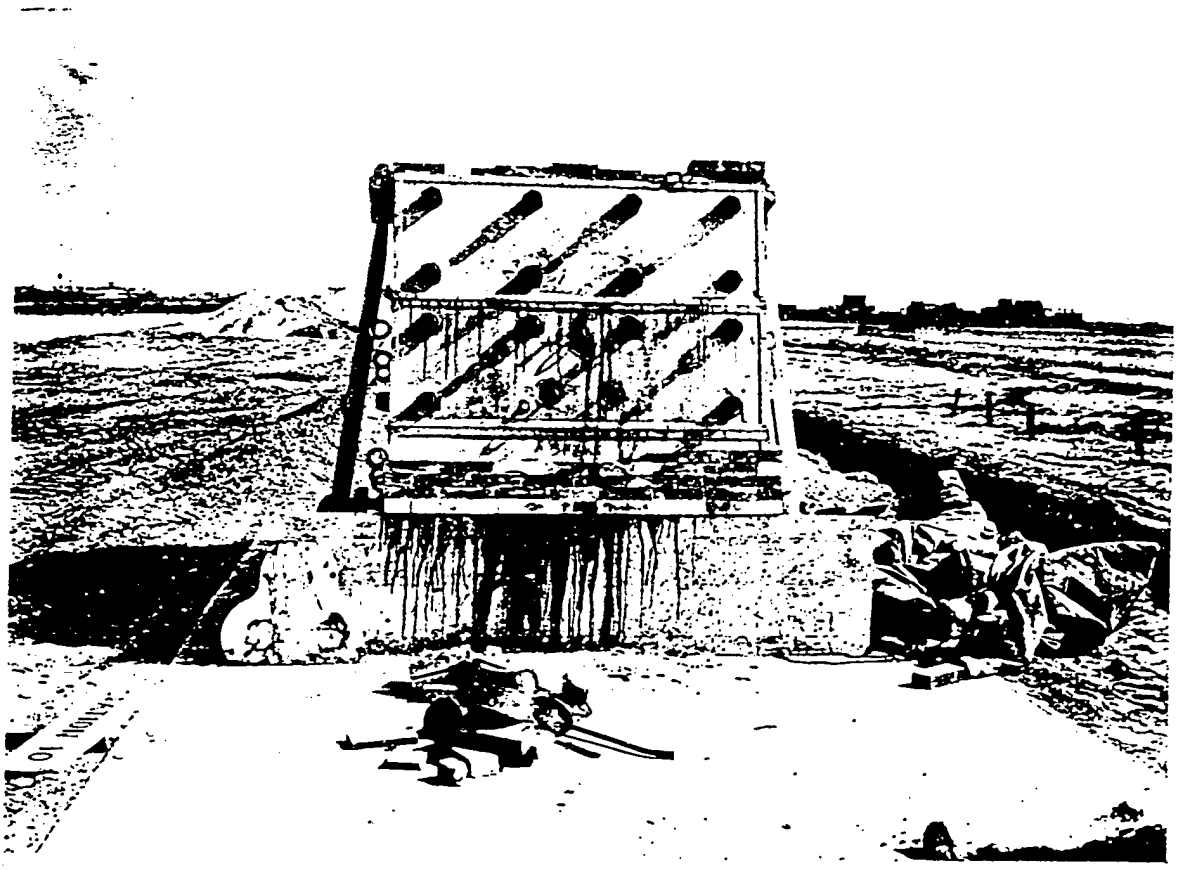

Fig. 2.4 Front View of Collimator Block Mounted at E-10. Front blast plate has been removed to show three collimator tubes.

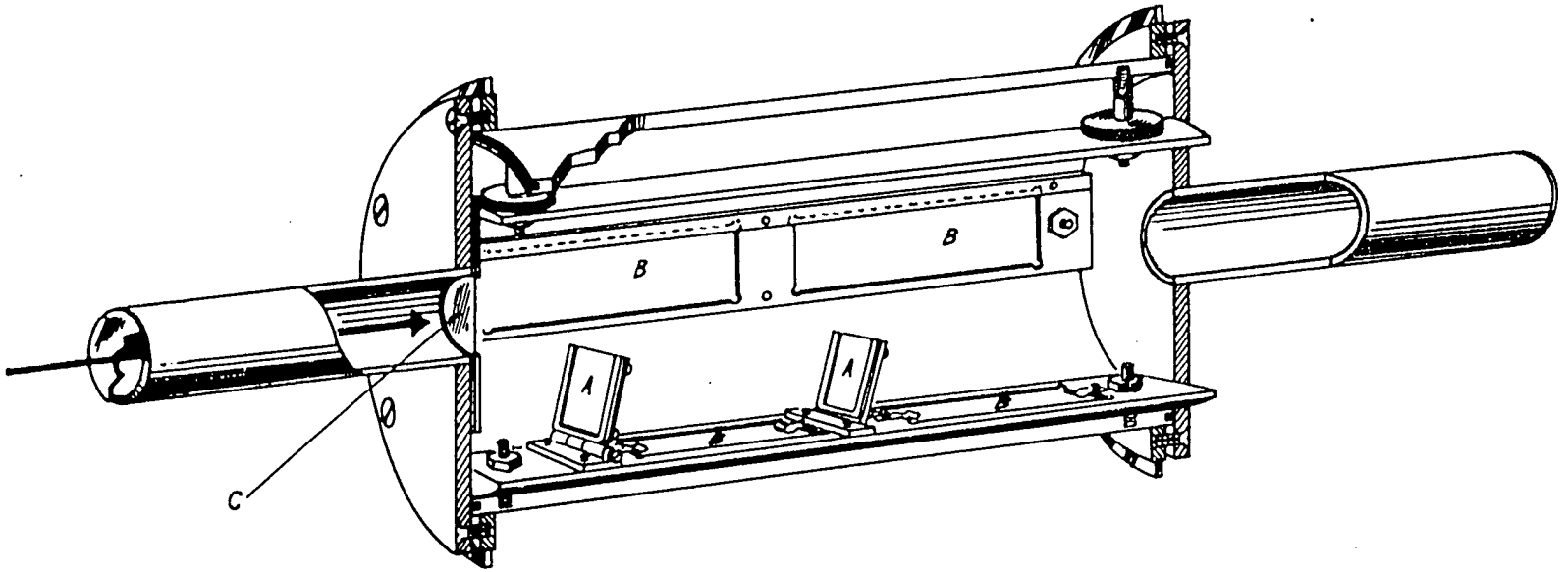

Fig. 2.5 Cutaway View of Camera. (A) Aluminum absorbers; (B) positions for nuclear plates; (C) polyethylene converter. The plate holders may be placed nearer the axis of the camera by means of the knurled spacers as shown at the top of the drawing; at the rear of the camera (not shown) are pumping lead, valve, and vacuum gauge.

This makes it unnecessary to remove the longitudinal bolts. The bolts are 2 in. in diameter, and the sleeves through which they pass are $2\frac{1}{4}$ in. in inside diameter. This space between bolt and sleeve is undesirable from the standpoint of shielding. The two sleeves in the top sections and the two sleeves in the middle sections nearest to the collimator tubes were removed before the heavy concrete was poured into the collimators. The collimator blocks were all made alike for reasons of interchangeability as well as economy.

The bases upon which the collimators rest vary in size depending upon their distances from zero point. A drawing for one of the bases is shown in Fig. 2.2, and pictures of one of the collimators in place on its base are shown in Figs. 2.3 and 2.4. The bases at some of the nearer stations have steel beams backing up the collimators. All bases point directly at zero point in the cab at the top of the tower. A piece of $\frac{1}{2}$-in. boiler plate 6 in. wide and 60 in. long is placed under the front end of each collimator. A fine adjustment on elevation can then be obtained by raising the rear end by means of the two rear vertical bolts which are threaded all the way through the bottom plate of the collimator. A lateral fine adjustment can be made by means of large setscrews at the four corners of the base. It is proposed to make the final alignment by taking pictures of the tower through the collimator tubes.

2.2 DESIGN OF CAMERAS

The general features of the cameras are shown in Fig. 2.5. The main portion of the camera consists of a cylindrical cavity 4 in. in diameter and 10 in. long. The 1- by 3-in. nuclear plates are generally placed as shown about the circumference of this cavity. In some cases the plates can be placed closer to the axis of the camera. At each end of the camera is a cylindrical extension 6 in. long and 1 in. in diameter. The ends of these extensions are closed by 0.015-in. platinum disks. By this arrangement it is possible to keep the photographic plates from seeing any metal which is in the direct beam of neutrons and gammas. The polyethylene radiator or converter is held in place between two washers at the front end of the main cavity. Provision is made for placing aluminum absorbers between the plates and the converter.

Each end of the camera is removable as are also the four plate holders which hold two plates each. The camera is vacuumtight, the end plates being sealed by means of O rings. The rear end plate has two eyebolts to facilitate removal of the camera from the collimator block. This end plate also has a pumping lead and valve as well as a vacuum gauge.

Ten of these cameras were constructed of mild steel, and thirty were made of aluminum with stainless-steel ends.

[redacted]

Chapter 3

Testing Program

3.1 GENERAL

The feasibility of measurement of fission neutron spectra from atomic weapons by means of the Phonex technique was established in 1949 by a series of neutron-spectra measurements using the Los Alamos fast reactor.[1] In these experiments a boron-steel collimator was substituted for the tamper and shielding at one of the top ports of the fast reactor. An evacuated chamber containing photographic plates was mounted above the collimator, and recoil protons produced in thin polyethylene radiators were recorded and observed as tracks in the photographic emulsions. A measurement of integrated gamma dosage during the run indicated that the plates received 1 r. The spectrum measured at that time is in essential agreement with other measurements of the fission spectrum from the fast reactor.[2] With these measurements as groundwork, the Phonex problem became essentially a technological one in design and testing of suitable techniques for bomb measurements. In general, the testing program has proved the original designs adequate, although in some instances minor modifications of the first concepts have been required.

The testing program which was considered necessary to ensure, in so far as possible, the success of the Phonex measurements included the following: (1) gamma-ray shielding and collimation; (2) fission spectrum collimation and spectrum alteration, if any; (3) 14-Mev neutron collimation; (4) mechanical tests, including shock and drop tests; (5) on-site tests. These will be considered in order.

3.2 GAMMA-RAY SHIELDING AND COLLIMATION

The completed and concrete-filled midsection of the prototype collimator was mounted so that its front was approximately 4 m from the target of the 20-Mev betatron (see Fig. 3.1). One of the three collimating tubes was aligned radiographically with the target. A prototype cylindrical neutron camera was inserted in the collimator and exposed to a measured r dosage, as determined by Victoreen r thimble measurements. In this geometry the size of the gamma-ray beam was essentially limited by the size of the firing snout through which the beam emerged. The face of the collimator was thus exposed to a circular spot of gamma radiation 14 in. in diameter, the beam being essentially unidirectional. Since the camera diameter is only 6 in., the interior of the camera was presumably subjected to a fairly uniform attenuated gamma flux, as well as to whatever ionizing radiation was produced in the end of the camera and the polyethylene radiator (i.e., scattered gammas, Compton recoils, and pairs).

Initially rather severe blackening of the photographic plates was produced. It appeared that this blackening was probably due to scattered radiation and particles. Accordingly the neutron camera was redesigned with snouts on each end (see Fig. 2.5), the gamma beam entering and leaving the camera through 15-mil platinum windows on the ends of the snouts. This geometry is such that the plates cannot see directly any heavy material struck by the gamma beam. With this modification the ex-

[redacted]

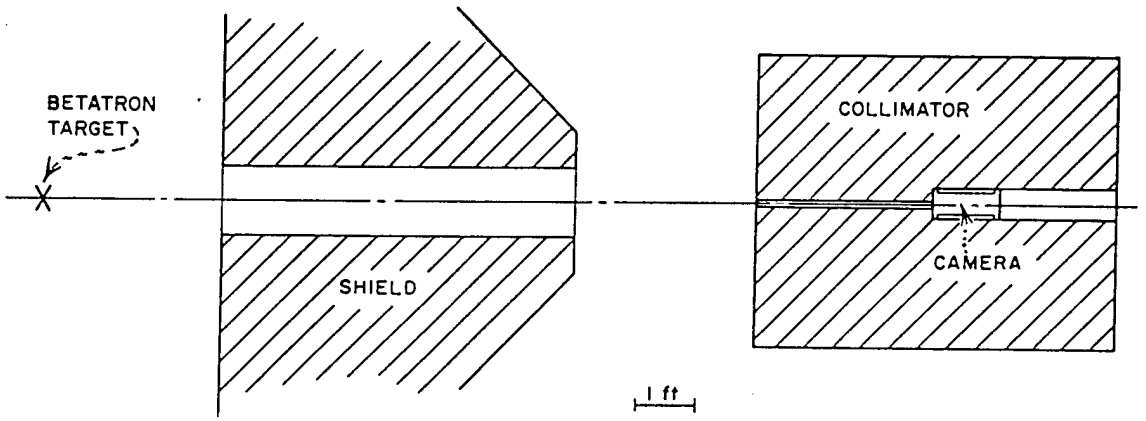

Fig. 3.1 Geometry for Gamma Shielding Test

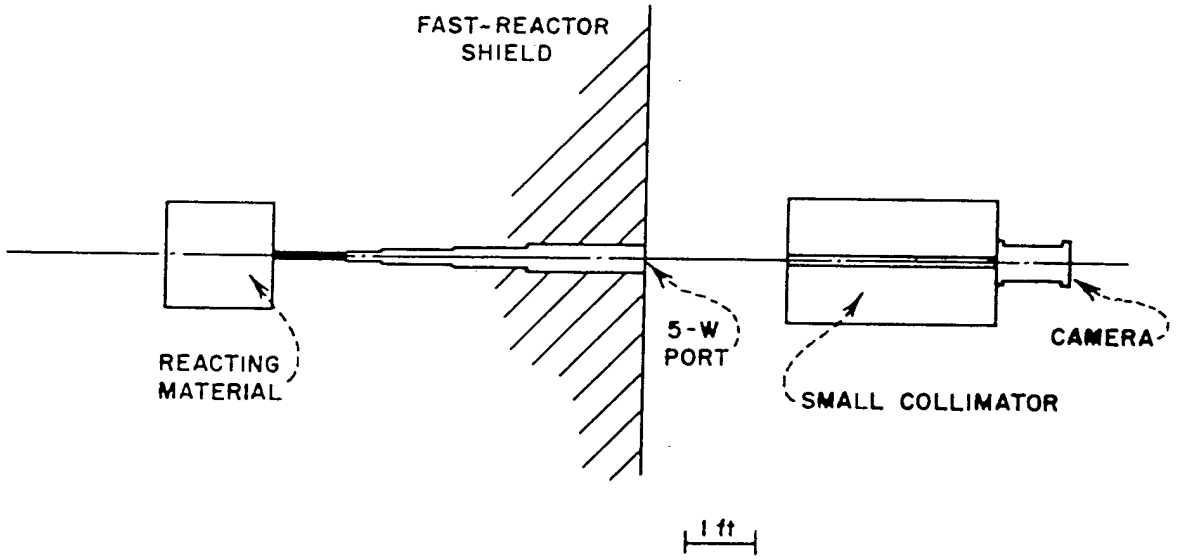

Fig. 3.2 Geometry for Fission Spectrum Measurement at Fast Reactor

periment was repeated, and it was found that a dosage of 1200 r at the radiator produced only very moderate blackening of the plates. Furthermore, the plates would have been readable even if the dosage had been increased by a factor of 10.

3.3 FISSION SPECTRUM COLLIMATION

For these tests a small collimator was constructed, which consisted of a $\frac{1}{2}$-in.-ID $\frac{5}{8}$-in.-OD steel pipe 36 in. long, embedded centrally in a limonite concrete block 36 in. long and 20 by 20 in. square, weighing approximately 2,100 lb. This unit corresponds essentially to the front center section of the large collimator. In this case, shielding of the direct beam may not be so good as for the actual collimator, whose steel collimating tube is 3 in. in outside diameter.

The initial tests were made at the Los Alamos fast reactor. Runs were made with the collimator previously described in alignment with a fast port (5-W) such that the collimator looked directly at the active material of the reactor (see Fig. 3.2). No collimating tube was used in the wall of the reactor. Thus the emergent neutron beam was conical and intersected the face of the collimator in a circle approximately 6 in. in diameter. A neutron camera was mounted behind the collimator coaxial with the collimating tube.

An exposure was made in which an integrated flux of approximately 10^{13} fission neutrons/cm^2 (based on power level, time, and conversion factor) was allowed to impinge on the front face of the collimator. A spectrum obtained from the reading of these plates was compared to a spectrum measured to much greater accuracy by Nereson.[2] The two were found to be in statistical agreement when normalized to each other. The slopes in various energy intervals likewise were found to be in good agreement. These results are shown in Fig. 3.3.

The plates used in making this measurement were themselves shielded by the collimator block. It is therefore possible to make a rough estimate of the attenuation of the shield by comparing the number of recoil-proton tracks produced in the emulsion to those tracks originating on the surface. In the 200-μ emulsion used, there were 1.4 times as many tracks originating in the emulsion as on the surface. Combining this figure with the ratio of the detection efficiencies of the emulsion and the radiator geometry, an attenuation factor for the limonite collimator of approximately 10^{-5} is obtained.

Subsequently a second measurement was undertaken at the fast reactor. This experiment was done to determine what the effect might be on the fission spectrum due to scattering, both elastic and inelastic, by the atmosphere between the bomb and a Phonex station.

DELETED

The expected attenuation of the neutron beam was observed. No change in the spectrum was apparent. The results are shown in Fig. 3.4. The attenuation is not obvious since approximately the same number of tracks were read for both spectra. Since there were no radical differences in the two spectra, it was decided to add the curves to improve the statistics. The resulting curve was compared with Nereson's data. The reciprocal slope, 3.5 Mev per decade, agrees with Nereson's result to 3 per cent, a result which is doubtless somewhat fortuitous. From this experiment it is concluded that in a good geometry spectrum measurement, such as is being undertaken in Phonex, the only important effect of air-scattering will be attenuation, at least in the low-energy region. Scaling is probably not too great a worry here since the geometry will be better for the actual test than for this experiment.

In order to investigate further the collimation of the fission spectrum and the shielding for thermal neutrons, the prototype collimator was placed, intact, into the Los Alamos Water Boiler at the position which the south thermal column normally occupies, as shown in Fig. 3.5. The collimator was surrounded by paraffin and lead shielding and became in effect a part of the reactor shield.

A 1-in. hole in the bismuth wall (8 in. thick) was drilled directly in line with one of the $\frac{1}{2}$-in. collimator holes. Thus the collimator tube could look directly at the reacting sphere

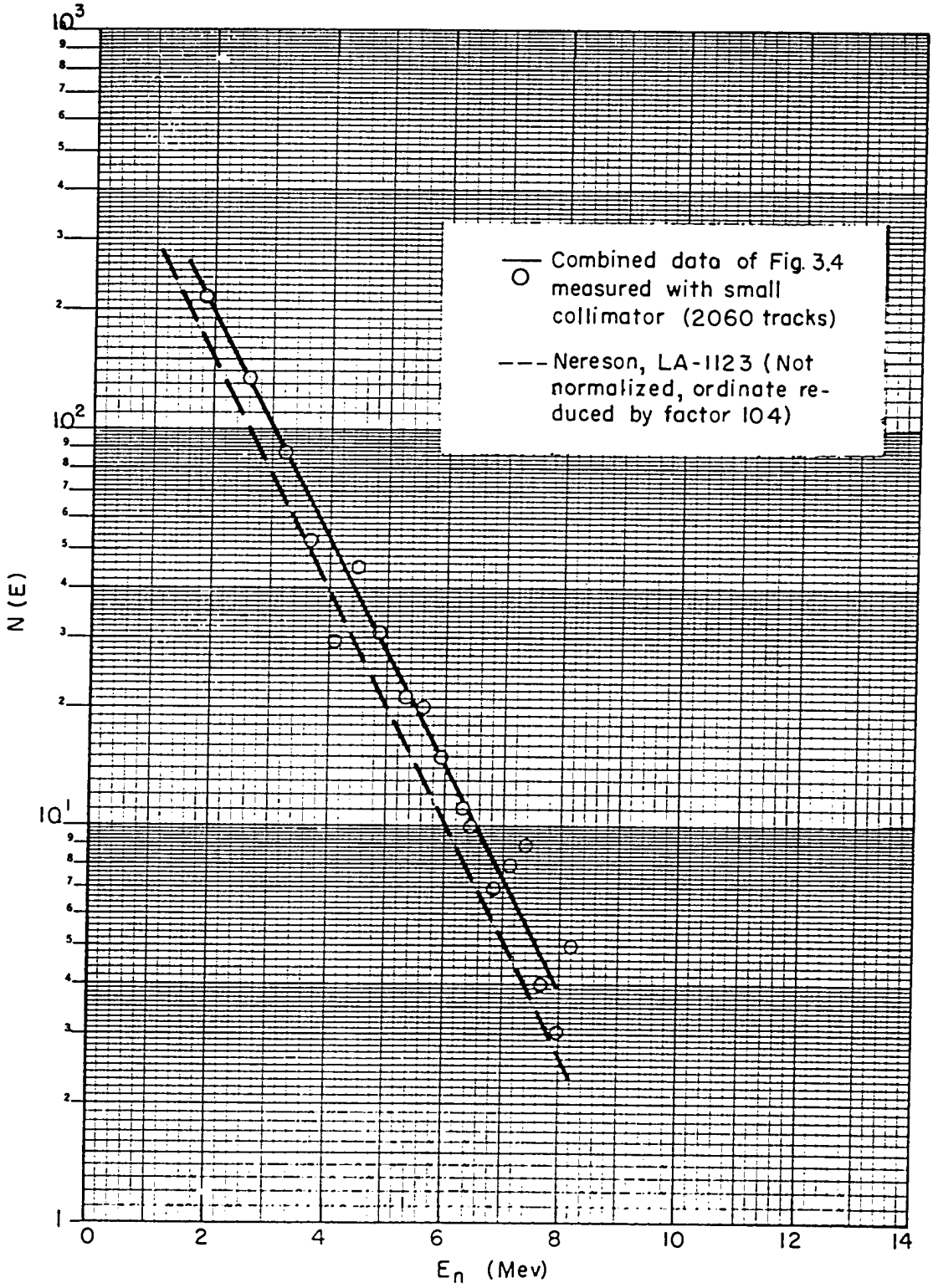

Fig. 3.3 Number vs Energy for 5-W Fission Spectrum of Los Alamos Fast Reactor

Page 40 is DELETED

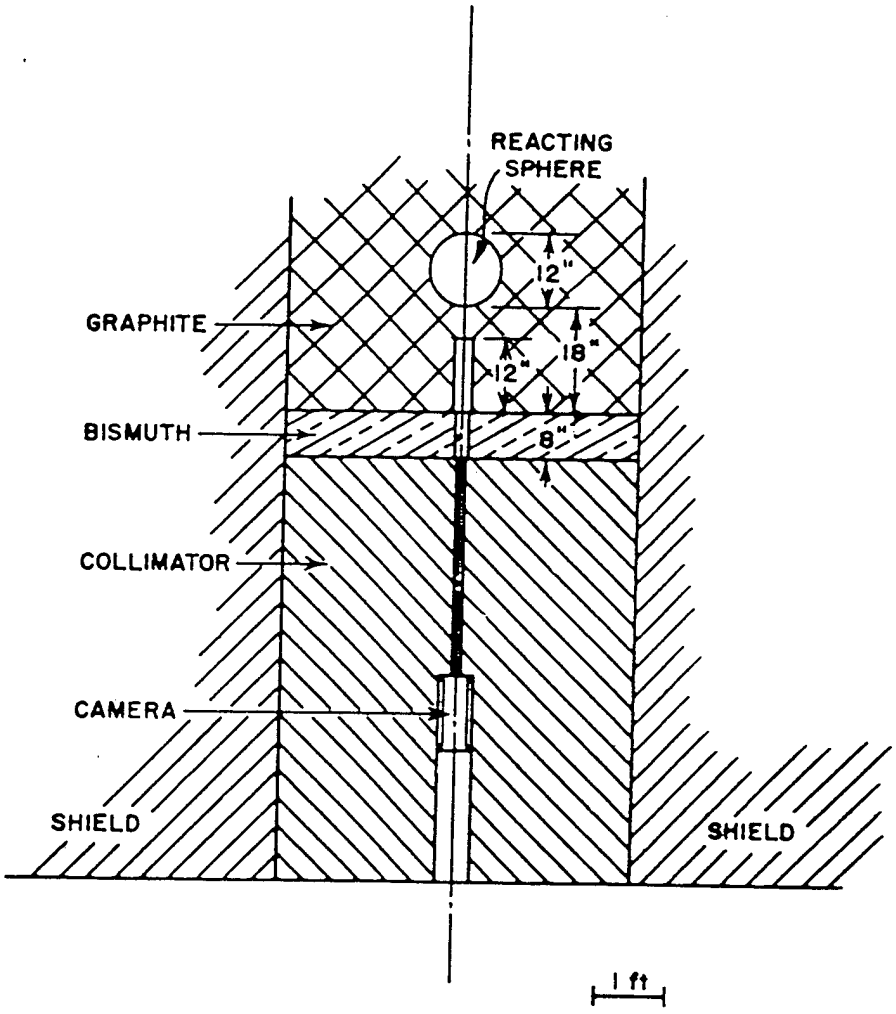

Fig. 3.5 Collimator Inserted in Position of South Thermal Column of Water Boiler for Fission Spectrum and Slow-neutron Testing as Viewed from Above

through graphite 18 in. thick. The bismuth shield inside the reactor has as its purpose the absorption of gamma radiation, while neutrons are more readily transmitted. Hence this test, although it was the most complete for neutron bombardment, left something to be desired from the standpoint of gamma-ray testing.

Exposures were made in the Water Boiler with a neutron camera in place. The first trial resulted in extreme blackening of the photographic plates. It was reasoned that the cavity for the camera inside the collimator comprised the essential design for a thermal-neutron catcher. Once inside this cavity, thermal neutrons remained there until their capture or decay.

In order to prevent this effect, a capsule $\frac{3}{4}$ in. long, containing 2.7 g/cm^2 of 95 per cent enriched B^{10}, was placed in the entrance end of the collimating tube. This measure overcame the blackening of the plates. As a consequence of this experiment, the collimating tubes in the standard collimators were altered to accept a similar B^{10} capsule. In addition, it was decided to redesign the rear plugs of the collimators so as to provide for a plug, 5 in. long, to be filled with B_4C containing B^{10} in its normal isotopic concentration.

With the previous alteration it became feasible to measure the fission spectrum of the Water Boiler as in the fast-reactor experiments.

DELETED

The fast-neutron spectrum observed is shown in Fig. 3.6.

3.4 14-MEV NEUTRON COLLIMATION

In order to investigate the effect of a collimating tube on a 14-Mev spectrum, the small test collimator described in connection with the fast-reactor experiments was used to look at the Cockcroft-Walton D-T source, as shown in Fig. 3.7. This source is, in the first approximation, an isotropic point source. The 220-kev atomic deuteron beam is focused to a spot less than 5 mm in diameter on a thick zirconium target containing absorbed tritium. As in the fast-reactor experiments, the collimator was aimed at the target spot. A neutron camera with an appropriate radiator was mounted behind the collimator and was coaxial with the collimating tube.

Initially it was found that the 14-Mev neutron flux, photographically measured through the collimator, was greater than that predicted by the alpha counter which observes the alphas coming from the target face. This discrepancy was approximately 25 per cent. Experiments were done with copper threshold detectors in an effort to determine whether or not this effect was due to small-angle scattering of neutrons from the inner wall of the collimator tube. This was found not to be the case. It is now believed that the extra flux arises as a result of penetration of the edges of the collimator tube at the end near the radiator and camera. This is a reasonable effect when the divergence of the neutron beam is considered. For the actual test, the neutrons observed should have essentially zero divergence angle, and the effect will be greatly reduced.

In any event this effect should cause only a small error in those Phonex measurements which are to be essentially relative. Also, calibrations will be made on ordinary fission bombs before the D-T shots so that if this effect exists corrections for it can be made. The spectrum measured at the D-T source is shown in Fig. 3.8.

3.5 MECHANICAL TESTS

In order to investigate the possibility of damage to the nuclear cameras or plates from shock due to the bomb blasts and the possible rolling of some collimators, drop and high-explosive blast tests were made.

Initially the collimator was hoisted to heights of 10, 20, and 30 ft by a crane, a loaded neutron camera having been placed inside the collimator, as for the actual tests (see Fig. 3.9). The brake of the crane was released, and the collimator was allowed to fall and strike the ground, as shown in Fig. 3.10. These tests did not correspond to free fall since a considerable amount of the potential energy of the collimator went into the cable drum of the crane as well as into the frictional losses of the pulley sys-

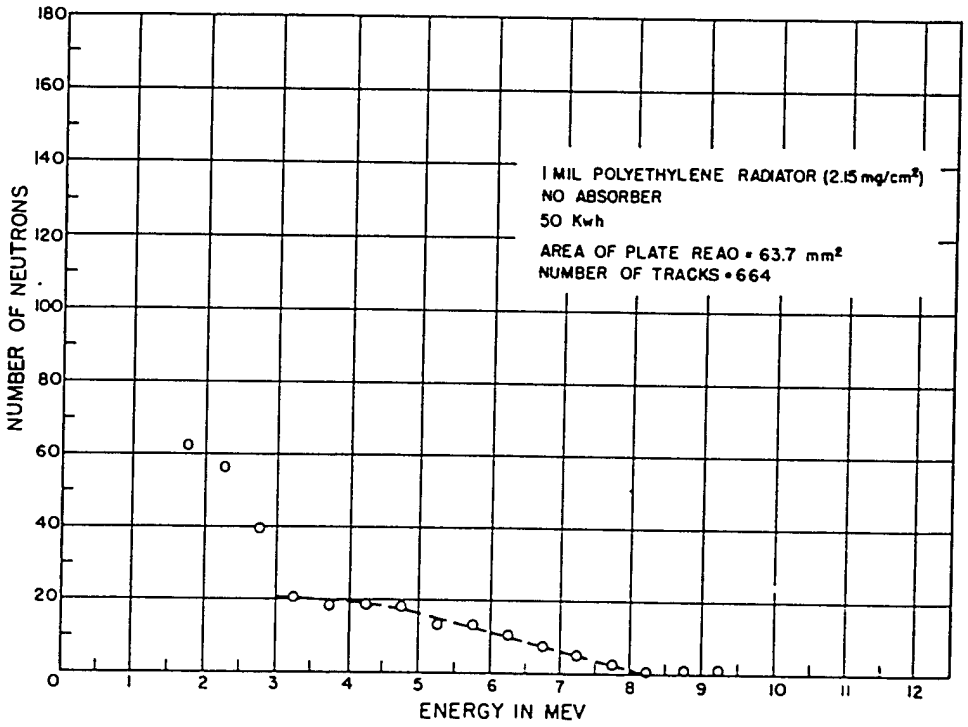

Fig. 3.6a Observed Neutron Spectrum from Water Boiler Using Collimator

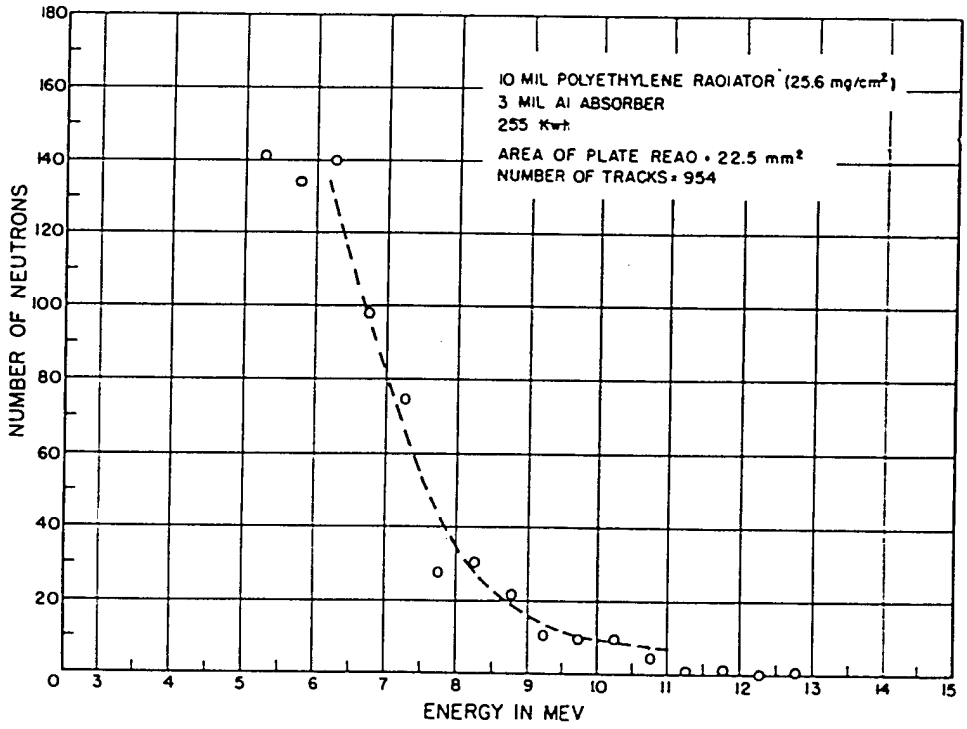

Fig. 3.6b Observed Neutron Spectrum from Water Boiler Using Collimator

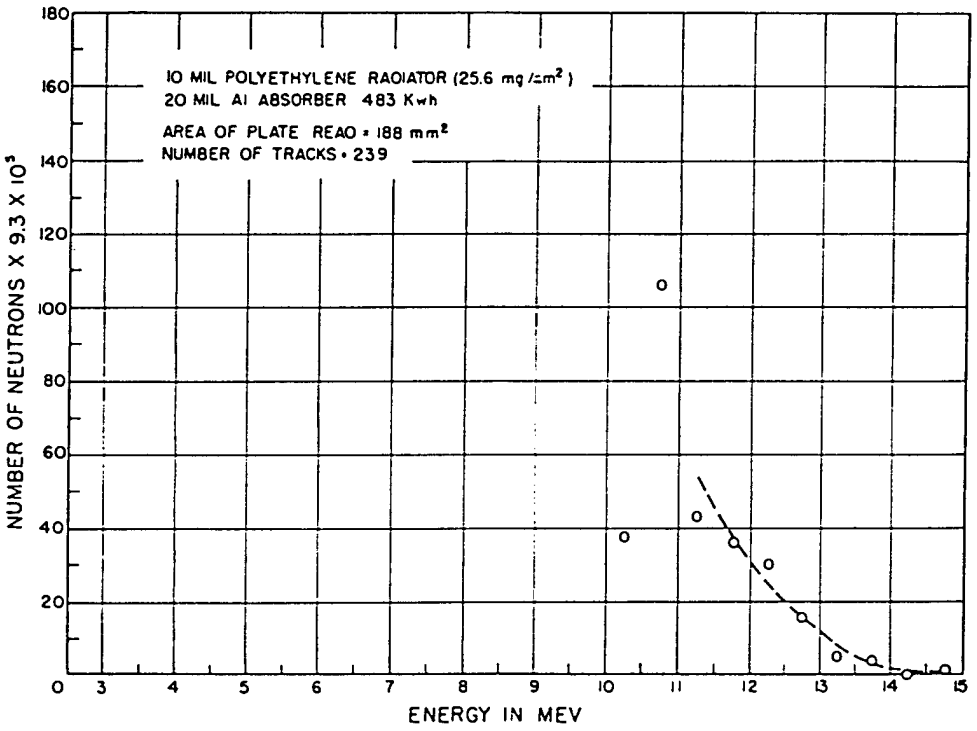

Fig. 3.6c Observed Neutron Spectrum from Water Boiler Using Collimator

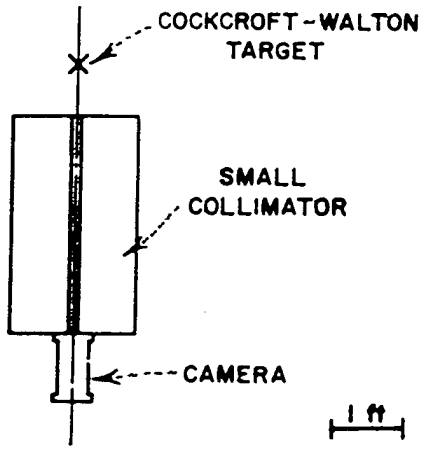

Fig. 3.7 Geometry for 14-Mev Neutron Collimator Testing as Viewed from Above

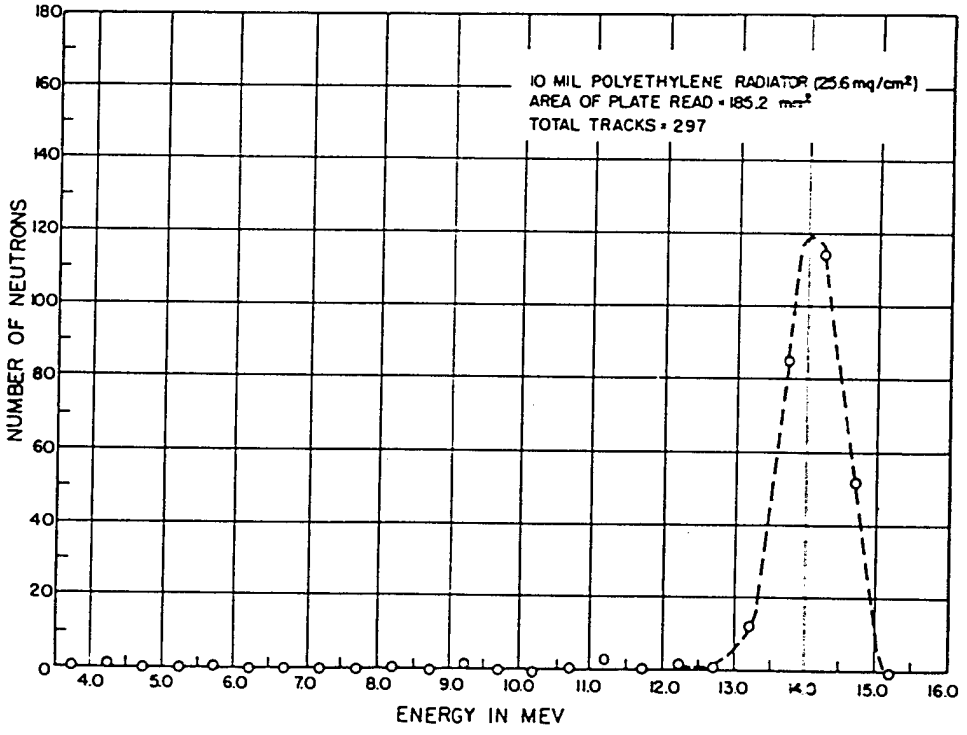

Fig. 3.8 Observed Neutron Spectrum from 14-Mev Source Using Collimator

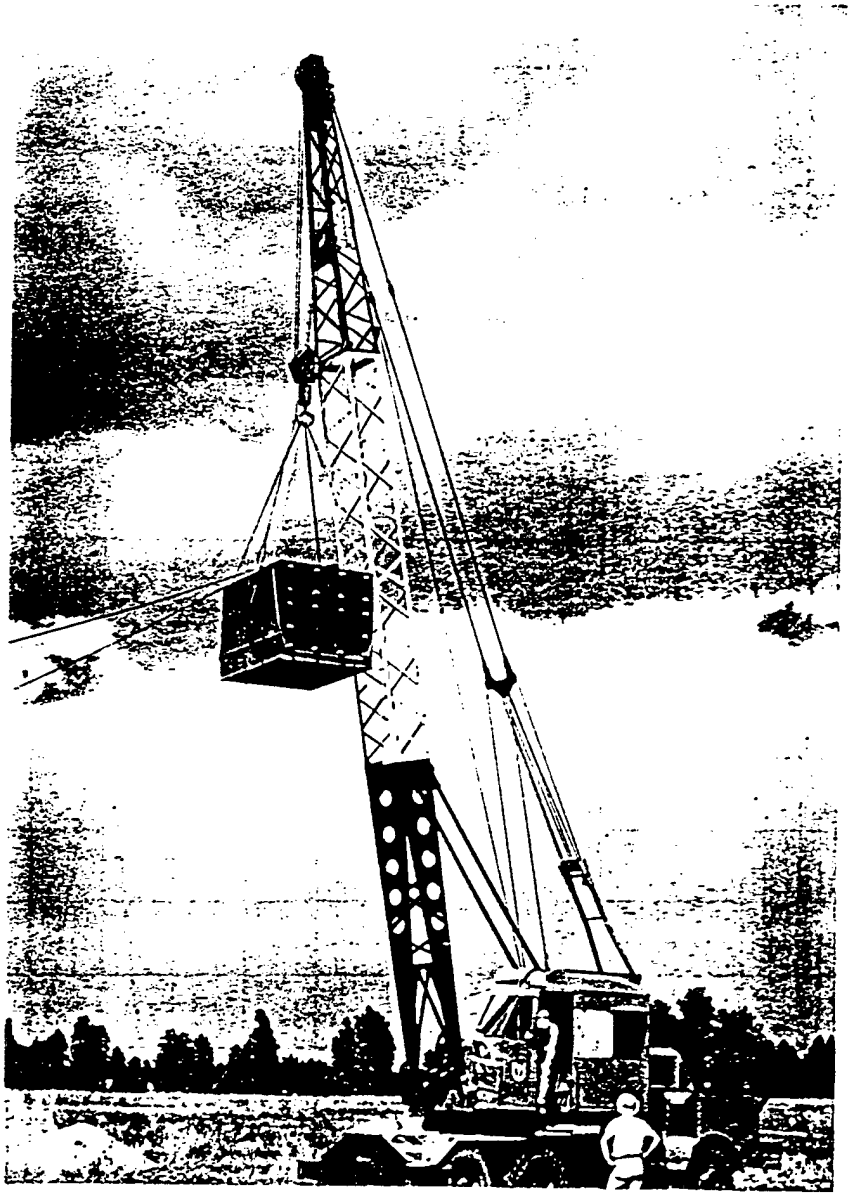

Fig. 3.9 Collimator in Position for Drop Test

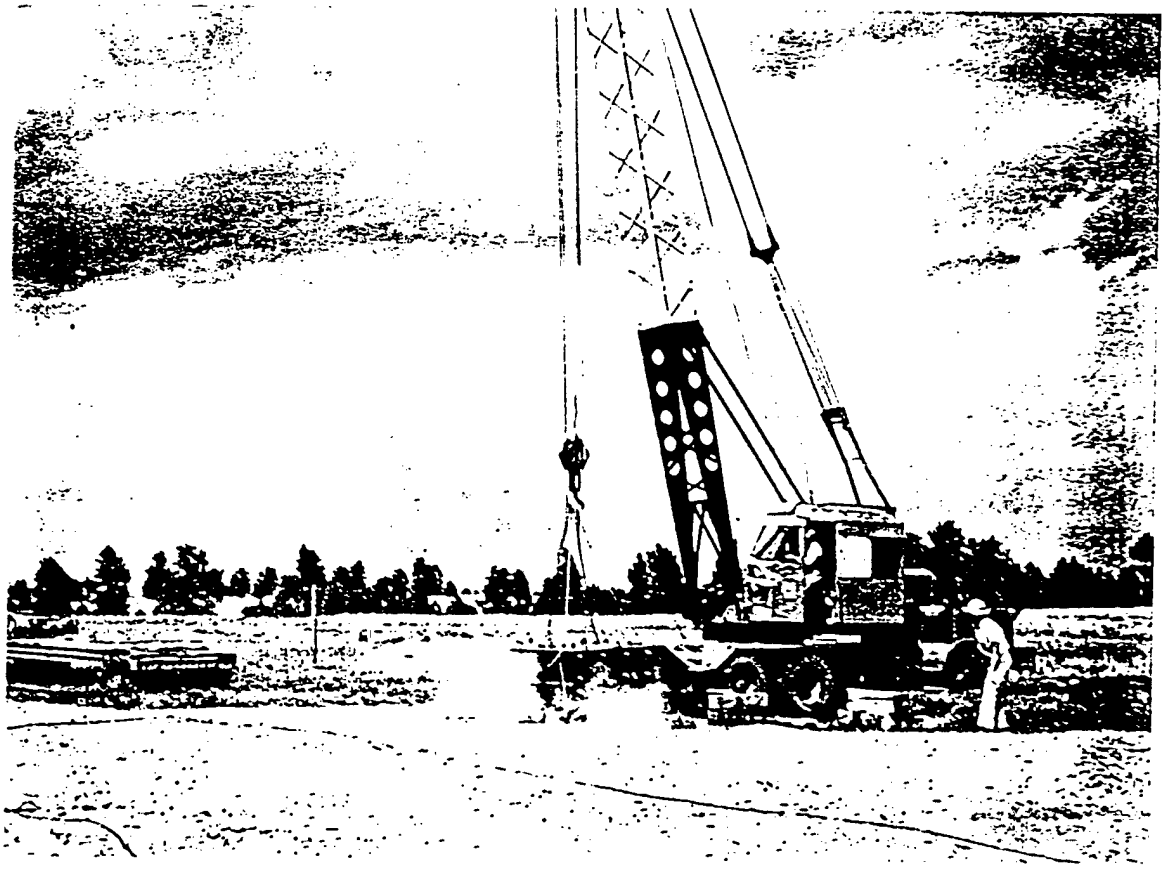

Fig. 3.10 Collimator Hitting Ground after Drop

tem. The terminal velocity for the 30-ft drop, for example, was 32 ft/sec, corresponding to a free fall of 16 ft. This was considered to be a sufficiently rigorous test of mechanical resistance to tumbling. A fourth drop of 20 ft was made in which the collimator was allowed to drop on one corner. After each drop examination was made of the camera and plates. No damage was detected. In addition, Fastax motion pictures made of the drops indicated that the various joints of the collimator did not open at impact.

To test the effect of blast, three high-explosive charges were fired in front of the collimator. These were as given in Table 3.1. The geometry for the blast tests is shown in Fig. 3.11, which shows the setup for shot 2. (The cable which is visible had fastened to it various threshold-detector holders for use with the Annex 1.5 measurements.) In no case was either the camera or the plates damaged. No deleterious effects were observed at all for shot 1. On shots 2 and 3, minor casualties were observed. These were the fracture of longitudinal bolts. One bolt broke on shot 2 and two on shot 3. It was observed that in all cases of bolt fracture, the end of the bolt toward the HE charge had been struck by some fast-moving object. In one case this object was known to have been a cable since the imprint of the wires of the cable was visible on the end of the bolt. In the other fractures, the striking object was presumably a rock.

This effect can be explained as being due to the fact that the bolts had been tightened to extreme tension. When the collimator was assembled, the bolts were tightened by using a pipe wrench on the nuts and pipe on the ends of the wrench and finally hitting the end of the pipe with a sledge hammer. It is reasonable that only a small additional stress might be necessary to surpass the fracture strength of the steel. It is now planned therefore that for the actual tests the collimator bolts will be tightened only with a long wrench. This should leave a reasonable reserve of strength. In addition, special high-tensile-strength bolts have been ordered for use in the collimators at close stations.

The effects of blast can be seen in Fig. 3.12. Note the indentations in the front steel plate covering the collimator tubes.

3.6 ON-SITE TESTS

In order to investigate the feasibility of the general operational plan for Phonex and to test the durability of equipment and manpower, a trip was made to Eniwetok in November 1950. A small scale of the actual operation was set up as follows:

One collimator of actual design was filled with limonite concrete and set on its base (Station E-10). The station was then completely assembled. All collimation tubes and rear plugs were greased and placed in the collimator. The collimator was aimed as nearly as possible at the position to be occupied by the bomb, and a lead-brick shield was placed in front and on top to the extent permitted by the alignment procedure. Photographs of this station are shown in Figs. 2.3 and 2.4.

A neutron camera was loaded with various types of plates, evacuated, and placed in the collimator. A Po-Be neutron source ($Q \cong 10^7$ neutrons/sec) was placed in the collimator just in front of the camera. The camera was allowed to remain in place for 96 hr. During the testing procedure the ambient temperature was about 90°F. On development the plates were found to be satisfactory with regard to readability of proton-recoil tracks. The gamma-ray dosage received by the plates

TABLE 3.1 HIGH-EXPLOSIVE CHARGES USED IN BLAST TESTING OF COLLIMATOR

Shot	Weight HE (lb)	Distance from Collimator (ft)	Estimated Minimum Peak Pressure (psi)
1	200	23.	200
2	100	7.5	1000
3	200	7.5	2000

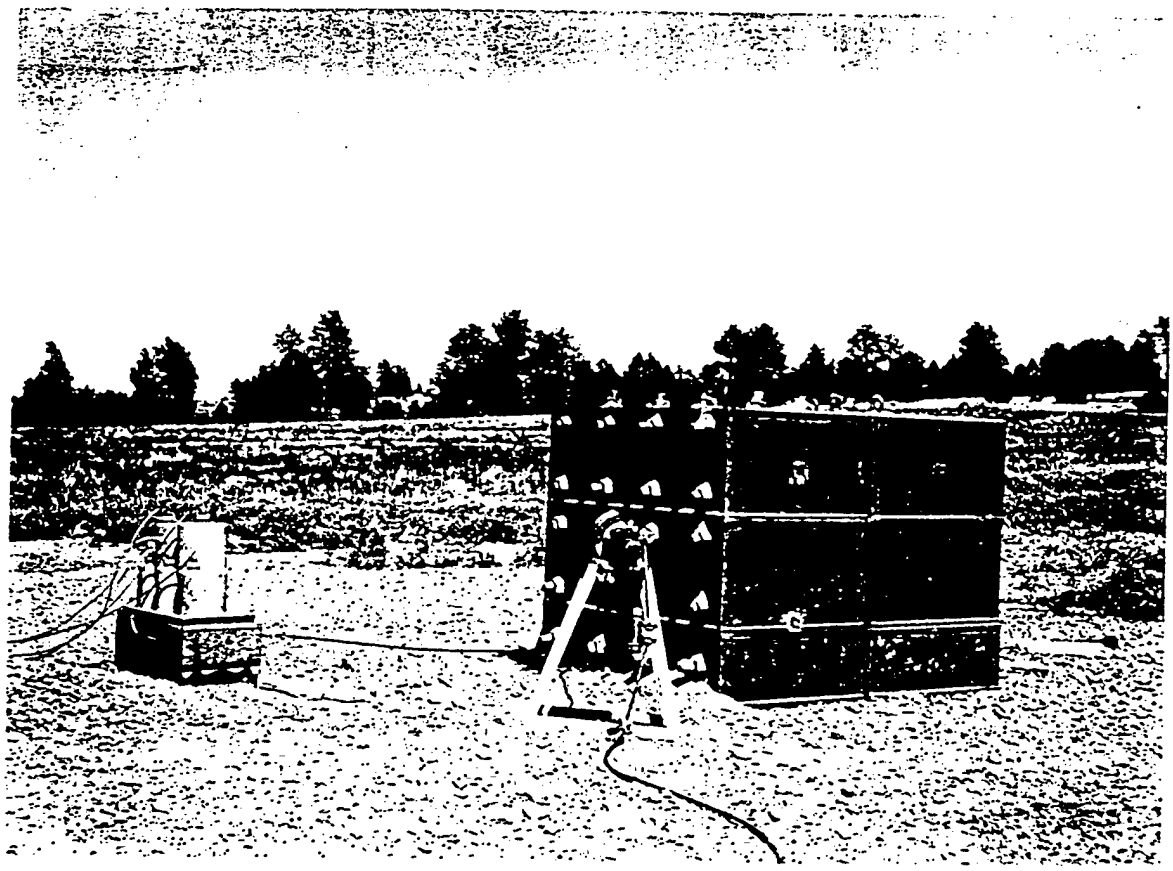

Fig. 3.11 Relative Positions of Collimator and HE for Blast Shot 2

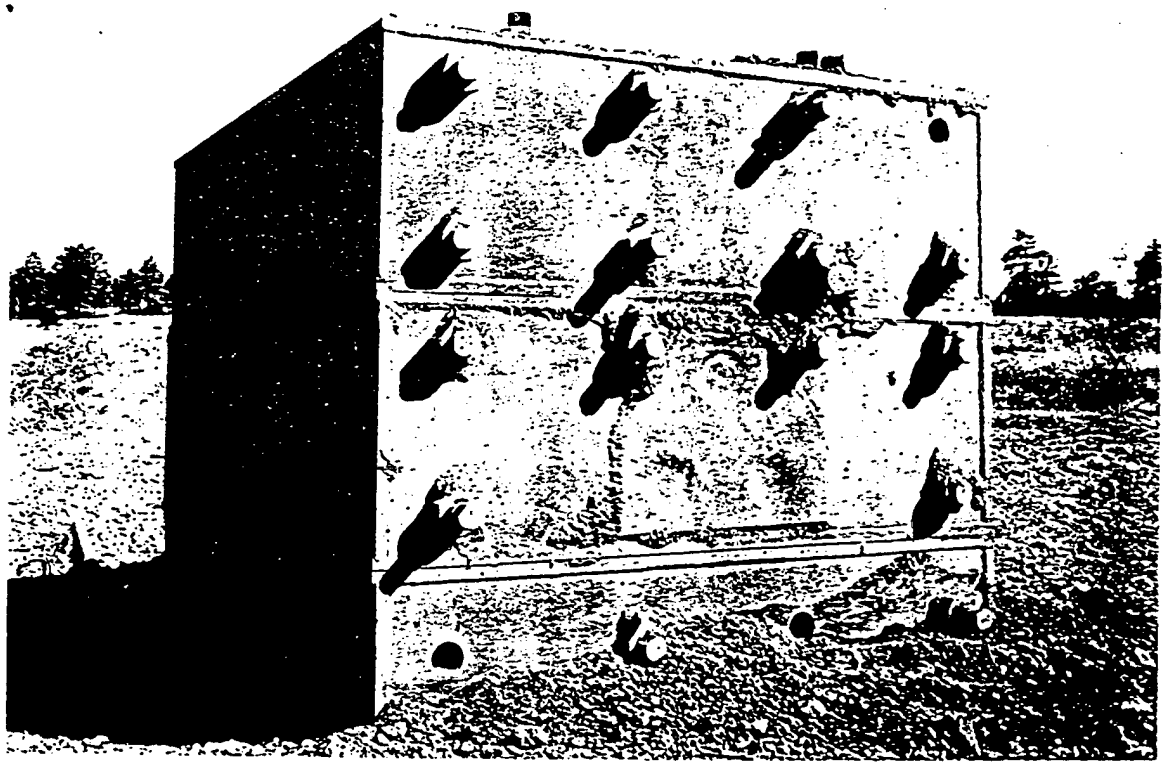

Fig. 3.12 Effect of Blast on Front of Collimator

was of the order of 5 r, but blackening was not sufficient to produce serious difficulty in distinguishing the tracks.

The results of this test were encouraging, in view of the fact that the plates suffered no appreciable deleterious effects due to temperature and extended time in vacuum. The developing technique for the plates was found to be satisfactory. Darkroom facilities were also found to be adequate.

3.7 CONCLUSIONS

As a testing program was evolved for the apparatus of the Phonex experiment, it soon become evident that it was impossible to mock-up completely the conditions which will exist at the firing of a weapon. This is true in the case of a weapon because of the extremely small neutron source of high intensity at a distance that is large compared to the length of the collimating tube. Even neglecting the time scale, this implies that for a proper test a laboratory source must be placed a great distance away, or the collimator thickness and hole size must be scaled down appropriately. For any laboratory sources available, considerations of intensity (as well as shielding) exclude either possibility. For the shielding problem, it would be desirable to bathe the collimator in a heterodirectional gamma-ray and slow-neutron field. These conditions are likewise impossible of achievement in the laboratory. Finally, the blast tests do not duplicate those to be experienced because of the relatively short duration of a high-explosive blast wave as compared to that from an atomic weapon. In spite of these shortcomings it is believed that the testing program has been sufficiently rigorous to justify a reasonable confidence in the outcome of the measurements.

REFERENCES

1. L. Rosen, Los Alamos Scientific Laboratory Report, LAMS-915.
2. N. Nereson, Los Alamos Scientific Laboratory Report, LA-1123.

Chapter 4

Modifications of Objectives and of Experimental Design

4.1 SUPPLEMENTARY OBJECTIVES OF PHONEX

After the first Greenhouse explosion (code name Dog shot), which was not a thermonuclear test, the success of the Phonex experiment prompted a reevaluation of the possibility of determining sufficiently precise neutron-spectra measurements from George shot to permit a measurement of the effective temperature at which the thermonuclear reaction proceeded. Since the temperatures at which the D-T reaction proceeds must be evidenced by a Doppler broadening of the distribution in energy of the 14-Mev neutrons, it is possible, in principle, to determine this temperature from the shape of the energy distribution of neutrons from the D-T reaction. However, the resolution necessary to permit a useful temperature determination turns out to be about 250 kv, and this was somewhat better than was at first thought possible. The reason for the original assumption that 0.5 Mev was the best resolution attainable with our method was that calculations showed it would be necessary to use considerable absorber thickness in front of the detectors to eliminate the low-energy proton recoils produced by fission neutrons. These absorbers would in turn introduce straggling and limit the resolution to 0.5 Mev.

DELETED

The geometry of the experiment was therefore altered to take advantage of this new development. The new geometry permitted a resolution of 0.25 Mev.

4.2 MODIFICATIONS OF CAMERAS

For Dog shot the camera geometry was as shown in Fig. 4.1. In order to achieve better resolution in the following shots, it was necessary to move the plates closer to the axis of the hole and hence to the neutron beam. The camera geometry for George and Item shots is shown in Fig. 4.2. The hoods were placed over the plates after the first test in order to decrease the number of proton recoils from water vapor in the camera since the camera was sealed off before being placed in the collimator. The camera geometry for Easy shot was identical with that for Dog shot with the exception that plates 13 and 14 occupied positions 1 and 2 as shown in Fig. 4.2.

4.3 MODIFICATION OF SUPPLEMENTARY SHIELDING FOR COLLIMATORS

The supplementary shielding for the collimators consisted of the following:

1. 8 in. of lead in front of all 200-, 400-, and 600-yd stations.
2. 4 in. of lead on top of all 200-, 400-, and 600-yd stations.
3. 18 in. of limonite on each side of all 200-, 400-, and 600-yd stations. The limonite blocks were girded by two 2-in. steel cables in the horizontal plane.
4. Dirt fill on each side and in front of all 200-, 400-, and 600-yd stations.

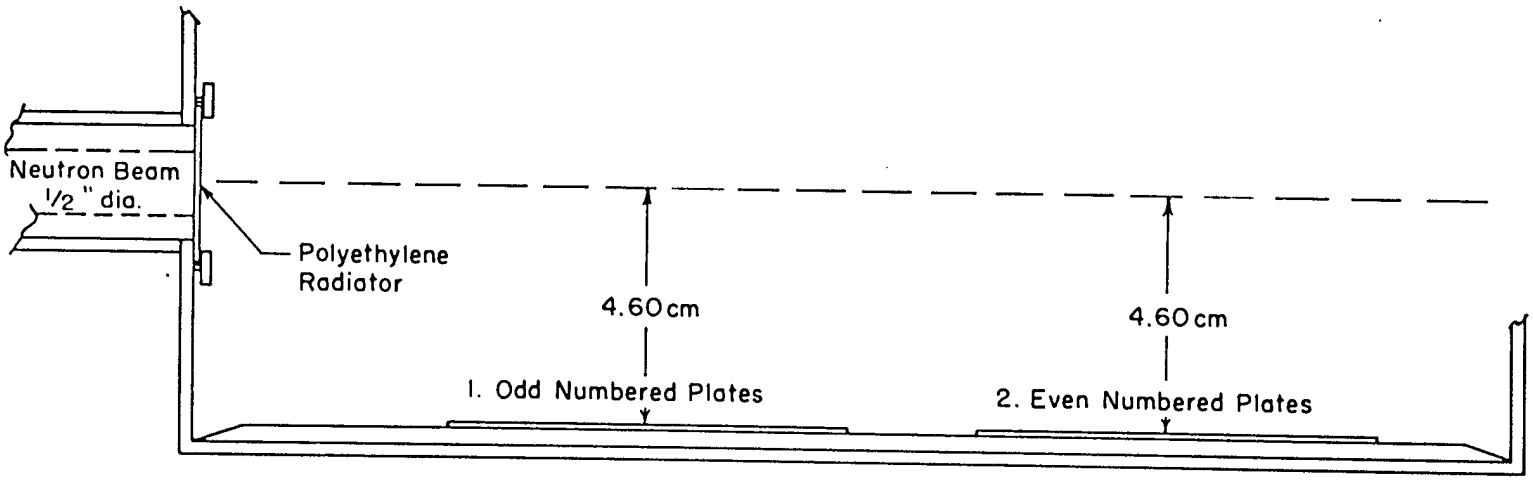

Fig. 4.1 Camera-plate Geometry for Dog and Easy Shots

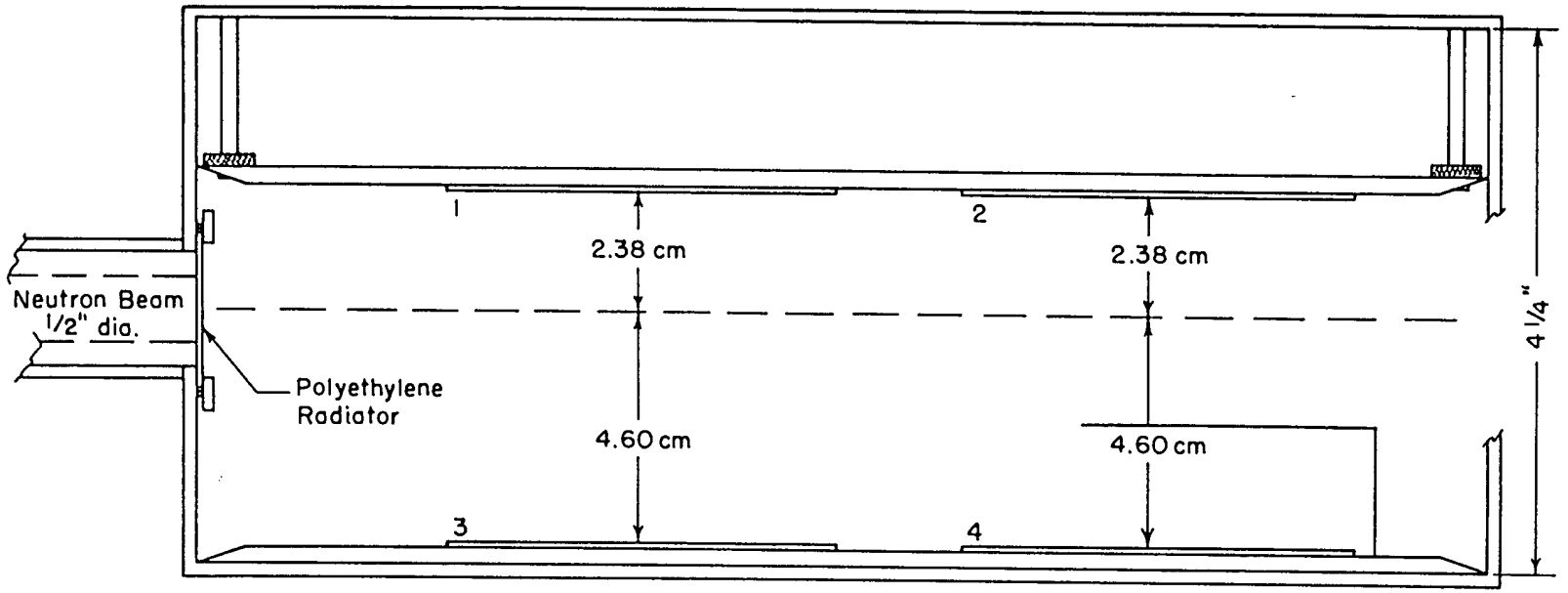

Position	Plate Numbers
1	3, 7, 13, 17
2	4, 8, 14, 18
3	1, 5, 11, 15, 21, 23, 25, 27
4	2, 6, 12, 16, 22, 24, 26, 28

Fig. 4.2 Camera-plate Geometry for George and Item Shots

5. Lead in all cases protected by $\frac{1}{2}$-in. boiler plate.

6. Lead-brick walls in front of the collimator, as well as the protective boiler plate, contained $\frac{7}{8}$-in. holes whose axes coincided with those of the collimator tubes.

Figures 4.3 to 4.7 are pictures of collimators prior to Easy shot; Figs. 4.8 to 4.10 are pictures taken after the blast.

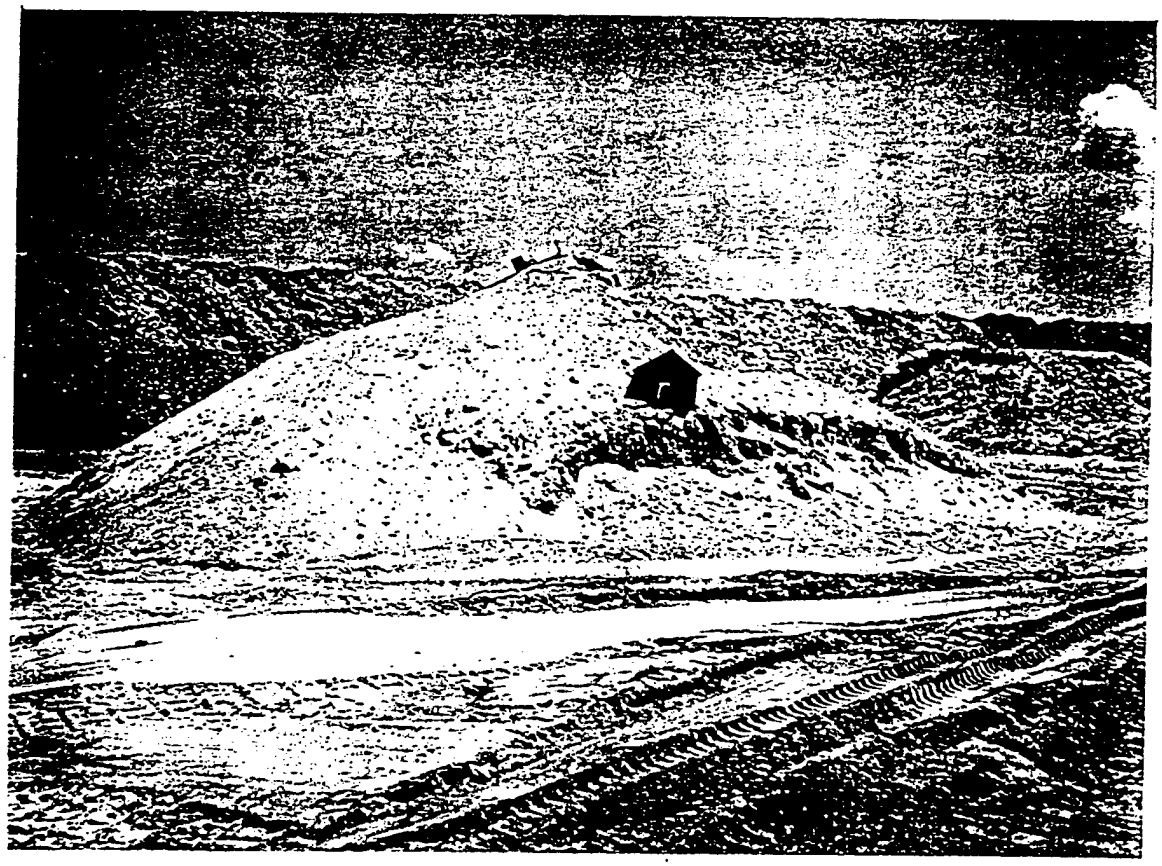

Fig. 4.3 Easy Shot 200-yd Collimator, Right Side (before Easy)

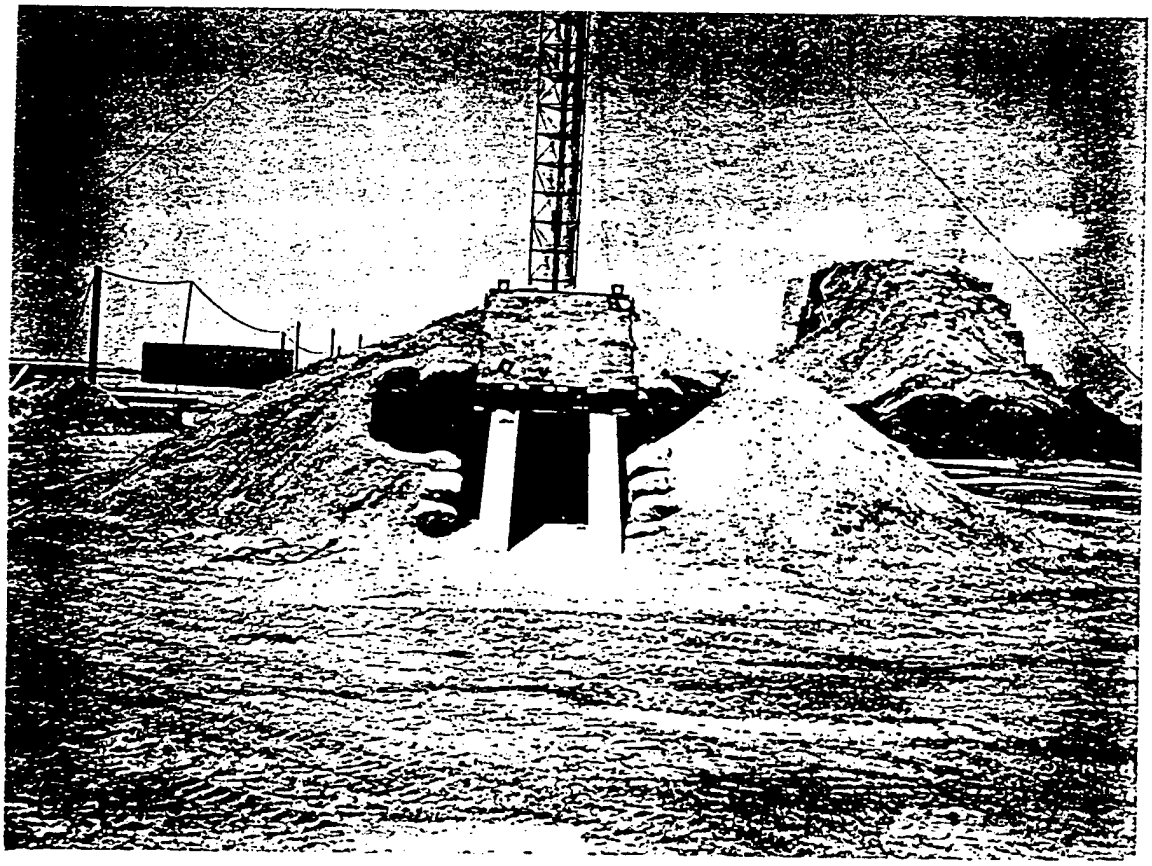

Fig. 4.4 Easy Shot 200-yd Collimator Rear View (before Easy)

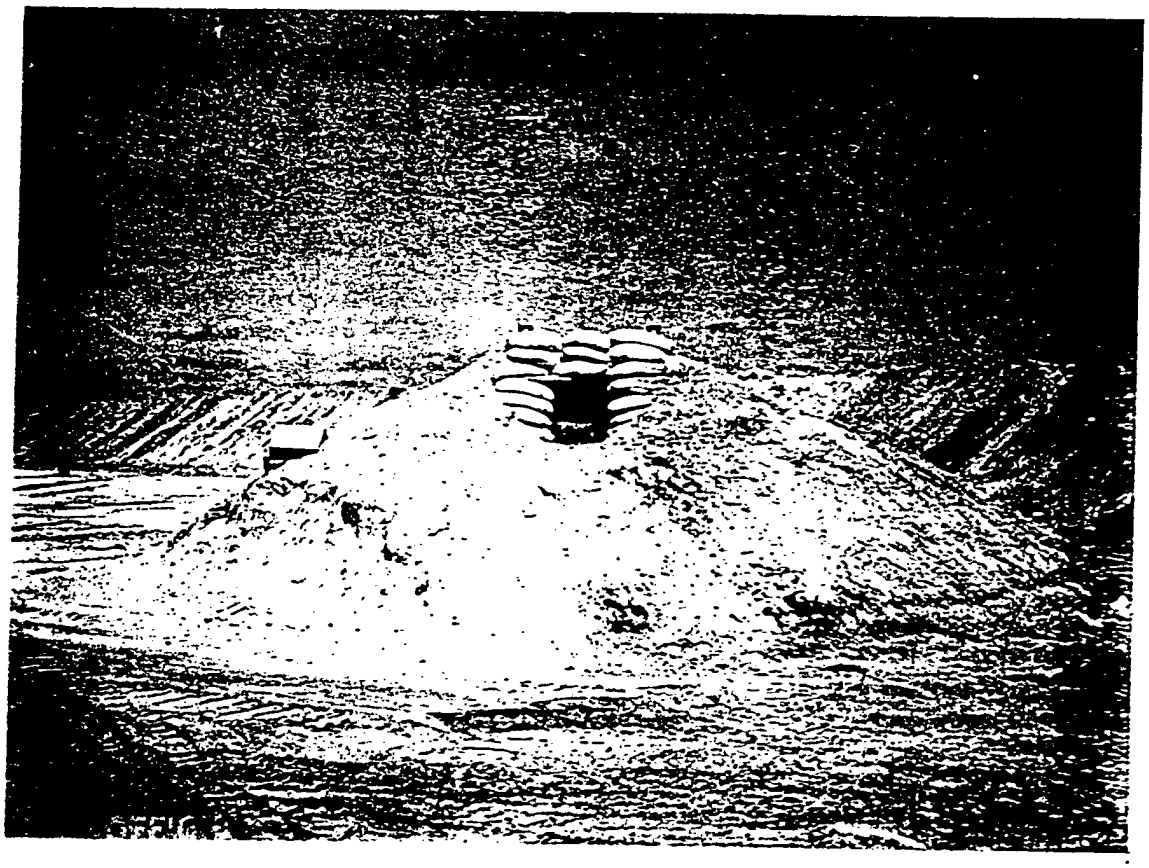

Fig. 4.5 Easy Shot 200-yd Collimator, Front View (before Easy)

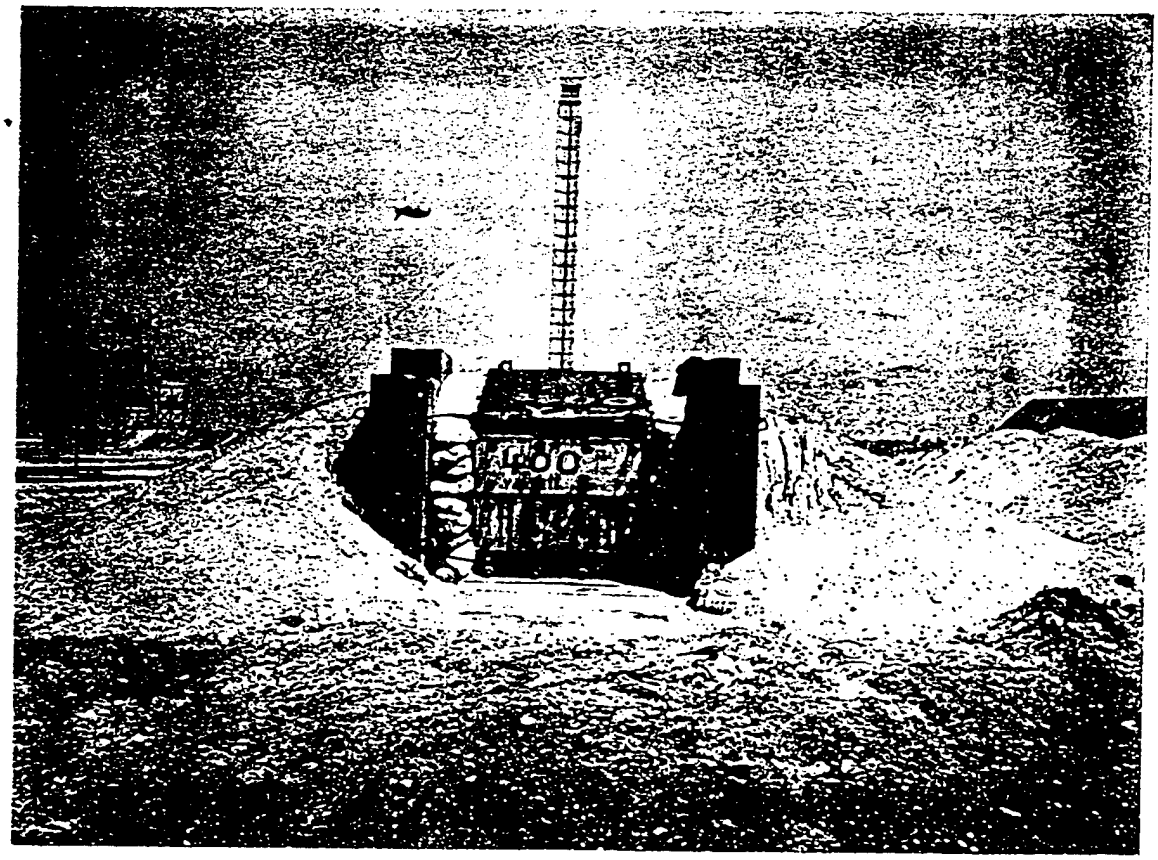

Fig. 4.6 Easy Shot 400-yd Collimator, Rear View (before Easy)

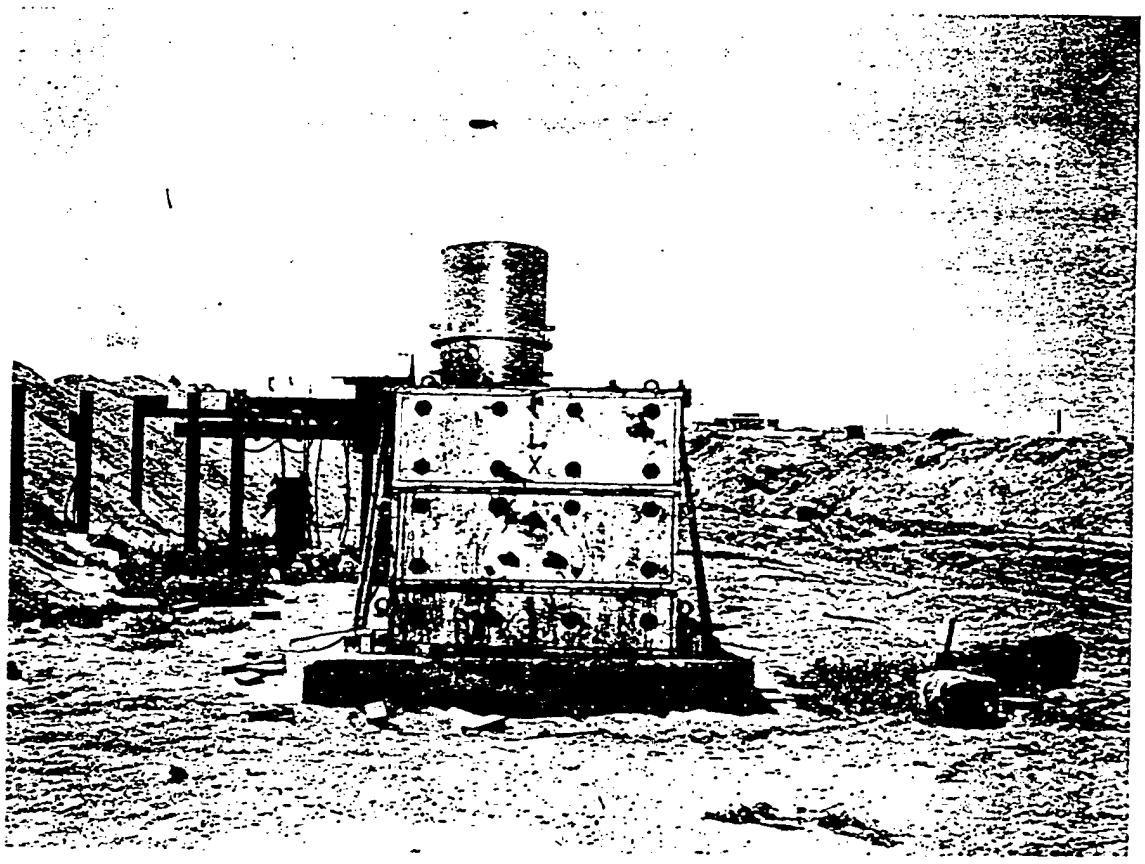

Fig. 4.7 Easy Shot 1000-yd Collimator, Front View (before Easy)

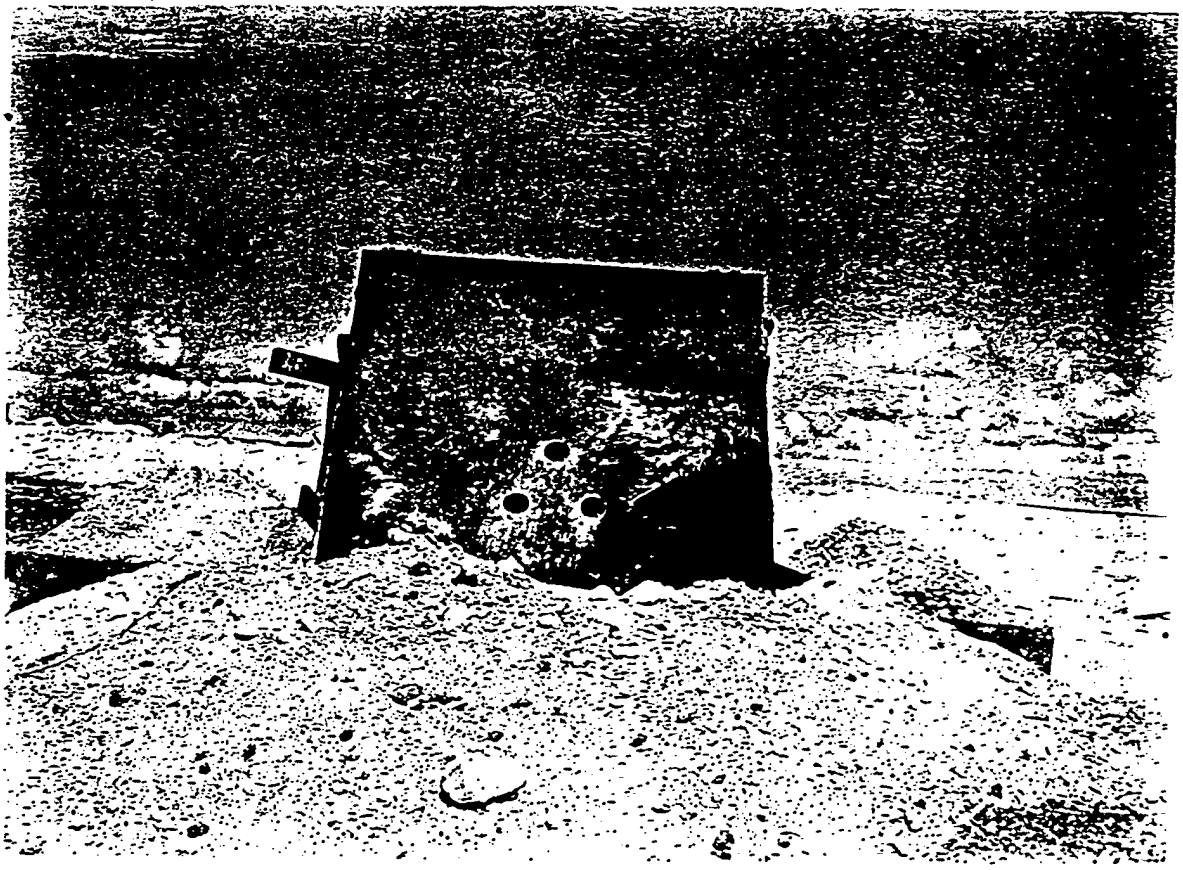

Fig. 4.8 Easy Shot 200-yd Collimator, Front View (after Easy)

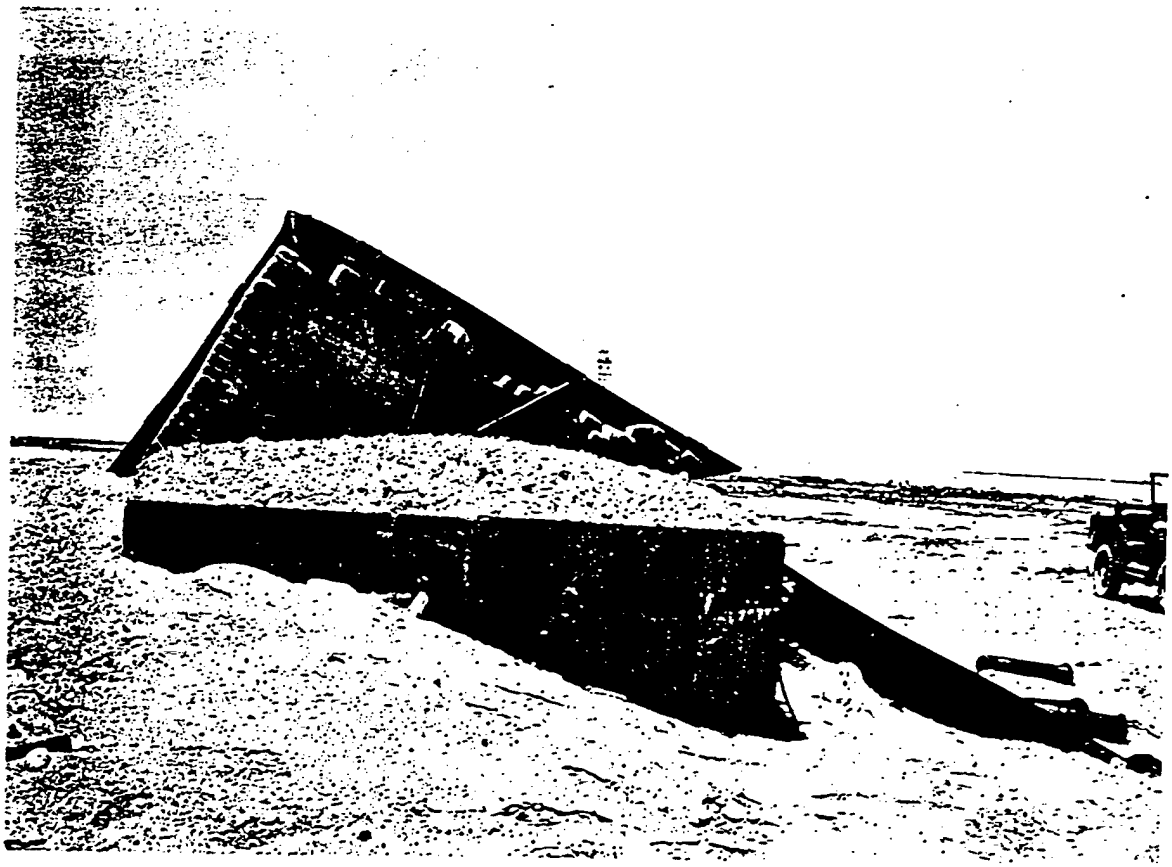

Fig. 4.9 Easy Shot 200-yd Collimator, Left Side (after Easy)

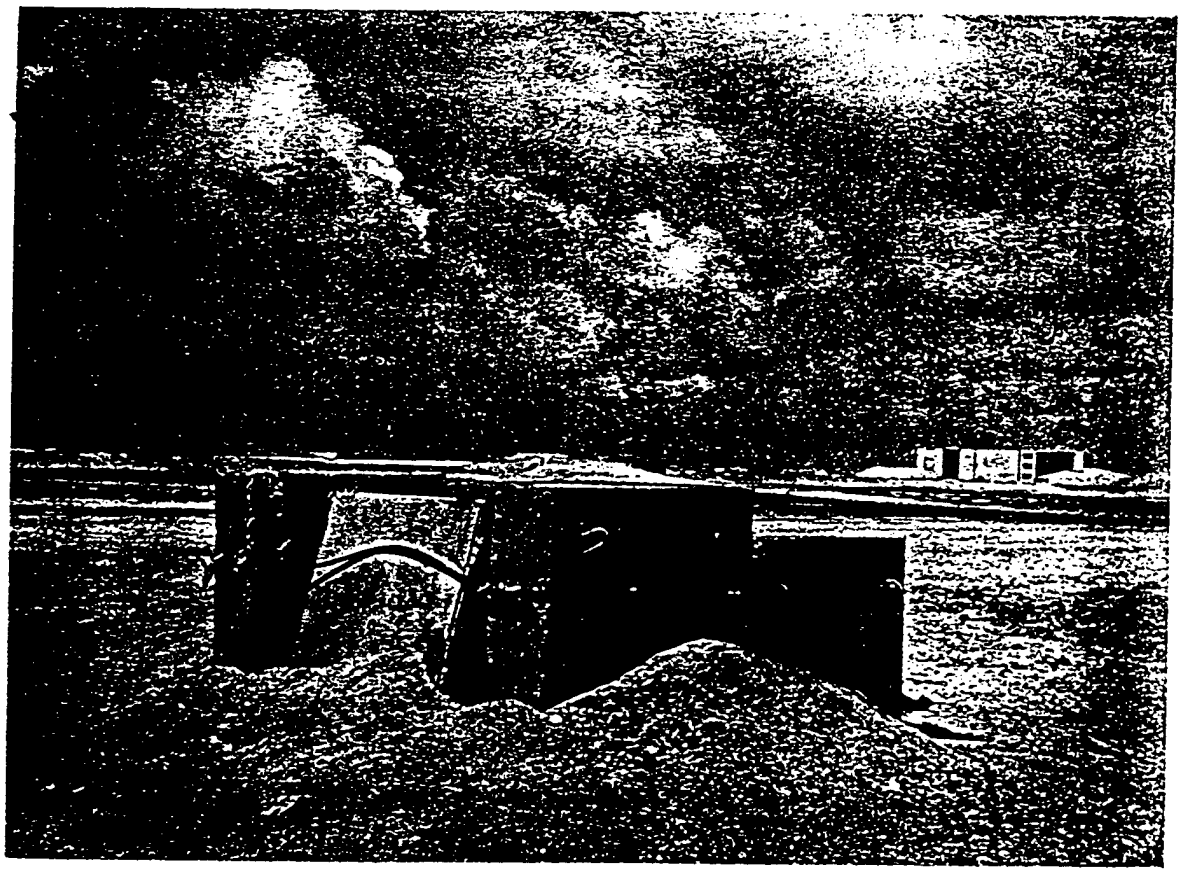

Fig. 4.10 Easy Shot 400-yd Collimator, Left Front (after Easy)

Chapter 5

On-site Experimental Procedure

5.1 FILLING AND ALIGNMENT OF COLLIMATORS

Most of the collimators were filled with limonite concrete according to the formula given in Chap. 2. Part of them, however, were filled with a somewhat heavier mix (approximately 290 lb/ft^3). The increase in density was realized by the addition of selected scrap iron. After filling, the collimators were set on their respective bases and pointed in approximately the right direction. The collimators were aligned by placing in the top collimator tube an accurately machined cylindrical brass plug through which was drilled a $\frac{1}{8}$-in. hole along its axis. One end of the plug was counterbored to an internal diameter of $\frac{3}{8}$ in. On insertion into the collimator tube the large hole opened to the back of the collimator, the axis of which coincided very accurately with the axis of the $\frac{1}{4}$- and $\frac{3}{4}$-in. holes in the alignment plug. At the back of the collimator was mounted a steel plate held in place with magnets. A $\frac{1}{16}$-in. "peep" hole had been drilled through the center of the steel plate. This peep hole was aligned with the axis of the collimator by sighting through it and moving the steel plate until the circle of direct light defined by the aperture in the brass plug at the front of the collimator tube and the circle of light scattered from the walls of the collimator tube were perfectly concentric. The steel plate could be aligned in this manner to approximately 0.001 in. Having thus aligned the peep hole with the collimator-tube axis, one then sighted along the collimator-tube axis, through the peep hole and the aperture in the brass plug, at a 200-w lamp placed at the position to be occupied by the center of the bomb in the case of Dog, Easy, and Item shots and by the center of D-T mixture in the case of George shot. The collimator was adjusted until the light was centered with respect to the aperture in the brass plug at the front of the collimator. By this method the axis of the top tube was aligned with the target on the tower to approximately ±1 in. for every 100 yd from bomb zero. For example, the axis of the tube which was aligned at the 400-yd station would pass within ±4 in. of the target center. Since each collimator contained three tubes and since these tubes were parallel to within ±0.001 in., precise alignment of one tube meant that the two remaining tubes would be slightly misaligned. Since the axes of the tubes were 10 in. apart, this meant a misalignment of 10 in. at bomb zero. A calculation was made to determine the magnitude of this effect on the observed neutron flux at the various converters. This misalignment was responsible for an apparent neutron-intensity decrease of 4 per cent at 600 yd and was corrected for in the final calculations of the absolute yield of neutrons as a function of neutron energy. The calculation of this correction is given in Appendix II.

After the collimators were aligned, the auxiliary shielding was put into place. Before each shot a rough check on the alignment was obtained by placing a light at the front of each collimator hole and observing this light with a telescope placed at the position which the center of the bomb was destined to occupy. Observation of the light through the channels in the lead wall showed that the lead wall would not block the line of sight along the axis of the collimator tubes.

5.2 PREPARATION OF CAMERAS

Approximately 48 hr before shot time all cameras were loaded, and their evacuation was begun. Each camera was pumped on for not less than 2 hr with a mechanical forepump. At the end of 2 hr the pressure in each camera was always below 100 μ. After evacuation the cameras were left for 8 hr to determine whether any of them leaked, as evidenced by the reading of the pressure gauge mounted on each camera. Approximately 24 hr prior to shot time, the operation of placing the cameras inside the collimators was begun. This operation was completed by 12 hr before shot time.

5.3 RECOVERY OF CAMERAS AND PROCESSING OF PLATES

Approximately 6 hr after shot time the recovery operation began. The cameras in the 1200-, 1000-, and 800-yd stations were always recovered during the first 8 hr after the shot. The 600-yd station became accessible approximately 48 hr after the shot, and the 400- and 200-yd stations became accessible within approximately 10 days after the shot. The following typical account of one of the recovery operations is quoted from Los Alamos Scientific Laboratory Notebook No. 3221, Apr. 8, 1951.

Runit Shot was fired this morning at 0634. About 10–15 minutes later a recovery party left Parry ramp. This consisted of Rosen, Allred, four Holmes and Narver personnel (T. Hoggatt, W. Jordan, P. Jakubowicz, J. Villareal) and two army monitors (G. Henry, T. Gibson). The six-by-six truck with recovery equipment on it was loaded on an LCM (M-Boat).

The eight men were divided into two recovery teams. These operated independently, the stand-by team remaining at the J-3 winch house while the other recovered as many stations as feasible at a time.

At about 0830 first recovery was made by Rosen and crew from 800 yard station. It was decided best to go in as far as possible and work back away from zero point. Thus if the truck bogs down, there is a better chance to save cameras. An upper limit of 2 R/hour was decided to be maximum working condition. On the average recovery operation took fifteen minutes total time from winch house and back for each station. Allred and crew recovered 1000 yard after first recovery, and party returned to Parry.

At 1415 party left Parry for second recovery operation. About 1515 Allred and crew went to 600 yard. Flux was 1.0 R/hr behind collimator, 1.5 R/hr at side of collimator. Lead bricks were still effectively in place except at side edges, where a few had been blown off. Boiler plate and tie welds were undamaged. Rosen and crew then recovered 1200 yard station. Level 20 mr/hr, so no rush at back stations. Party returned to Parry.

High contamination of Parry Island due to fall out occurred during the morning. It was decided on Runit to bring back only six cameras since space for these was available in 2 inch lead boxes. This proved especially fortuitous on account of fall out. Level was 20–200 mr/hr, and this would have blackened plates by the time cameras were back in lab.

After the cameras were recovered, they were cleaned with alcohol and taken to the darkroom. The plates were developed from two stations at a time, but not all the plates from a given station were developed at the same time. This precaution was taken as insurance against darkroom mishaps. After the plates were developed, they were briefly scanned; and then a representative assortment, comprising half the total number, was sent by courier to Los Alamos for analysis.

[redacted]

Chapter 6

Analysis of Data

6.1 CODING OF PLATES

The coding system utilized was so designed that the number scribed on each plate revealed the nuclear detonation during which it was exposed, the thickness of converter used, the absorber thickness in front of the plate, and the converter-detector geometry. The following description of the coding system used is reproduced as recorded in Los Alamos Scientific Laboratory Notebook No. 3221. This record was made Apr. 4, 1951.

A plate is marked with two letters and a number between 0 and 28, i.e., AB 10. The first letter designates the shot in chronological order—"A" for the first shot, "B" for the second, and so on. The second letter designates the station. Station "A" is closest to the bomb at 200 yards from ground zero; "B" at 400 yards, "C" Station at 600 yards, etc. (Note that for George shot the "C" Station is 640 yards from ground zero and for Item shot the "D" Station is 808 yards).

Plates in all three cameras at a given station are numbered serially and uniquely, such that the number of a plate describes the location in a particular camera and the thickness of the polyethylene radiator in the camera. A collimator has a total of 27 plates.

Of these, three are background plates and are designated 0, 10, and 20, these numbers corresponding to the camera in which they are placed. The numbers 1 through 8 inclusive, 11 through 18, and 21 through 28 are data recording plates. Odd-numbered plates are nearest the radiator. Thus the designation AB 10 means that the plate is for the first shot, second (400 yard) station, and a background plate for the second camera.

The number of a plate also describes the aluminum foil absorber which is associated with the particular plate position for a given shot. [A complete listing of plate numbers, radiators, and absorbers is given in Tables 6.1 to 6.3.]

The absorbers are set at one of three distinct angles. All odd-numbered absorbers, which are in the front positions of the camera, are adjustable and are set at an angle of 56° 00' to the plane of the plate.

In the rear positions, six absorbers are mounted in fixed-angle foil holders. These absorbers make an angle of 81° 30' with the plate. Plate numbers 4, 6, 12, 14, 16, and 18 are placed in these positions. In the other six rear positions, namely, 2, 8, 22, 24, 26, and 28, the foils are adjustable and are set at an angle of 76° with the plate.

6.2 READING OF PLATES

The plates were read in the manner outlined in Sec. 1.5. Binocular research microscopes (Leitz and Cooke, Troughton, and Simms) were used with high-numerical-aperture optical components. Either a 45× or a 90× oil-immersion apochromatic objective was utilized in conjunction with 6× compensating eyepieces. One of the eyepieces contained a graticule ruled into 100 squares. This grid was utilized to determine the angle which a given track makes with the long axis of the plate. The angle of dip of the track was determined by a depth measurement (using the fine adjustment on the microscope) on two sections of the track equidistant from the center of the field.

The track lengths are measured in one of two ways. In the case of long tracks (greater than 100 μ) one edge of the graticule is made to coincide with the beginning of the track, and a micrometer screw is used to move the stage (and plate) until the end of the track coincides with the same edge of the graticule. This

[redacted]

Page 66, 67, and 68 are DELETED.

micrometer screw is activated by a calibrated drum by means of which the stage displacement can be measured to approximately 2 μ. This procedure measures the projection of the track along the long plate axis in the emulsion plane. In the case of short tracks the projected-length measurement was made using the graticule divisions, the graticule having first been calibrated to $\frac{1}{2}$ per cent by means of an accurate stage micrometer. The field of view defined by the graticule is approximately 100 μ on a side.

Figure 6.1 is a drawing of the radiator-detector geometry showing the angles which must be considered in setting up the criteria for track acceptance and for corrections to the measured projected length.

6.3 CRITERIA FOR ACCEPTANCE OF TRACK FOR MEASUREMENT

Only tracks which start on the surface of the emulsion and proceed away from the converter in a direction indicating that they originated in the converter were accepted for measurement. Tracks which did not satisfy this criterion were due either to proton recoils from collisions of neutrons with hydrogen in the emulsion or to proton recoils from collisions of neutrons with hydrogen in the water vapor in the camera. Neither source was sufficiently prolific to give rise to significant background.

Since some scattering is to be expected both in the nuclear emulsion and in absorbers, when these are used, the angular criteria were increased by 20 per cent in the case of no absorbers and by 30 per cent in the case of absorbers, to take such scattering into account. The more liberal acceptance criteria were arrived at by plotting the number of tracks vs horizontal and vertical angles in the plate. Some plates showed that 95 per cent of the tracks starting on the surface of the emulsion did indeed arise in the radiator. Some concern was at first felt that tracks arising from proton recoils in the water vapor might to a large extent be indistinguishable from tracks arising from proton recoils in the converter. However, a calculation (see Appendix III) showed that the intensity of tracks arising from proton recoils in the water vapor would be a maximum for a dip angle twice as large as the acceptance angle. Since this angle is far outside the angular criteria it is concluded that the background from this source is negligible.

The projection was always measured along the long plate axis (line AB, Fig. 6.1) except in cases where large-angle scattering took place. In these cases the absolute length of each of the track segments was recorded. In addition, β [arctan (d cos α)/r] had to be scrutinized for each track, as did α (arctan v/r), since these were the acceptance-criteria parameters. In setting up the angular criteria, it was found necessary to take the emulsion shrinkage into account; i.e., β' = arctan sd cos α, where β' is the angle of dip in the unprocessed emulsion and s is the factor by which the emulsion shrinks on processing; s $\approx$ 2.3. From a range analysis of the tracks and the neutron-proton scattering cross section as a function of neutron energy it is possible to arrive at the shape of the neutron spectrum incident on the converter. In order to determine the absolute number of neutrons, as a function of energy, which strike the converter, it is necessary to define accurately the solid angle subtended at the converter by the plate area analyzed (see Sec. 1.5). The plate area analyzed is determined by the number of swaths read and the width of each swath as defined by the height of the graticule, which is calibrated with a stage micrometer in the same way as the graticule width is calibrated. The swath widths were taken at 1 cm for reasons of energy resolution.

6.4 TABULATION OF DATA

In order to avoid calculating the energy of the neutron corresponding to each proton-recoil trajectory, the calculations were essentially reversed, and the projected range of recoil protons was calculated as a function of neutron energy every $\frac{1}{4}$ or $\frac{1}{2}$ Mev over the neutron-energy range of 2 to 16 Mev. It was necessary to make a calculation for each combination of radiator thickness, absorber thickness, and plate area analyzed. The width of the energy intervals taken was determined by the resolution attainable for a given position on a given plate.

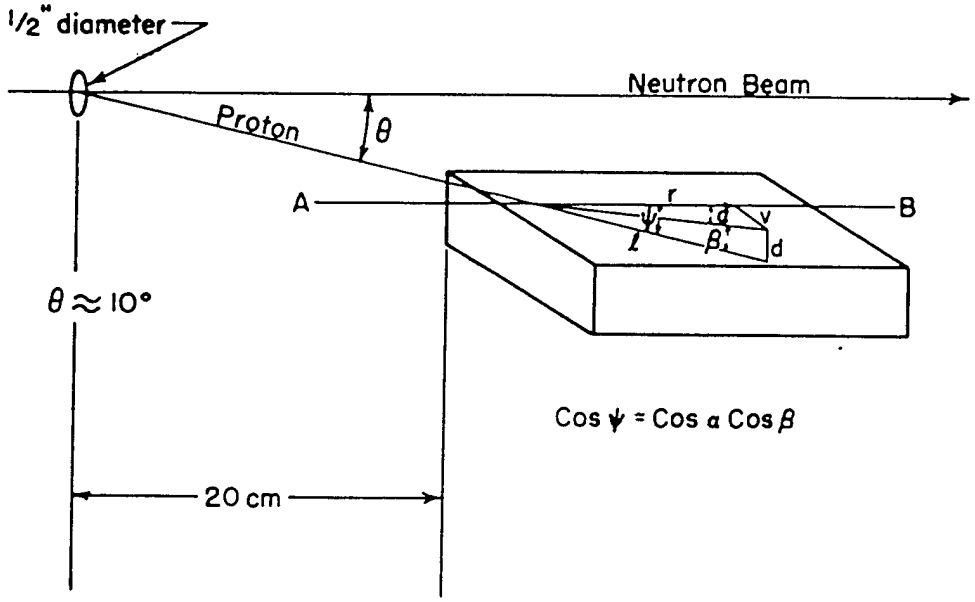

Fig. 6.1 Schematic of Radiator-detector Geometry

Page 71 is DELETED.

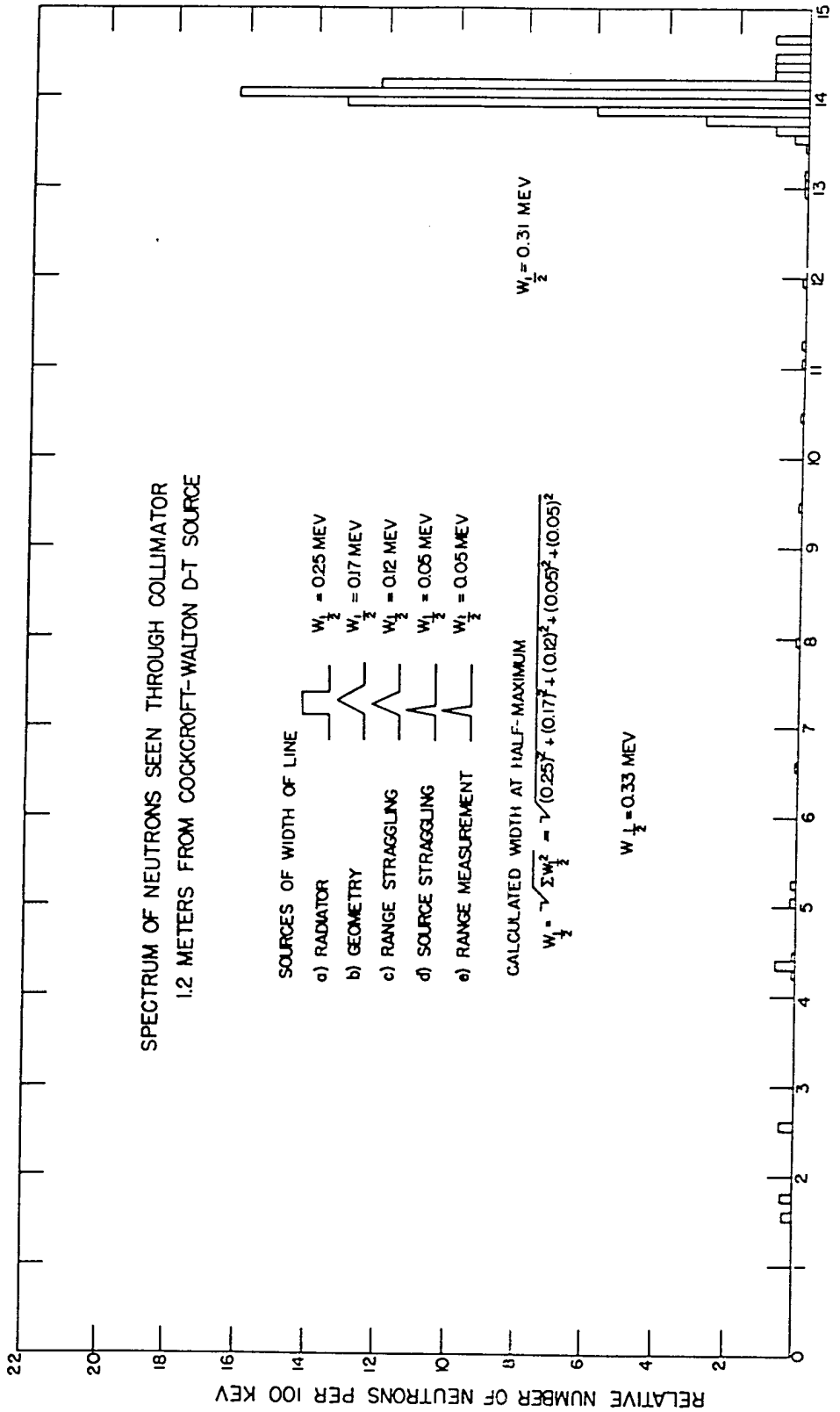

Fig. 6.2 Neutron Spectrum of Cockcroft-Walton D-T Source

Table 6.4 shows a representative record of data from one of the plates. The headings are self-explanatory and essentially explain each step of the calculation for going from a projected-proton-range distribution to a relative neutron-energy spectrum. In order to go to an absolute neutron-energy spectrum, see Eq. 1.8.

6.5 ENERGY RESOLUTION OF NEUTRON SPECTRUM

The energy of a recoil proton is given by $E_p = E_n \cos^2 \theta$. Since $dE_p \leq 2E_n \sin \theta \cos \theta \, d\theta + \cos^2 \theta \, dE_n$, it is immediately obvious that resolution varies inversely with both $\sin \theta$ and $d\theta$ and that these should therefore be as small as possible, consistent with intensity considerations. Also, the converter should be as thin as possible, again consistent with intensity considerations since, for a given E_n, dE_p is determined, to a first approximation, by the converter thickness. Both $\sin \theta$ and $d\theta$ are geometrical factors and easily evaluated. The value of dE_p depends upon the converter thickness, range straggling, and measurement errors. The various factors entering into energy resolution for plates C-4 and C-14, for example, may be evaluated as follows:

Factor	Mev
Radiator	0.25
Geometry	0.17
Range straggling	0.12
Source straggling	0.05
Range measurement	0.05

If all these factors are combined, assuming each to be Gaussian, the width at half-maximum is $\sqrt{(0.25)^2 + (0.17)^2 + (0.12)^2 + (0.05)^2 + (0.05)^2} = 0.33$ Mev.

In order to check this point, a collimator and camera were set up in front of the Cockcroft-Walton D-T source with exactly the same converter thickness and converter-detector disposition as was used for the highest resolution results at Greenhouse (plates C-4 and C-14). The neutron spectrum obtained for this run is shown in Fig. 6.2. The experimental setup is substantially the same as that illustrated in Fig. 3.7. It can be seen from Fig. 6.2 that the width at half-maximum calculated in the manner just outlined is in satisfactory agreement with the observed width at half-maximum. Also the absolute neutron flux as determined from the plates agreed within 5 per cent with the flux determined by counting alphas from the D-T reaction. The width at half-maximum of Fig. 6.2 is henceforth referred to as the natural width at half-maximum for this particular converter-detector arrangement. (Source straggling is seen to be negligible.)

One point which was somewhat troublesome covered the applicability of the range-energy curves in measurements involving a projected length which is later converted to a true length by the relation

$$\text{Actual length} = \frac{\text{projected length}}{\cos \psi},$$

where $\cos \psi$ is the angle between the axis along which the projection is measured and the true direction of the track. A calculation shows that the actual length measured in this way differs (owing to multiple small-angle scattering) from the true track length by less than $\frac{1}{2}$ per cent. (See Appendix IV for the details of this calculation.) A $\frac{1}{2}$ per cent difference in range corresponds to a $\frac{1}{4}$ per cent difference in energy at 14 Mev.

Chapter 7

Evaluation of Elastic- and Inelastic-scattering Effects

7.1 DELETED

DELETED

The transmission is given by the ratio of the two intensities observed, each intensity being first normalized to the number of neutrons generated during equivalent exposure times.

DELETED

The transmission was determined to be 53 per cent along the Phonex line of sight.

DELETED

7.2 DELETED

DELETED

The neutron spectrum was measured at 1 m from the D-T source by exposing 200-μ C-2 nuclear emulsions in such geometry that the plane of the emulsion made an angle of approximately 5° with the line from the D-T source to the center of the plates.

DELETED

In this method of measuring neutron spectra, the nuclear emulsion is used as both radiator and detector. The neutrons collide with H^1 nuclei in the photographic emulsion. After the plate is processed, the trajectories of the proton recoils can be seen as rows of silver grains. The analysis consists in measuring all tracks of proton recoils projected into a given solid angle as defined by a square pyramid of convenient half-angle. See Fig. 7.2 for a diagrammatic representation.

In practice it is usually most convenient to measure the projected track length, h, along the long plate axis. The true track length is obtained from the projected track length by

$$l = \frac{h}{\cos \psi}, \qquad (7.1)$$

where $\cos \psi = \cos \alpha \cos \beta$. From l the energy

Page 75 is DELETED.

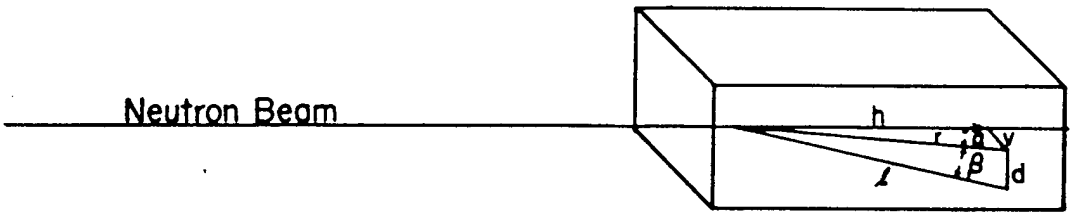

Fig. 7.2 Geometric Relations Involved When Using Plate as Both Radiator and Detector

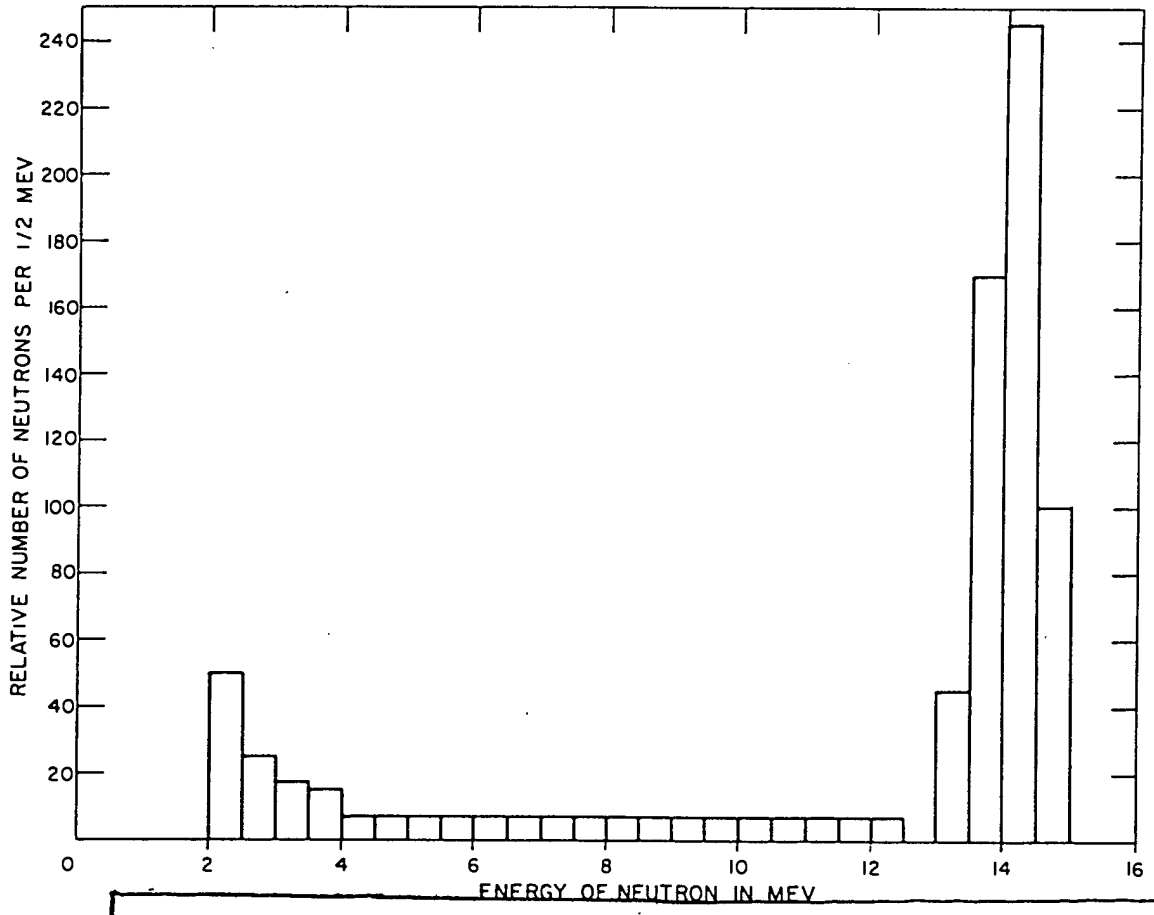

Fig. 7.3 DELETED

of the proton recoil E_p is obtained. The energy of the neutron producing the recoil is given by

$$E_p = E_n \cos^2 \psi. \qquad (7.2)$$

The neutron spectrum may be calculated in much the same way as previously outlined for the case of the camera geometry with but two exceptions. In the first place, no correction to the range need be made for radiator thickness since the emulsion serves as both radiator and detector. Secondly, a correction must be made for the fact that long tracks have a higher probability of leaving the emulsion than the short tracks.

DELETED

Figure 7.5 gives the spectrum corrected for the background, the background correction being made on the assumption that the number of low-energy background tracks is proportional to the number of high-energy neutrons reaching the detector.

DELETED

7.3

DELETED

DELETED

In this experiment the 14.1-Mev neutrons from the Cockcroft-Walton source were again used to simulate the neutrons from the George shot thermonuclear reaction. DELETED

DELETED

The geometry was such that the solid angles were duplicated wherever possible.

DELETED

The Dinex shield was also mocked-up by using paraffin. The cab wall, which consisted of $\frac{3}{8}$-in. plywood with a $3\frac{3}{4}$-ft hole, coaxial with the Phoenix line of sight, was likewise mocked-up to subtend the same solid angle at the neutron source. Figure 7.6 is a picture of the mock-up minus the plywood. Figure 7.7 is a schematic of the experimental arrangement.

DELETED

Figure 7.9 gives the neutron spectrum obtained in the arrangement shown in Fig. 7.7. Figure 7.10 is a background run; i.e., all the scattering material was removed. Figure 7.11 gives the neutron spectrum corrected for background. The corrected spectrum was arrived at in the same manner as outlined in Sec. 7.2.

DELETED

In order to determine the magnitude of this effect, the nuclear emulsions were replaced by copper threshold detectors, and a determination was made of the intensity of neutrons above the Cu(n,2n) threshold (12 Mev) with and without the above-mentioned scattering materials around the Cockcroft-Walton 14-Mev neutron source. The result of this experiment was that the intensity of neutrons as measured by copper threshold detectors is 5.5 per cent higher with the scattering materials surrounding the neutron source than with these materials removed.

DELETED

This correction was applied to the final results.

[redacted]

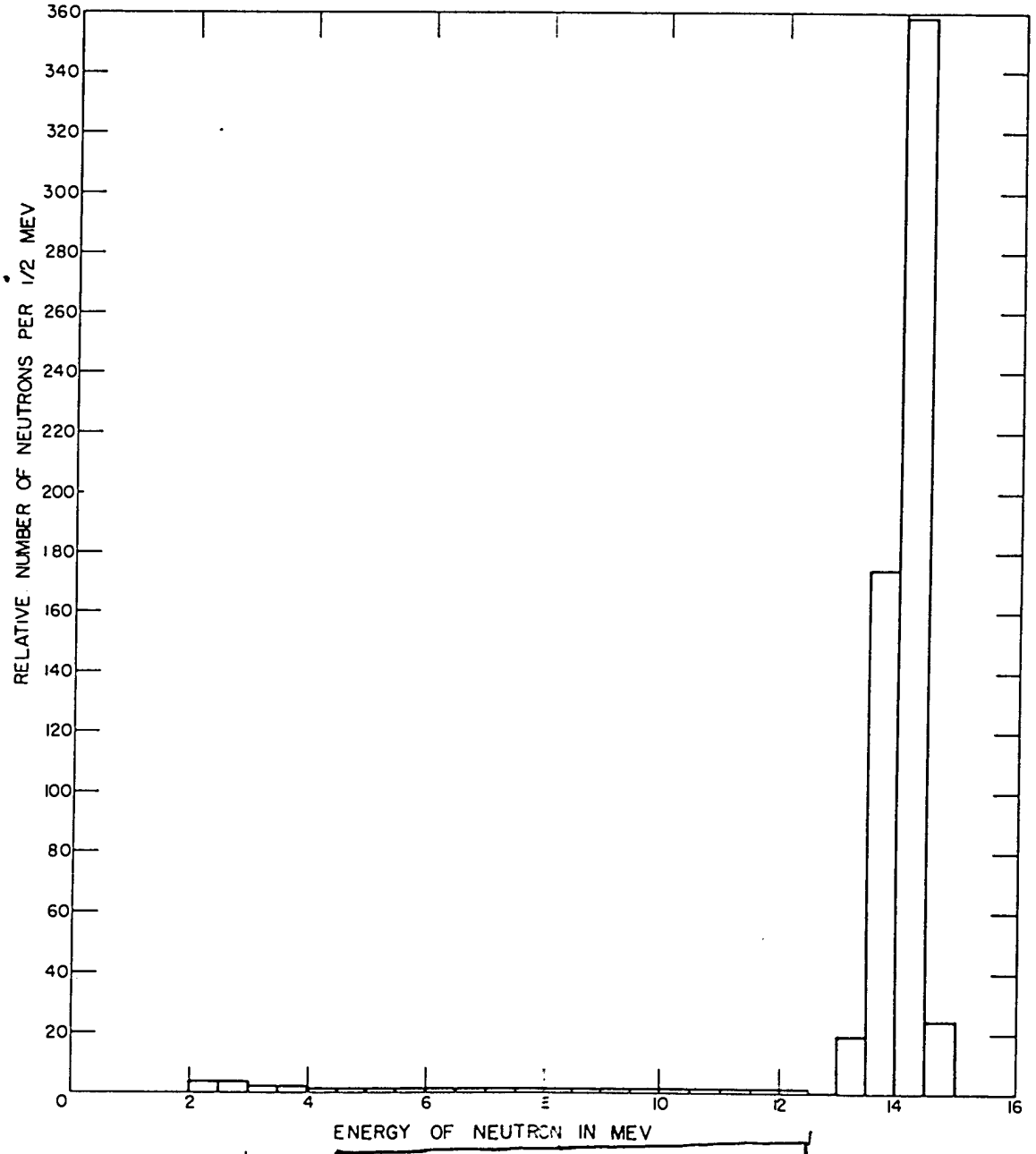

Fig. 7.4 DELETED

[redacted]

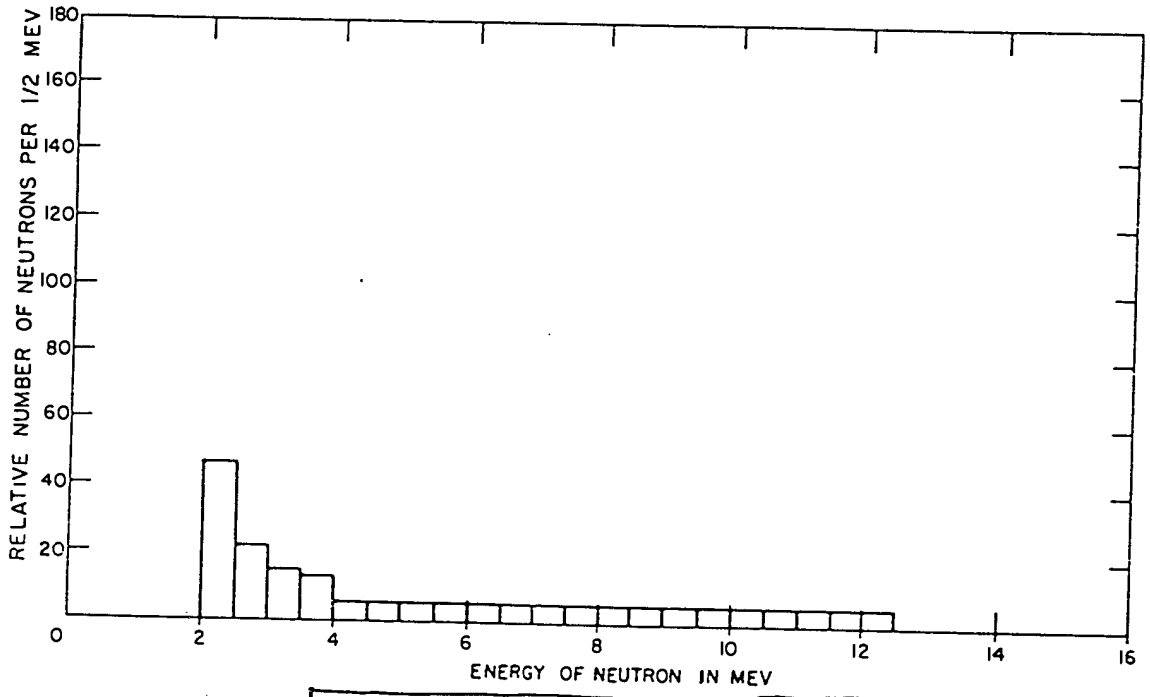

Fig. 7.5 DELETED

Pages 80, 81, 82, 83 are DELETED

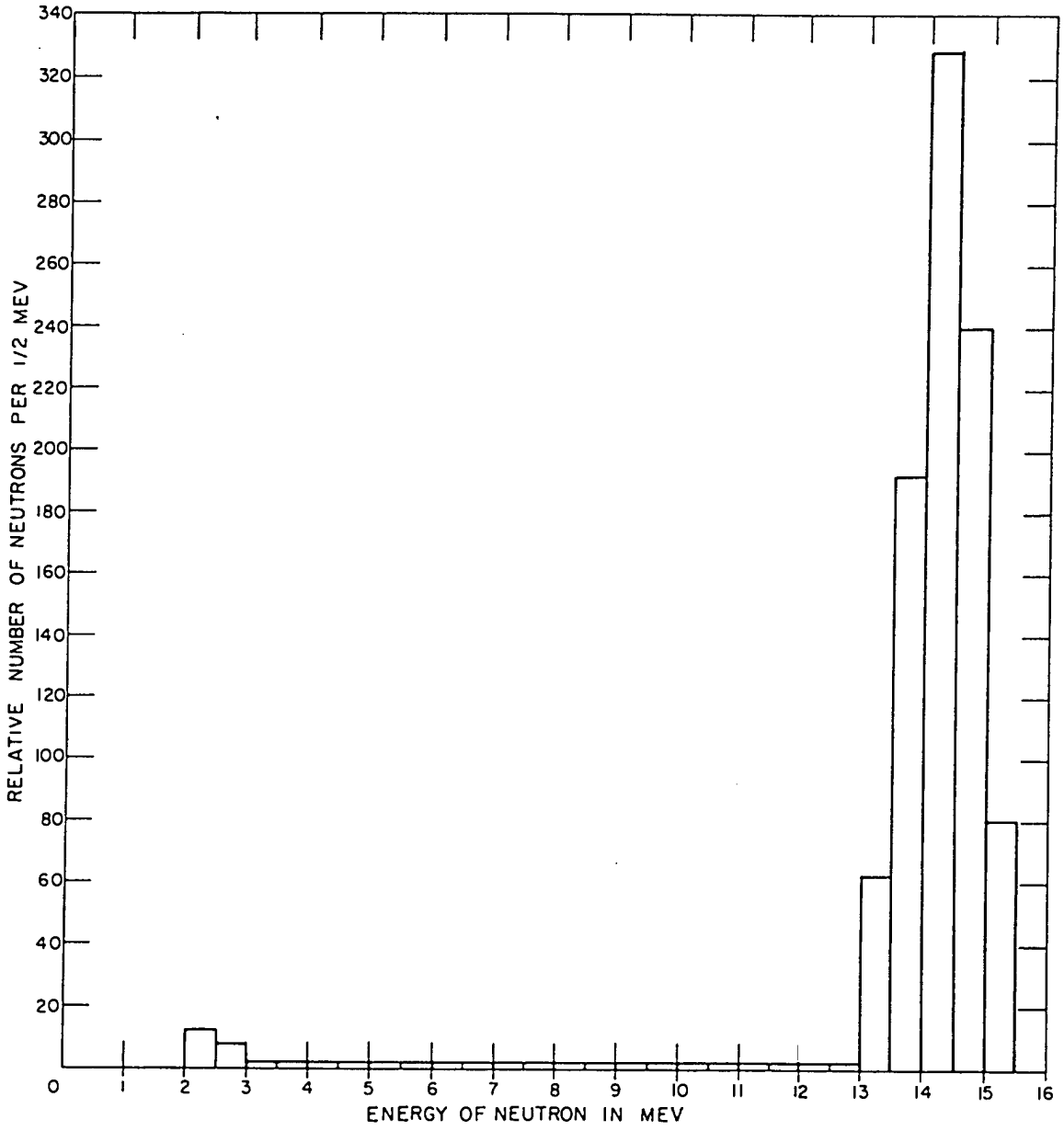

Fig. 7.10 Background Run for Fig. 7.9

Page 85 is DELETED.

7.4 TRANSMISSION OF X UNIT FOR 14-MEV NEUTRONS (ITEM SHOT)

In order to evaluate the Item shot data it is necessary to know the transmission of the bomb at the time the chain reaction is proceeding. This was mocked-up by J. H. Coon for the bomb proper. Unfortunately, the Phonex line of sight looked through the X unit as well as through the fundamental bomb components. Since only the fundamental bomb components were mocked-up in Coon's experiment, it was necessary, for interpretation of the D-T neutron part of the spectrum, to measure the transmission of the X unit for 14-Mev neutrons.

DELETED

Although this was not a good geometry experiment, it approached a true mock-up of the actual case for the following reasons:

1. The X unit was placed sufficiently far from the source so that the angle between the direction of a neutron striking any part of the X unit and its direction after scattering in such a way that it passed through the detectors was approximately the same for both the mock-up experiment and the actual shot.

2. It is realized that the neutrons incident on the X unit come from a point source in the mock-up experiment and from an extended source in the case of the bomb. However, in the case of the bomb, comparatively few 14-Mev neutrons would arrive at the X unit from directions other than the center of the bomb. In order to come from other directions they would have to undergo scattering. If scattered by light nuclei (hydrogen in the HE, for example) they would lose considerable energy upon collision and would therefore no longer have 14 Mev energy. As for scattering by heavy nuclei, it is known that large-angle elastic scattering is highly improbable. Finally, inelastic scattering would again reduce the neutron energy even more, on the average, than does elastic scattering from hydrogen.

DELETED

7.5 TRANSMISSION OF BORON PLUGS AND STEEL BLAST PLATE IN FRONT OF COLLIMATOR TUBES (ALL SHOTS)

As was pointed out in Chap. 3, it was necessary to use B^{10} plugs in each end of the collimator tubes in order to keep thermal neutrons from reaching the cavity containing the camera. It was also necessary to cover the front of the collimator with a $\frac{3}{8}$-in. steel blast plate. Neutrons incident on the converter were first obliged to pass through $\frac{7}{16}$ in. of steel and $\frac{3}{4}$ in. of powdered B^{10}. The B^{10} was contained in a steel capsule with $\frac{1}{32}$-in. ends. Since the converter saw both the B^{10} capsule and blast plate in good geometry, it is necessary to correct the neutron flux incident on the converter by a factor which takes account of the total cross section for neutrons of the B^{10} and steel. A good geometry transmission experiment was therefore performed with 14-Mev neutrons incident on a plug of B^{10} and on a flat cylinder of steel. (The outside diameter of both was 1 in., which is the same as the diameter that was effective when these were used with the collimators.) The transmission of the steel and B^{10} was 65 per cent for 14-Mev neutrons. In making the corrections to the flux incident on the converter, it was assumed that the transmission of the B^{10} and steel is independent of neutron energy. Calculations indicate the error introduced by this assumption for energies below 14 Mev is probably less than 5 per cent.

Chapter 8

Results

8.1 DISPOSITION OF COLLIMATORS

Table 8.1 gives the positions at which neutron-spectra determinations were made for the various shots.

TABLE 8.1 DISTANCE OF COLLIMATORS FROM GROUND ZERO FOR VARIOUS SHOTS

Distance from Ground Zero (yd)			
Dog	Easy	George	Item
200*	200†	400†	200†
400†‡	400	640	400
600§	600	800	600
800	800	1000	808
1000	1000¶	1200	1000¶
1200¶			

*Collimator destroyed by jets from bomb. The cameras were recovered but the plates were black.

†Plates could not be analyzed because of extensive gamma fogging.

‡NBS film dosimeters inside collimator showed a gamma intensity of approximately 17 r.

§Relatively clear plates were obtained. NBS film dosimeters inside collimator showed a gamma intensity of approximately 1.8 r.

¶Plates were not analyzed because of low intensity.

8.2 DOG SHOT

Figures 8.1 to 8.3 and Table 8.2 give the neutron spectra obtained from Dog shot.

8.3 EASY SHOT

Figures 8.4 to 8.6 and Table 8.3 give the neutron energy distributions obtained from Easy shot at the various stations.

8.4 GEORGE SHOT

Figures 8.7 to 8.10 and Table 8.4 give the neutron spectra obtained from George shot. Figures 8.11 and 8.12 display the high-energy portion of the distribution in $\frac{1}{3}$- and 0.1-Mev intervals, respectively. It can be seen from the 0.1-Mev data that plotting the data with this resolution is not quite justified.

8.5 ITEM SHOT

Figures 8.13 to 8.15 and Table 8.5 give the energy spectra obtained from Item shot.

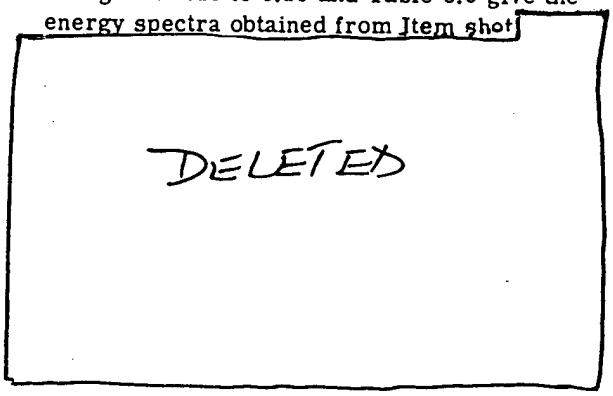

8.6 COMPARISON OF NEUTRON-SPECTRA DATA FROM VARIOUS SHOTS AT APPROXIMATELY 600 YD

Figure 8.16 is a comparison of the neutron spectra from various shots at approximately

TABLE 8.2 SUMMARY OF RESULTS FROM VARIOUS STATIONS, DOG SHOT

DELETED

600 yd.

DELETED

8.7 MEAN FREE PATH IN AIR OF NEUTRONS AS A FUNCTION OF ENERGY

One of the primary objectives of Phonex was the determination of the distribution in energy of the neutrons emitted by the various bombs, this distribution to be on an absolute scale both as to number and energy. It is possible to arrive at these data from the spectrum at any one of the stations at which data were obtained, if the mean free path of the neutrons as a function of their energy is known. Since George shot yielded the most useful spectra for mean-free-path determinations, these spectra were analyzed to determine the energy dependence of neutron mean free paths in air over the neutron energy region available. These mean free paths were of course determined from the atmospheric conditions existing at the time of George shot, which were as follows: temperature, 29°C; relative humidity, 90 per cent; and

Pages 89 through 92 are DELETED.

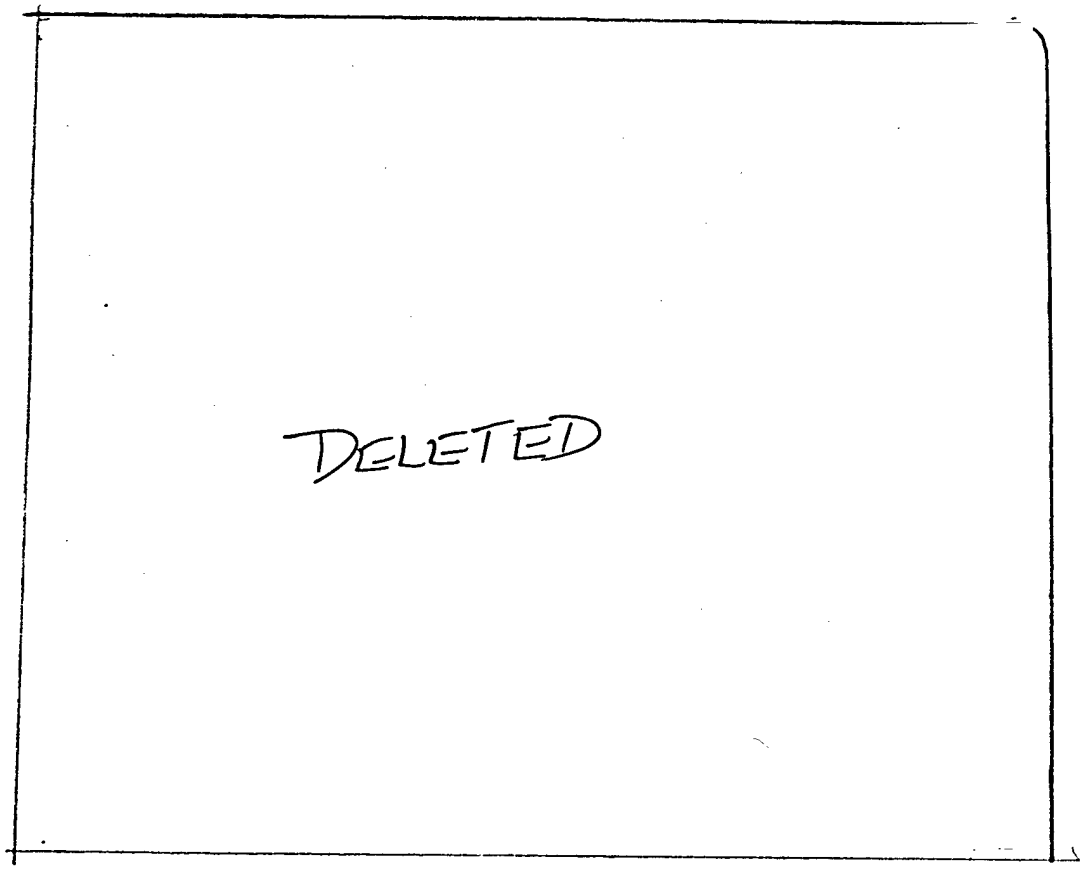

atmospheric pressure, 75.4 cm Hg. The mean free paths applicable to Dog, Easy, and Item shots were calculated from the mean free paths obtained for George shot by making appropriate corrections for atmospheric conditions.

The flux F_n of neutrons of energy E observed in good geometry at a distance R from a source which emits Q neutrons of energy E is given by

$$F_n(E) = \frac{Q}{4\pi R^2} e^{-R/\lambda}, \qquad (8.1)$$

where λ is the mean free path of neutrons of energy E, i.e.,

$$\lambda(E) = \frac{1}{\Sigma_i \sigma_i(E)\, n_i},$$

where $\sigma_i(E)$ is the total cross section of type i atoms for neutrons of energy E, and n_i is the number of such atoms per cubic centimeter. From Eq. 8.1 it is seen that $\ln [4\pi R^2 F_n(E)] = -R/\lambda + \ln Q(E)$. If $\ln [4\pi R^2 F_n(E)]$ vs R is plotted, a straight line is obtained. The reciprocal of the negative slope of this line is obviously equal to the mean free path of neutrons of energy E, and the intercept yields the total number of such neutrons emitted by the source.

Figures 8.17 to 8.21 give the graphs of Eq. 8.1 as obtained from George shot data.

Table 8.6 gives the mean free paths obtained from the slopes of the straight lines fitted to the points plotted in Figs. 8.17 to 8.21. The straight-line fits were made by least-squares analyses. Column 2 of Table 8.6 gives the mean free path as a function of energy under the atmospheric conditions of the experiment. In addition to the mean free paths, the values of Q(E) and the errors assigned to $\lambda(E)$ and Q(E) were determined from least-squares analyses. The errors calculated for $\lambda(E)$ and Q(E) are based on the errors assigned to $F_n(E)$ at the various distances from the bomb. The

Pages 98 through 113 are DELETED.

TABLE 8.6 MEAN FREE PATHS FOR NEUTRONS IN AIR

Neutron Energy (Mev)	λ Experimental (yd)	λ (STP) for Dry Air (yd)	σ_t (STP) for Dry Air (barns)
2 – 3	166.1 ± 4.88	168.1	1.21
3 – 4	153.5 ± 11.10	154.1	1.32
4 – 5	193.2 ± 8.85	193.9	1.05
5 – 6	194.2 ± 11.22	194.2	1.05
6 – 7	183.6 ± 10.16	182.4	1.12
7 – 8	169.9 ± 11.43	168.2	1.20
8 – 10	185.5 ± 9.33	183.6	1.11
10 – 12	164.1 ± 9.18	161.6	1.26
12 – 13	146.5 ± 12.92	143.8	1.41
13 – 16	147.0 ± 6.24	144.2	1.41

errors assigned to $F_n(E)$ are made up of the following:

Error Source	Per Cent
Geometry	4
Radiator	3
Plate area analyzed	1
Statistical	$\frac{100}{\sqrt{\text{No. of counts}}}$

Appendix V outlines the least-squares calculations which were used to obtain λ(E), Q(E), and the corresponding standard errors. These calculations were made by Mrs. Lee Stewart of LASL. Column 3 of Table 8.6 gives the mean free paths as a function of energy for dry air at standard temperature and pressure. The correction for the water vapor was made on the basis of the known n-p scattering cross section as a function of energy and on the assumption that the cross section for oxygen is the same as the average atomic cross section for air. The correction for temperature and pressure was made by

$$\lambda(E)_{STP} = \lambda(E)_{measured} \times \frac{273}{273 + t} \times \frac{P}{76 \text{ cm Hg}}$$

Column 4 gives the total average atomic cross section of dry air at standard temperature and pressure for neutrons as a function of neutron energy.

8.8 INFERRED NEUTRON ENERGY DISTRIBUTIONS AT BOMB ZERO

Table 8.7 lists the energy distributions of neutrons emitted by the various bombs as inferred from the energy distribution of the neutrons observed at the experimental stations. The neutron energy distributions at the various stations are given in Tables 8.2 to 8.5. In order to extrapolate back to the bombs, the mean free paths given in Table 8.6 were utilized. These were converted, where necessary, for atmospheric conditions. Since the mean free paths were determined from George shot, no correction for atmospheric conditions was necessary for this shot. The corrections to λ(E) for the remaining shots were as follows:

Shot	Correction (%)
Dog	1.35
Easy	0.42
Item	0.25

Figure 8.22 shows the neutron spectra at bomb zero from all shots. All these data are plotted in 1-Mev intervals. [redacted] DELETED

Figures 8.23 to 8.25 are more detailed graphs of the George shot data; Fig. 8.26 is a more detailed graph of the Item shot data. It should be noticed that the spectra at bomb zero do not show erratic fluctuations. This is a good

TABLE 8.7 BOMB SPECTRA AT ZERO
(Using Mean Free Paths Calculated from George Data)

Energy Interval (Mev)	George Shot Mean Free Path (yd)	George Shot Number of Neutrons Emanating from Bomb $\times 10^{-22}$	Item Shot Mean Free Path (yd)	Item Shot Number of Neutrons Emanating from Bomb $\times 10^{-22}$	Easy Shot Mean Free Path (yd)	Easy Shot Number of Neutrons Emanating from Bomb $\times 10^{-22}$	Dog Shot Mean Free Path (yd)	Dog Shot Number of Neutrons Emanating from Bomb $\times 10^{-22}$
2–3	166.1	DELETED	165.7	DELETED	165.4	DELETED	163.9	DELETED
3–4	153.5		153.1		152.9		151.4	
4–5	193.2		192.7		192.4		190.6	
5–6	194.2		193.7		193.4		191.6	
6–7	183.6		183.1		182.9		181.1	
7–8	169.9		169.5		169.2		167.6	
8–10	185.5		185.0		184.8		183.0	
8–9								
9–10								
10–12	164.1		163.7		163.4			
10–11								
11–12								
12–13	146.5		146.1					
13–16	147.0		146.6					
13–14								
14–15								
15–16								

[redacted]

Pages 116 through 120 are DELETED.

indication that the mean free paths given here are quite accurate; otherwise large fluctuations in these spectra would have resulted from the extrapolation over several mean free paths.

8.9 EVALUATION OF NEUTRON-SPECTRA DATA FROM DOG AND EASY SHOTS

DELETED

DELETED

8.10 EVALUATION OF NEUTRON-SPECTRA DATA FOR ITEM SHOT

The data from Item shot do not lend themselves to reliable interpretation because of the large, and to some extent, unknown attenuation of the bomb for neutrons at the time that these neutrons are generated and also because of the unknown energy dependence of this attenuation.

DELETED

8.11 EVALUATION OF GEORGE SHOT NEUTRON-SPECTRA DATA

8.11.1 Corrections to Neutron Spectra

DELETED

(See Appendix VI for contributions from secondary D-D, D-T, and T-T reactions.) The neutrons produced by the D-T reaction could suffer energy degradation by the following processes:

1. Elastic scattering by deuterium.

[redacted]

2. Elastic scattering by tritium.

DELETED

DELETED

Each of the factors just presented will be considered in turn, starting with the last.

DELETED

The method of making the calculations of the spectra of elastically scattered neutrons is outlined in Appendix VII.

DELETED

[redacted]

Pages 123 through 129 are DELETED.

[redacted]

DELETED

1. Figure 8.23 is replotted as Fig. 8.32a. This is the neutron spectrum emitted by the bomb as inferred from the neutron-spectra measurements at the collimators.

DELETED

3. Figure 8.32c represents the difference between the spectra illustrated by Figs. 8.32a and b.

4. Figure 8.32c is reproduced as Fig. 8.32d; the spectrum shown in Fig. 8.31 is replotted as Fig. 8.32e after normalizing to the spectrum of Fig. 8.32d at 8 to 10 Mev, and then Fig. 8.32e is subtracted from the spectrum in Fig. 8.32d. The resulting spectrum is shown in Fig. 8.32f.

DELETED

Figure 8.32h shows the normalized fission spectrum which was subtracted from the spectrum given by Fig. 8.32g to yield Fig. 8.32i. The high-energy part is the spectrum of unscattered D-T neutrons.

DELETED

The fraction of such neutrons as a function of neutron energy is shown in Fig. 8.33a. Figures 8.33b to g result from multiplying the number of neutrons in a given energy interval as observed at the distances indicated by the factor for that energy interval as given by Fig. 8.33a.

DELETED

Figure 8.33h gives the spectrum of the Cockcroft-Walton 14-Mev neutron source.

8.11.2 Fraction of Tritium Burned in George Shot

The amount of tritium burned in George shot may be calculated from the basis of the following considerations:

DELETED

It is here assumed that the neutrons from deuteron and triton disintegrations have approximately the same distribution in energy as do the neutrons elastically scattered from D and T (Fig. 8.31). Although the assumption is obviously unjustified, the error introduced is small owing to the small number of neutrons for D and T disintegrations.

DELETED

8.11.3 Average Temperature at Which D-T Mixture Burned

Ken Ford of LASL has calculated the shape of the energy distribution of the D-T neutrons at the time they are generated as a function of

[redacted]

Pages 131 through 142 are DELETED.

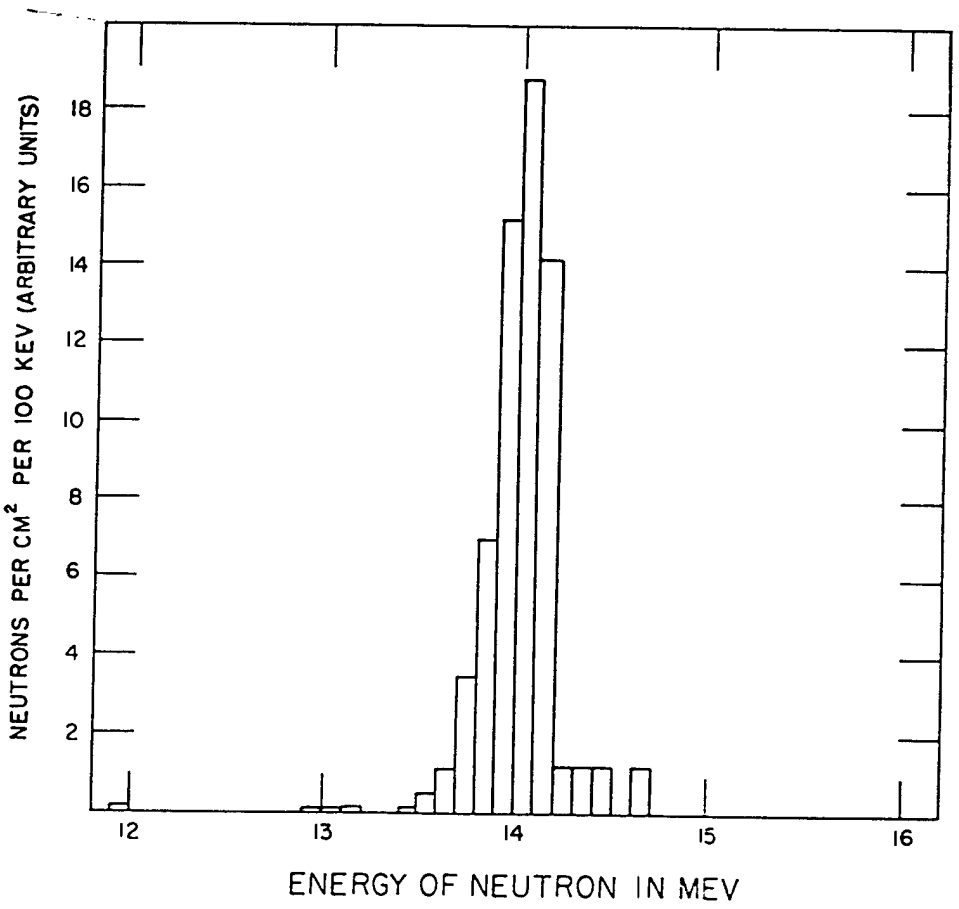

Fig. 8.33h Spectrum of the 14-Mev Neutrons from Cockcroft-Walton ($\frac{1}{10}$-Mev Intervals)

temperature of burning. His data are reproduced in Fig. 8.34. From the corrected neutron-spectra data (Fig. 8.33) an inference may be made of the width at half-maximum of the unmodified D-T neutron energy distributions.

DELETED

8.11.4 Average Compression of D-T Mixture

DELETED

It has also been assumed that the inelastically scattered neutrons have the same energy distribution as the elastically scattered neutrons.

Once I/I_0 has been determined, it is possible to calculate the number of mean free paths that a path along the radius of the D-T mixture presents to the D-T neutrons. The values of mean free paths vs I/I_0 have been calculated for the core of a sphere in which neutrons are uniformly produced. These calculations were made by Group T-1 of LASL and are given in Los Alamos Scientific Laboratory Report, LA-990. The following values of number of mean free paths (N_λ) vs I/I_0 are taken from that report:

DELETED

Page 145 is DELETED.

[redacted]

DELETED

8.12 CONCLUDING REMARKS

It is recognized that the interpretation of the data in this report leaves much to be desired. However, it is anticipated that T Division of LASL will correct and improve upon the calculations made in Chap. 8. As soon as additional cross-section data become available, it should be possible to calculate values for the fraction of tritium burned, apparent temperature during burning, and compression of D-T mixture during burning with much better precision than was possible in this report.

It is hoped that making available the experimental data will act as a stimulant to their further interpretation and to the precise measurement of the various cross sections which enter into the evaluation of the data and which, to a large extent, determine the accuracy of the results.

8.13 SUMMARY

Phonex was designed to make measurements on the distribution in energy of the neutrons emanating from nuclear detonations. It was proposed to look at only those neutrons which came directly (without air scattering) from a given bomb and to determine their spectra at various distances from the bomb. From these spectra it is possible to determine the mean free path in air as a function of neutron energy. It is then a simple matter to derive the neutron spectrum existing at the bomb. From the neutron spectrum of a given bomb it is possible to deduce a number of important results.

DELETED

The method chosen to achieve the objectives of Phonex is in principle very simple. It essentially consists in exposing a hydrogen-containing material to a collimated beam of neutrons from the bomb and recording in photographic emulsions a known fraction of the complete trajectories of the protons projected by the neutrons. A collimator permits the radiator to see only those neutrons coming directly from the bomb, and the geometry is such that the range of a proton in the emulsion is a unique function of the energy of the neutron which projected that proton. In order to determine the spectrum on an absolute scale, the nuclear plate is arranged in such a way that any given area of a plate subtends an accurately calculable solid angle at the radiator. The foregoing conditions are realized by housing the converter and detector inside a large limonite shield which has a collimation channel of circular cross section. The total solid angle seen by the converter was 2.5×10^{-3} steradian.

Page 147 is DELETED.

[redacted]

The number of proton recoils $N(E_p)$ in the energy range dE_p is given by

$$N(E_p)\,dE_p = N(E_n)\,dE_n\,n_o t A_c\,\sigma_{n\text{-}p}(E)\,\frac{A_p \sin\theta\,(4\cos\theta)}{4\pi D^2},$$

where $N(E_n)$ = number of neutrons per square centimeter in energy range dE_n,
n_o = number of H atoms per cubic centimeter of radiator,
A_p = area of plate analyzed,
t = thickness of radiator,
A_c = area of collimation channel,
$\sigma_{n\text{-}p}(E)$ = total n-p scattering cross section at energy E,
θ = angle between proton recoil and incident-neutron direction,
D = distance from center of radiator to center of plate area analyzed,

and

$$E_p = E_n \cos^2\theta,$$

or

$$dE_p = \cos^2\theta\,dE_n.$$

The plates and converters were contained in evacuated cameras in order to eliminate air scattering. The plates were analyzed by making a range analysis of all proton tracks which start on the surface of the emulsion and which have the proper angle to have originated in the converter. This procedure eliminated essentially all background.

If the neutron spectra are obtained at various distances from a given bomb, it is possible to determine the mean free path of the neutrons in air as a function of neutron energy. This in turn permits an extrapolation of the spectrum back to the bomb.

The mean free path as a function of neutron energy is obtained from

$$N(E_n) = \frac{Q(E_n)}{4\pi R^2}\,e^{-R/\lambda(E)}$$

or

$$\ln N(E_n)4\pi R^2 = -\frac{R}{\lambda(E)} + \ln Q(E_n).$$

Here $Q(E_n)$ is the total number of neutrons of energy E emitted in the energy interval dE_n at the bomb. R is the distance at which the spectrum is obtained, and $\lambda(E)$ is the mean free path in air for neutrons of energy E.

If $4\pi N(E_n)R^2$ vs R is plotted on semilog paper, $-1/\lambda(E)$ is obtained for the slope and $Q(E_n)$ for the intercept on the semilog axis. From the spectrum at the bomb the yield of D-T neutrons is obtained.

DELETED

The results of the Phonex experiment may be summarized as follows:

1. Neutron spectra were obtained from all Greenhouse shots for at least three distances from each bomb.
2. The mean free paths of neutrons in air were obtained as functions of neutron energy in the energy interval of 2 to 16 Mev.
3. The neutron spectra at bomb zero were determined for all shots.
4.

DELETED

Appendix IA

Neutron Scattering in Air*

DELETED

It is desired to calculate two quantities: (1) the proportion of neutrons that arrive inside a collimator having suffered only elastic scattering to those that have suffered no scattering at all and (2) the total number of neutrons at 14 Mev as a function of distance. It will be assumed that:

1. The mean free path, considering both elastic and inelastic scattering, is 140 m.
2. Elastic and inelastic scattering are equal.
3. A neutron that suffers inelastic scattering is lost as far as either means of detection is concerned (nuclear plates or threshold detectors).

The intensity of neutrons reaching a distance R from the source and having had nothing at all happen to them is

$$N_{direct} = \frac{Qe^{-R/\lambda}}{4\pi R^2}, \qquad (IA.1)$$

where $\lambda = 140$ m.

The number of neutrons at distance R that have suffered either elastic or no scattering (that is, considering elastic as no process) is

$$N_{direct + elastic} = \frac{Qe^{-R/2\lambda}}{4\pi R^2}. \qquad (IA.2)$$

The difference between Eqs. IA.1 and IA.2 is just the elastic scattering; i.e.,

$$N_{elastic} = \frac{Q}{4\pi R^2}\left(e^{-R/2\lambda} - e^{-R/\lambda}\right). \qquad (IA.3)$$

Thus at any point the ratio of elastically scattered neutrons to nonscattered is

$$\frac{N_{el}}{N_{direct}} = \frac{e^{-R/2\lambda} - e^{-R/\lambda}}{e^{-R/\lambda}} = e^{R/2\lambda} - 1. \qquad (IA.4)$$

If it is now assumed that neutrons are elastically scattered preferentially forward and that the mean scattering on one collision is through an angle θ, then on n collisions the mean angle with the original direction is $\theta\sqrt{n}$.

Here, however, since those particles are being considered which have undergone only elastic scattering, the n is not the number of mean free paths, but half that number; i.e.,

$$\bar{\theta} = \theta\sqrt{R/2\lambda}. \qquad (IA.5)$$

This angle then represents a solid angle given by

$$\bar{\theta}_S = \pi \sin^2\theta\,\sqrt{R/2\lambda} \qquad (IA.6)$$

for values of θ that are not too large.

If consideration is now given to a collimator that accepts over a solid angle α, the proportion of elastically scattered neutrons accepted will be approximately

$$\frac{\alpha}{\bar{\theta}_S} = \frac{\alpha}{\pi \sin^2\theta\,\sqrt{R/2\lambda}}, \qquad (IA.7)$$

and hence, from Eqs. IA.4 and IA.7, the ratio of elastically scattered neutrons to direct neutrons accepted by the collimator is

$$\frac{N_{sc}}{N_{direct}} = (e^{R/2\lambda} - 1)\,\frac{\alpha}{\pi \sin^2\theta\,\sqrt{R/2\lambda}}. \qquad (IA.8)$$

* Reproduced from a paper by W. Ogle.

If it is assumed that a ratio $N_{sc}/N_{direct} = \frac{1}{10}$ is acceptable, an equation for α may then be written:

$$\alpha = \tfrac{1}{10} \frac{\pi \sin^2 \theta \sqrt{R/2\lambda}}{e^{R/2\lambda} - 1}. \qquad \text{(IA.9)}$$

Then, assuming $\sin^2 \theta = \frac{1}{100}$ or $\sin^2 \theta = \frac{1}{4}$ (J. Coon's data), Table I is obtained.

The solid angle of acceptance on the present collimators is

$$\frac{\pi/16}{36^2} = \frac{4\pi}{64 \times 36^2} = 1.5 \times 10^{-4},$$

which on the basis of Coon's scattering data is appreciably better than required. Thus it seems that the present collimators are satisfactory.

Now consider the case of the uncollimated threshold detectors. It will be assumed that the detector sees all neutrons which either have not been scattered at all or have suffered only elastic collisions. The total intensity at a point is then given by Eq. IA.2:

$$N_T = \frac{Qe^{-R/2\lambda}}{4\pi R^2}.$$

It is recognized that this equation is not strictly correct because it ignores diffusion. However, it indicates that extrapolation back to zero is not too bad.

TABLE I

For R Equal to	$R/2\lambda$	$e^{R/2\lambda} - 1$	$\sqrt{R/2\lambda}$	α	
				$\sin^2 \theta = 1/100$	$\sin^2 \theta = 1/4$
λ = 153 yd	1/2	0.649	0.707	3.42×10^{-3}	79.2×10^{-3}
2λ = 306 yd	1	1.72	1.00	1.82×10^{-3}	45.6×10^{-3}
3λ = 459 yd	3/2	3.48	1.22	1.10×10^{-3}	27.6×10^{-3}
4λ = 612 yd	2	6.39	1.41	6.92×10^{-4}	17.3×10^{-3}
5λ = 765 yd	5/2	11.18	1.58	4.43×10^{-4}	11.09×10^{-3}
6λ = 918 yd	3	19.1	1.73	2.84×10^{-4}	7.10×10^{-3}
7λ = 1071 yd	7/2	32.1	1.87	1.83×10^{-4}	4.34×10^{-3}

Appendix IB

Experimental Determination of Theta

The value of θ for these calculations was deduced from experiments by James Coon and his group.

The experiments consisted in making transmission measurements of 14-Mev neutrons through O_2 and N_2 in various geometries. The results may be illustrated as follows:

Assume a disk scatterer of radius R made of O_2 or N_2 and imagine it divided into an arbitrary number of concentric rings. Further, assume a detector at an arbitrary point on the axis of this disk at a distance D from the center of the disk. The results of this experiment showed that each ring contributed approximately the same number of elastically scattered neutrons per atom in the ring at the detector in the region $30° > \arctan R/D > 0$; i.e., there does not appear to be preferential scattering into very small angles as was at first expected. It should be pointed out that the disk geometry is quite applicable to the geometry of this experiment. The mean scattering for one collision was consequently taken to be 15° for the calculations given in Appendix IA.

In the foregoing discussion it has been assumed that the ground makes no contribution to the number of scattered neutrons which find their way into the collimator tube. Although this assumption is obviously not true, it can readily be shown that the effect of the ground must be less than the effect of air scattering. The argument is as follows: Assume a neutron source S at a distance d above ground level. Then the effect of the ground can be estimated by considering the scattering contribution from an image source a distance d below ground level, as illustrated in the figure below.

Since most of the elastic scattering is small-angle scattering, it is immediately apparent that the collimator will see fewer scattered neutrons which had their origin at S' than at S.

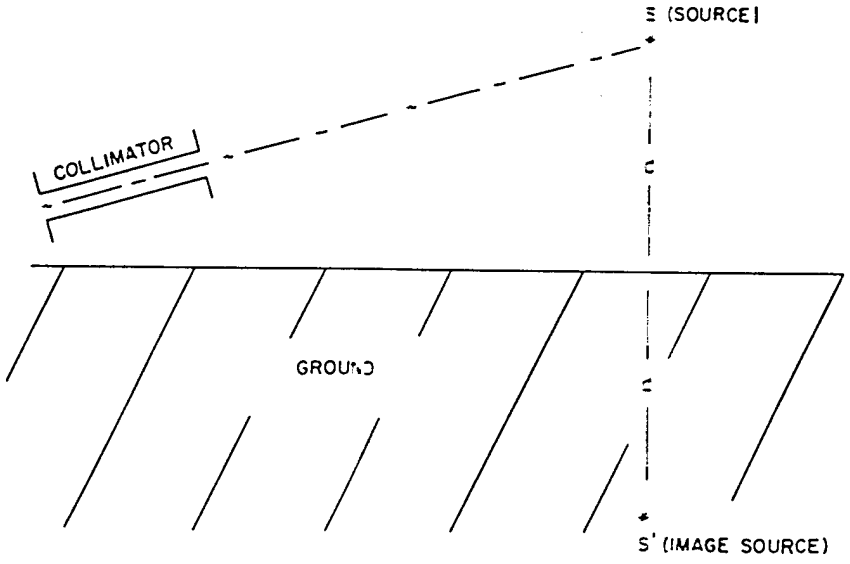

Appendix II

Collimation Geometry Corrections

In the figure below, AB is a collimator of length L, with a circular collimating tube of radius r. S is the distance to the bomb, and X is the misalignment of the bomb from the center line of the collimator; that is, X/S is the angle of displacement in radians, since X ≪ S.

Also, the projection of A is slightly larger than A itself. In linear dimensions this will be a factor of (L + S)/S = 1 + (L/S), and in area approximately 1 + (2L/S); the correction will be 1 per cent at the 200-yd station and 0.2 per cent at the 1000-yd station.

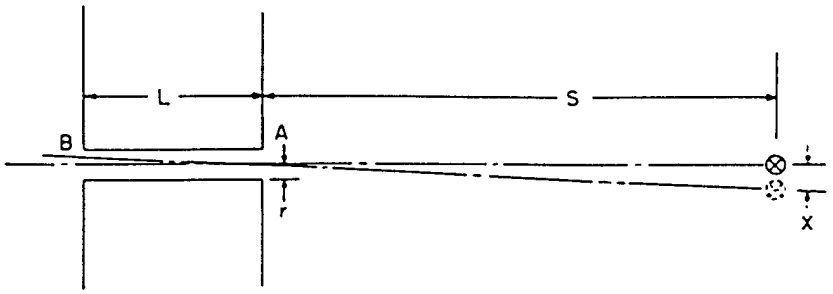

Assume perfect collimation; i.e., a neutron which does not pass through the opening is lost. The efficiency of the collimator for seeing the source will then be given by the projection of circular aperture A on plane at B, the effective radiator area being the intercept of projection of diaphragm A on diaphragm B as a function of X.

Plane B will look like

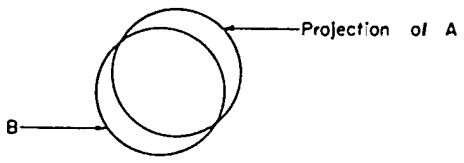

The displacement of the projection of A will be designated as b:

$$\frac{b}{L} = \frac{X}{S}.$$

Neglecting this correction, the area common to the two circles as a function of d will be found as shown in the following calculation. The circles are of radius r.

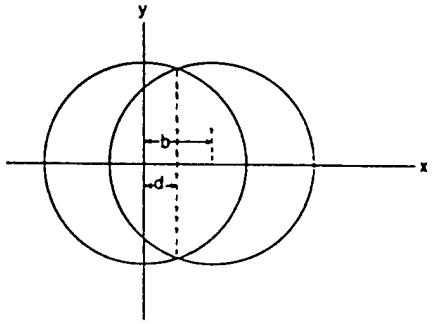

$$x^2 + y^2 = r^2.$$

$$(x^2 - b^2) + y^2 = r^2.$$

$$A + \Delta A = 2\int_d^r \int_{-\sqrt{r^2-x^2}}^{\sqrt{r^2-x^2}} dy\, dx$$

[redacted]

$$= 4\int_d^r \sqrt{r^2 - x^2}\, dx$$

$$= 2\left(x\sqrt{r^2 - x^2} + r^2 \sin^{-1}\frac{x}{r}\right)_d^r$$

$$= 2\left(r(0) + r^2 \sin^{-1} 1 - d\sqrt{r^2 - d^2} - r^2 \sin^{-1}\frac{d}{r}\right)$$

$$= \left(\frac{2\pi}{2} r^2 - 2d\sqrt{r^2 - d^2} - 2r^2 \sin^{-1}\frac{d}{r}\right)$$

$$b = X\frac{L}{S} = 2d \qquad d = \frac{XL}{2S}$$

$$A + \Delta A = \pi r^2 - 2\frac{XL}{2S}\sqrt{r^2 - \left(\frac{XL}{2S}\right)^2} - 2r^2 \sin^{-1}\frac{XL}{2rS}$$

$$\frac{\Delta A}{A} = \frac{-2\frac{X}{2S} L \sqrt{r^2 - \left(\frac{X}{2S}\right)^2 L^2} - 2r^2 \sin^{-1}\frac{X}{2S}\frac{L}{r}}{\pi r^2}$$

$$\frac{\Delta A}{A} = \frac{-2}{\pi}\left[\frac{X}{2S}\frac{L^2}{r^2}\sqrt{\left(\frac{r}{L}\right)^2 - \left(\frac{X}{2S}\right)^2} + \sin^{-1}\frac{X}{2S}\frac{L}{r}\right]$$

for $r = \frac{1}{4}$ in. and $L = 36$ in.

$$\frac{\Delta A}{A} = \frac{-2}{\pi}\left[\frac{X}{2S} 144^2 \sqrt{\frac{1}{144^2} - \left(\frac{X}{2S}\right)^2} + \sin^{-1} 144\frac{X}{2S}\right]$$

$$= \frac{-2}{\pi}\left[1.04 \times 10^4 \frac{X}{S}\sqrt{\frac{1}{2.07 \times 10^4} - 0.25\left(\frac{X}{S}\right)^2} + \sin^{-1} 72\frac{X}{S}\right]$$

$$= \frac{-2}{\pi}\left[1.04 \times 10^4 \frac{X}{S}\sqrt{4.83 \times 10^{-5} - 0.25\left(\frac{X}{S}\right)^2} + \sin^{-1} 72\frac{X}{S}\right].$$

Values for $\frac{\Delta A}{A}$ are computed below.

Loss of Radiation Efficiency

$\frac{X}{S}$	$\frac{\Delta A}{A}$
0.001	−0.09
0.002	−0.18
0.003	−0.28
0.005	−0.45
0.01	−0.83

[redacted]

[redacted]

Appendix III

Effectiveness of Water Vapor in Camera as a Neutron-Proton Converter

The following notation is used:

N_p = number of proton recoils.

N_n = integrated number of neutrons.

Ω = solid angle.

$\frac{d\sigma}{d\Omega}$ = differential n-p scattering cross section at angle θ and energy E.

$\sigma_t(E)$ = total n-p scattering cross section at energy E.

b, l = camera dimensions.

n_0 = number of hydrogen nuclei per cubic centimeter in water vapor in camera.

n_1 = number of hydrogen nuclei per square centimeter in radiator at end of camera.

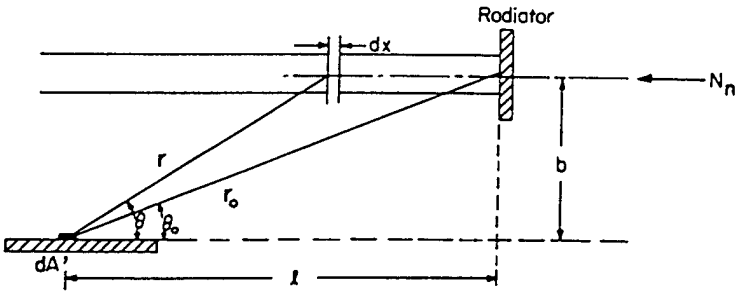

For water vapor,

$$dN_p = N_n n_0 \, dx \frac{d\sigma}{d\Omega} d\Omega,$$

$$d\Omega = \frac{dA \sin \theta}{r^2},$$

$$\frac{d\sigma}{d\Omega} = \frac{\sigma_t(E)}{4\pi} 4 \cos \theta = \frac{\sigma_t(E)}{\pi} \cos \theta,$$

$$dx = \frac{r \, d\theta}{\sin \theta} \qquad \frac{b}{r} = \sin \theta,$$

$$dN_p = N_n n_0 \frac{r \, d\theta}{\sin \theta} \frac{\sigma_t(E)}{\pi} \cos \theta \frac{dA}{r^2} \sin \theta,$$

$$\frac{N_p}{dA} = \frac{N_n n_0 \sigma_t(E)}{\pi b} \int_{\theta_0}^{\frac{\pi}{2}} \sin \theta \cos \theta \, d\theta,$$

$$\theta_0 = \tan^{-1} \frac{b}{l}. \qquad \text{Set } K = \frac{N_n n_0 \sigma_t(E)}{\pi b},$$

$$\frac{N_p}{dA} = \frac{1}{2} K (1 - \sin^2 \theta_0) = \frac{1}{2} K \left(1 - \frac{b^2}{b^2 + l^2}\right).$$

Hence

$$\frac{N_p}{dA} = \frac{N_n n_0 \sigma_t(E)}{2\pi b} \left(\frac{l^2}{b^2 + l^2}\right).$$

For the radiator, having n_1 atoms/cm^2,

$$N_p = \frac{N_n n_1 \sigma_t(E) \cos \theta_0}{\pi} \frac{dA}{r_0^2} \sin \theta_0,$$

$$\frac{N_p}{dA} = \frac{N_n n_1 \sigma_t(E)}{\pi} \frac{bl}{(b^2 + l^2)^2}.$$

[redacted]

The ratio of tracks in dA due to water vapor to those due to the radiator is, then,

$$R = \frac{(N_p/dA)_{W.V.}}{(N_p/dA)_{RAD}} = \frac{n_0}{n_1}\left[\frac{l(b^2 + l^2)}{2b^2}\right].$$

For a water-vapor pressure of 1 cm Hg, the value for n_0, neglecting the temperature correction, is

$$n_0 = \frac{2 \times 6.023 \times 10^{23} \text{ atoms H}}{2.24 \times 10^4 \text{ cm}^3} \frac{1 \text{ cm Hg}}{76 \text{ cm Hg}}$$

$$= 7.1 \times 10^{17} \frac{\text{atoms H}}{\text{cm}^3},$$

and, for a 1-mil radiator, the thinnest used,

$$n_1 = 2.4 \times 10^{20} \frac{\text{atoms H}}{\text{cm}^2}.$$

Typical dimensions of the cameras are $b = 5$ cm and $l = 15$ cm.

$$R = \frac{7.1 \times 10^{17}}{2.4 \times 10^{20}} \frac{15 \times 250}{2 \times 25} = 2.2 \times 10^{-1},$$

or 22 per cent, an appreciable fraction of the total number of tracks.

It may be observed, however, that the intensity distribution with angle for the protons scattered from water vapor is

$$D(\theta) \propto \frac{\sin\theta \cos\theta}{\sin\theta\, r} \approx \sin\theta \cos\theta.$$

Maximizing, set

$$\frac{dD}{d\theta} = 0,$$

$$\sin^2\theta - \cos^2\theta = 0,$$

$$\theta = 45°.$$

Hence dip discrimination permits rejection of a considerable fraction of the spurious tracks. Actually, after the first short hoods were placed over the plates, where practicable, and this effect was reduced to practically zero for those plates. See Fig. 4.2.

Appendix IV

Range-straggling Calculations

The problem to be considered here is an evaluation of the difference between the true mean range l of a particle and the measured mean range h. By definition

$$l = \int_0^E \left(-\frac{dE}{dx}\right)^{-1} dE. \qquad \text{(IV.1)}$$

In other words, half the particles travel a range greater than l, and half travel less than l.

On the other hand, h is the distance from the entrance point in the emulsion of a plane perpendicular to the initial direction of the beam through which half the particles pass. Because of multiple small-angle scattering, $l > h$. If the range is divided into small lengths l_i and if θ_i is the angle between l_i and the direction of the incoming particles, then, for small θ_i,

$$l - h = \sum_i l_i(1 - \cos\theta_i) \approx \sum_i \frac{1}{2} l_i \theta_i^2. \qquad \text{(IV.2)}$$

The average value of θ_i^2 is given by

$$\theta_i^2 = \left(\frac{Zm}{M}\right) \log E_0/E_i, \qquad \text{(IV.3)}$$

where m is the mass of the electron, M is the mass of the proton, and Z is the atomic number of the element. The above formula is an approximation of Williams' formula and Bethe's stopping-power equation.

$$-\frac{dE}{dx} = \frac{4\pi e^4}{mv^2} NZ \left[\log \frac{2mv^2}{I(1-\beta^2)}\right]. \qquad \text{(IV.4)}$$

The sum is now replaced by an integral in Eq. IV.2, and Eq. IV.3 is used to obtain

$$l - h = \frac{Zm}{2M} \int_0^l \log E_0/E(x)\, dx. \qquad \text{(IV.5)}$$

If it is assumed that $l \approx E^{1.75}$, which is a good approximation of the range-energy relation in nuclear emulsion, then, where $t = 1.75$, $l = E^t$, and $E = l^{1/t}$,

$$\int_0^l (\log l_0^{1/t} - \log l^{1/t})\, dx$$
$$= \frac{1}{t} l_0 \log l_0 - \frac{1}{t}(l \log l + l)$$
$$= \frac{1}{t}(l_0 \log l_0 - l \log l + l). \qquad \text{(IV.6)}$$

But, in the limit, $l = l_0$; therefore,

$$l - h \simeq \frac{Zml_0}{2Mt},$$

or

$$\frac{l-h}{l_0} = \frac{Zm}{2M(1.75)} = \frac{Z}{6400}.$$

In nuclear emulsion the highest Z is that of silver (Z = 47), which means that $(l - h)/l_0 < 1$ per cent.

Appendix V

Statistical Analysis of Beta

A detailed analysis of the neutron data was made in order to determine the spectra at the bomb for each shot. First, it was necessary to evaluate the mean free paths for neutrons from George shot. From Eq. 8.1, taking logarithms,

$$\ln 4\pi R^2 F_n(E) = -R/\lambda + \ln Q(E). \qquad (V.1)$$

The experimental points were weighted according to the errors of statistics and geometry, the weighting factors being

$$w_i = \left(\frac{Y_i}{\Delta Y_i}\right)^2, \qquad (V.2)$$

where $Y = 4\pi R^2 F_n(E)$ and ΔY = the error in Y.

Using the above notation, a least-squares analysis was made to evaluate λ and ln Q(E) and associated errors.

$$y = mx + b,$$

where $y = \ln Y$, $b = \ln Q(E)$, $m = -1/\lambda$, and $x = R$.

$$\Delta = y - y_i = mx_i + b - y_i.$$

$$\Delta^2 = m^2 x_i^2 + b^2 + y_i^2 + 2mx_i b - 2mx_i y_i - 2by_i.$$

$$\Sigma w_i \Delta^2 = m^2 \Sigma w_i x_i^2 + b^2 \Sigma w_i + \Sigma w_i y_i^2 + 2mb \Sigma w_i x_i - 2m \Sigma w_i x_i y_i - 2b \Sigma w_i y_i.$$

$$\frac{\partial \Sigma w_i \Delta^2}{\partial m} = 2m \Sigma w_i x_i^2 + 2b \Sigma w_i x_i - 2 \Sigma w_i x_i y_i = 0.$$

$$\frac{\partial \Sigma w_i \Delta^2}{\partial b} = 2b \Sigma w_i + 2m \Sigma w_i x_i - 2 \Sigma w_i y_i = 0.$$

$$m \Sigma w_i x_i^2 + b \Sigma w_i x_i = \Sigma w_i x_i y_i.$$

$$m \Sigma w_i x_i + b \Sigma w_i = \Sigma w_i y_i.$$

This gives

$$\lambda = -\frac{1}{m} = \frac{\Sigma w_i x_i^2 \; \Sigma w_i - (\Sigma w_i x_i)^2}{\Sigma w_i x_i \; \Sigma w_i y_i - \Sigma w_i x_i y_i \; \Sigma w_i}, \qquad (V.3)$$

and the antilog of b, the intercept, gives the number of neutrons originating at the bomb.

$$b = \frac{\Sigma w_i y_i + \frac{1}{\lambda}(\Sigma w_i x_i)}{\Sigma w_i}. \qquad (V.4)$$

Since the errors in the quantities which are of interest are rather large, it becomes important to evaluate them as accurately as possible. The fact that the spectra at the bomb are derived only by a rather devious extrapolation from the original data makes estimation of the errors not entirely unambiguous. A discussion of this type of problem is given by Birge' in which he emphasizes the two means of estimating errors. One (referred to as "internal consistency") finds the error in a derived quantity as the result of estimated errors in individual measurements, whereas the other ("external consistency") examines derived quantities to see whether or not their deviations are in accordance with the statistical analysis. The latter is not very accurate but serves to locate undetected errors in the original experiment. In the experiment under consideration it is found that in nearly all cases the external-consistency criterion is more than satisfied. Indeed, the external consistency of the data is sometimes surprising. Nevertheless, it is believed that any lessening of the errors given here is not justified considering the small number of stations for recording data.

In order to calculate the errors in the intercept, b, the test for external and internal consistency must therefore be applied; that is, if

$$\sqrt{\frac{\Sigma w_i (y - y_i)^2}{2}} \geq 1, \qquad (V.5)$$

the error in b (which is written E_b) may be found by

$$E_{b_1} = \sqrt{\frac{\Sigma w_i (y - y_i)^2}{2}} \frac{\Sigma w_i x_i^2}{\Sigma w_i \ \Sigma w_i x_i^2 - (\Sigma w_i x_i)^2}. \quad (V.6)$$

If the left-hand member of Eq. V.5 is less than 1,

$$E_{b_2} = \sqrt{\frac{\Sigma w_i x_i^2}{\Sigma w_i \ \Sigma w_i x_i^2 - (\Sigma w_i x_i)^2}}. \quad (V.7)$$

Since the data used in evaluating λ were not always confined to the 1-Mev energy intervals needed to plot the zero bomb spectrum, the evaluation of b and associated errors was not always carried out in the same manner. The preceding equations apply to the energy intervals of George shot where both λ and b were evaluated for 1-Mev intervals, namely, 2 to 3, 3 to 4, 4 to 5, 5 to 6, 6 to 7, 7 to 8, and 12 to 13 Mev.

For the high-energy peak (13 to 16 Mev) where F_n and $(dF_n)/(dE_n)$ are rapidly changing, and for the 8- to 10- and 10- to 12-Mev intervals, an average λ for the entire interval was calculated. Putting this λ into Eq. V.4, b was evaluated as a least-squares average for each of the 1-Mev intervals. The b found in this manner will hereafter be referred to as b′.

Following the same line of reasoning, the error in b′ must also take into account the error in the slope, m; that is,

$$E_m = \sqrt{\frac{\Sigma w_i}{\Sigma w_i x_i^2}} E_{b_k}, \quad (V.8)$$

where E_{b_k} is the error in b over the entire interval used in evaluating λ (Eq. V.6 or V.7 as the case may be).

With this notation, the error in b′ may be calculated from the well-known formula for the propagation of errors.[1] For the case under consideration here, this formula takes the form

$$E_{b'} = \sqrt{\left(\sum E_{y_i} \frac{\partial b}{\partial y_i}\right)^2 + \left(E_m \frac{\partial b}{\partial m}\right)^2}, \quad (V.9)$$

which becomes

$$E_{b'} = \frac{1}{\Sigma w_i} \sqrt{(\Sigma \sqrt{w_i})^2 + E_m^2 (\Sigma w_i x_i)^2}. \quad (V.10)$$

$E_{b'}$ was also calculated by external consistency using the following equations:

$$w_{b_i} = \frac{w_i}{1 + w_i E_m^2 x_i^2}, \quad (V.11)$$

$$E_{b''} = \sqrt{\frac{\Sigma w_{b_i} (b - b_i)^2}{\Sigma w_{b_i} (n - 1)}}, \quad (V.12)$$

and the equation which gave the largest error was used.

The error in λ is yet to be evaluated. Since $\lambda = -1/m$, Eq. V.8 may be readily used in this calculation.

Figure 8.23 shows the bomb spectrum at zero with the calculated errors for George shot. Table 8.6 gives the calculated errors for the mean free paths.

The mean free paths from George shot were used to evaluate the spectra at bomb zero for Dog, Easy, and Item shots. These values were first corrected for differences in atmospheric conditions. Errors were not calculated for these shots, but they could be evaluated in the same manner as the errors in b′ from George shot using Eqs. V.9 to V.12.

REFERENCE

1. R. T. Birge, Phys. Rev., 40: 207–227 (1932).

Appendix VI (page 159) IS DELETED.

Appendix VII

Collision Mechanics Calculation

Let M_1 be the incident nucleus and M_2 the target nucleus. The problem is to derive the energy distribution of the scattered M_1 particles.

Let N(E) dE represent the number of M_1 particles scattered in the interval dE; i.e.,

$$N(E) = \frac{dN}{dE}.$$

Now

$$N(E)\,dE = K_1\,\sigma(\phi)\,d\Omega,$$

where $\sigma(\phi)$ is the cross section per unit solid angle in the laboratory coordinate system and $d\Omega$ is the element of solid angle in the same coordinate system.

$$N(E)\,dE = K_1\,\sigma(\phi)\,2\pi \sin\phi\,d\phi,$$

and

$$\int_{E_1}^{E_2} N(E)\,dE = K_2 \int_{\phi_1}^{\phi_2} \sigma(\phi)\,d(\cos\phi).$$

If $\sigma(\phi)$ vs $\cos\phi$ is now plotted, it is an easy matter to perform graphical integration over any interval ϕ_1 to ϕ_2.

It now only remains to correlate E_1 with ϕ_1 and E_2 with ϕ_2. From conservation of energy and momentum it can be shown quite readily that

$$E_{M_1} = E_{OM_1} \frac{M_1^2}{(M_1 + M_2)^2}\left[\cos\phi + \left(\frac{M_2^2}{M_1^2} - \sin^2\phi\right)^{\frac{1}{2}}\right]^2,$$

where E_{M_1} is the energy of the incident nucleus after collision and E_{OM_1} is its energy before collision. The following table gives the values of ϕ for n-d and n-t elastic scattering for various values of E_{M_1}, where E_{OM_1} = 13.5 and 14.5 Mev. The cross sections used are for 14.1-Mev neutrons.

Energy of Neutron (Mev)	Laboratory Angle of Scattering of Neutron (deg)			
	n-d Scattering		n-t Scattering	
E_{M_1}	ϕ E_{OM_1} = 14.5 Mev	ϕ E_{OM_1} = 13.5 Mev	ϕ E_{OM_1} = 14.5 Mev	ϕ E_{OM_1} = 13.5 Mev
14.5	0.0	-	0.0	-
14.0	16.0	-	19.5	-
13.5	21.5	0.0	27.0	0.0
13.0	26.5	16.0	33.5	20.0
12.5	31.0	23.0	39.2	28.0
12.0	35.0	27.5	44.3	34.5
11.5	39.0	32.0	49.5	40.5
11.0	42.5	36.5	53.8	46.0
10.5	46.0	40.5	58.5	51.0
10.0	49.7	44.5	63.3	56.0
9.5	53.5	48.5	67.8	61.0
9.0	57.0	52.3	72.2	66.0
8.5	60.5	56.0	77.0	71.0
8.0	64.0	60.0	82.3	76.0
7.5	67.5	63.5	87.5	81.5
7.0	71.0	67.5	93.0	87.5
6.5	75.0	71.5	99.0	93.5
6.0	79.0	75.5	106.0	100.0
5.5	83.5	80.0	113.3	107.0
5.0	88.5	85.0	122.0	115.0
4.5	94.0	90.5	134.0	125.5
4.0	99.3	96.0	149.0	139.0
3.5	106.0	102.5	-	160.0
3.0	115.0	111.0	-	-
2.5	127.0	122.0	-	-
2.0	146.0	137.0	-	-
1.5	-	180.0	-	-
1.0	-	-	-	-

AEC, Oak Ridge, Tenn., A11935